

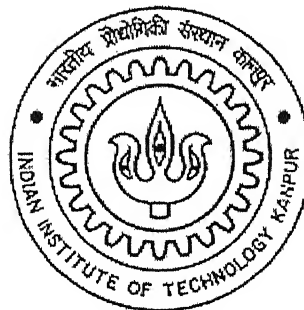
Design and Tuning of Power System Stabilizer for Kaiga Nuclear Power Plant

*A Thesis Submitted
in Partial Fulfillment of the Requirements
For the Degree of*

MASTER OF TECHNOLOGY

by

SAKTI PRASAD PANDA



to the

**DEPARTMENT OF ELECTRICAL ENGINEERING
INDIAN INSTITUTE OF TECHNOLOGY, KANPUR**

MAY 2005

TH
EE/2005/M
P. 22

12 JUL 2005/EE

पुस्तकालय काशीनाथ केलकर पुस्तकालय
भारतीय प्रौद्योगिकी संस्थान कानपुर
अवधि क्र. A...152052.....

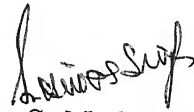


A152052

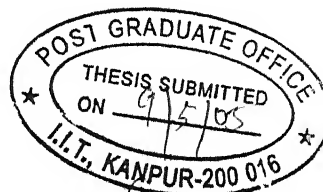
CERTIFICATE

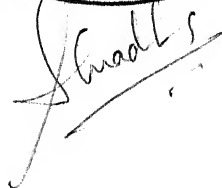
This is to certify that the work contained in this thesis entitled “**Design and Tuning of Power System Stabilizer for Kaiga Nuclear Power Plant**”, has been carried out by Mr. Sakti Prasad Panda (Y3104081) under my/our guidance and that this work has not been submitted elsewhere for a degree.

May, 2005.


(Dr. S. N. Singh)

Associate Professor,
Department of Electrical Engineering,
Indian Institute of Technology,
Kanpur-208016.





Acknowledgement

I express my deep sense of gratitude towards my thesis supervisor Dr. S. N. Singh for his invaluable guidance, moral support and constant encouragement, which was the source of inspiration for me to complete this thesis work successfully. My sincere thanks to him, for tolerating me and solving my academic and personal problems without any hesitation. I also thank Dr. S.C. Srivastava without whose kind support this thesis would have remained incomplete. I also thank Dr. L. Behera, who constantly guided my personal life, like the pole star.

My special thanks to Er. M.K. Kannan, Er. N.S.M. Rao and Er. Rajesh Laad of NPCIL, for sharing with me their invaluable practical experience and for their kind help during my visit to Mumbai. I also acknowledge the financial support provided by Department of Atomic Energy, Government of India, under DGFS scheme, for carrying out this project work.

I thank Mr. B. Kalyan Kumar, Mr. J.G. Singh, and Mr. Sanjoya Parida for their guidance and excellent company. I also thank Praveen, Gaurav, Srikanth, Prabodh and Rajinder for their excellent company and their help.

I thank Mr. Ranjan Kumar Behera and Mr. Gopal Krishna Das for sharing their valuable time with me, standing besides me during the rough patches of my life and making my stay in IIT a memorable event.

I thank my parents, brother and sister, and other good friends from UCE, whose love, concern and blessings enabled me to reach this stage.

Sakti Prasad Panda

Dedicated to
Lord Krishna, the Supreme Controller

CONTENTS

List of Figures	iv
List of Tables	vii
Abstract	viii
1. Introduction	
1.1 General	1
1.2 Rotor Angle Stability	2
1.2.1 Small Signal Stability	3
1.2.2 Transient Stability	4
1.3 Voltage Stability and Frequency Stability	5
1.4 State of The Art	5
1.5 Motivation	7
1.6 Thesis Organization	9
2. System Modeling and Coordination of PSS parameters	
2.1 Introduction	10
2.2 Modeling of Power System Components	10
2.2.1 Synchronous Machine	11
2.2.2 Exciter Modeling	12
2.3 Complete Differential Algebraic Equations	15
2.4. System Linearization	18
2.5. Power System Stability and Power System Stabilizer	20
2.6 PSS Structure	22
2.7 Multi Machine PSS tuning	24
2.7.1 Co-ordination of PSS parameters	24
2.7.2 Determination of coordinated PSS parameters	25
2.7.2.1 Determination via Structurally Constrained Optimal control	25
2.7.2.2 Determination by strip Eigen Value Assignment Method	29

2.8 Results and Discussion	30
2.8.1 WSCC 9-bus system	31
2.8.2 New England 39-bus System	35
2.9 Conclusion	38
3. PSS tuning for Kaiga Nuclear Power Plant	
3.1 Introduction	39
3.2 Exciter and AVR Dynamic Equations for Kaiga NPP	40
3.2.1 PSS Block Diagram at Kaiga NPP	41
3.3 SMIB Analysis and PSS Tuning	41
3.3.1 Phase Plot	42
3.3.2 Eigen Value Analysis	43
3.3.3 PSS Tuning	44
3.4 Simulink Models for NPC System	46
3.5 Simulation and Results	53
3.5.1 NPC Reduced System without PSS	53
3.5.2 NPC Reduced System with PSS at Generator-1	53
3.5.3 Detailed NPC System without PSS	54
3.5.4 Detailed NPC System with PSS at Generator-1	54
3.5.5 Reduced NPC System with 16 Other Generators	54
3.5.6 Reduced NPC System with 16 Generators and PSS at Kaiga-1	55
3.6 Conclusion	74
4. Fuzzy Logic Based PSS design	
4.1 Introduction	75
4.2. Fuzzy Logic Controller (FLC)	76
4.3 FLC Design	77
4.4 FLPSS design	82
4.4.1 FAM Table Formation	83
4.4.2 FLPSS Parameter Tuning	84
4.5. Simulink Model for FLPSS	84

4.6 Simulation and Results	85
4.7 Conclusion	95
5. Conclusions	
5.1 General	96
5.2 Future Scope of Research	98
References	99
Appendix	
A WSCC 3-Machine, 9-Bus System	103
B New England 10-Machine, 39-Bus System	105
C System and Machine Parameters for Kaiga NPP	109

List of Figures

1.1: Stability Classification	2
1.2: Kaiga NPP and nearby generators	8
2.1: Synchronous machine two-axis model dynamic circuit	11
2.2: IEEE type-1 exciter	14
2.3: Phasor diagram for universal rotating frame	16
2.4: Inter connection of synch. Machine and rest of the network	17
2.5: Stabilizer with speed input-system block diagram	20
2.6 PSS block diagram	22
2.7 (a) Single vertical line	30
(b) Vertical strip	30
2.8: Eigen value for 3-machine and 9-bus system	32
2.9: Eigen value for WSCC with pseudo decentralization	33
2.10: Eigen value for WSCC with strip eigen value placement	34
2.11: Eigen value for 10-machine, 39-bus system	35
2.12: Eigen value for New-England system with Pseudo decentralization	38
3.1: AVR block diagram	39
3.2: Simplified AVR block diagram	40
3.3: PSS block diagram for Kaiga NPP	41
3.4: Phase plot for Kaiga NPP	42
3.5: Gain plot for Kaiga NPP	43
3.6: Eigen value without PSS for Kaiga	45
3.7: Eigen value with PSS on generator-1	46
3.8: Simulink blocks of reduced NPC system	47
3.9: Exciter and AVR signal collection	48
3.10: Exciter and AVR Simulink model	48
3.11: Simulink model for PSS	49
3.12: Detailed model for NPC system	50
3.13: Kaiga system with 16 other generators	51
3.14: Kaiga system with IEEE-1 exciter	52
3.15: Load angle oscillation of mac-1 for reduced NPC system	55

3.16: Power output of Kaiga-1	55
3.17: Speed difference between Kaiga-1 and 2	56
3.18: Speed difference between kaiga-1 and swing generator	56
3.19: Load angle of swing generator	57
3.20: Terminal voltage of Kaiga-1	57
3.21: Load angle of Kaiga-1 for reduced NPC system with $T_1/T_2=0.25$	58
3.22: Speed difference between kaiga and swing generator	58
3.23: Load angle of swing generator	59
3.24: Power output of Kaiga-1	59
3.25: Load angle of Kaiga-1 with PSS on generator-1	60
3.26: Speed difference between kaiga-1 and 2	60
3.27: Speed difference between Kaiga-1 and swing generator	61
3.28: Load angle of swing generator	61
3.29: terminal voltage of Kaiga-1	62
3.30: Power output of Kaiga-1	62
3.31: Load angle of Kaiga-1 in detailed model without PSS	63
3.32: Speed difference between Kaiga-1 and Kadra hydro	63
3.33: Load angle of Kudasalli hydro	64
3.34: Speed difference between kaiga-1 and 2	64
3.35: Load angle of Kaiga-1 for detailed system with PSS on machine-1	65
3.36: Speed difference between Kaiga-1 and 2	65
3.37: Load angle at Kadra hydro	66
3.38: Speed difference between Kaiga-1 and Kadra hydro	66
3.39: PSS output at Kaiga-1	67
3.40: Terminal voltage at Kaiga-1	67
3.41: Load angle at Kaiga-1 for Kiaga with 16 other generators and 3 phase fault	68
3.42: Speed difference between Kaiga-1 and 2	68
3.43: Load angle of generator at 200km from Kaiga	69
3.44: Terminal voltage at Kaiga-1	69
3.45: Load angle of swing generator	70
3.46: Speed difference between Kaiga-1 and infinite generator	70

3.47: Load angle of Kaiga-1 with PSS on amchine-1	71
3.48: Load angle of swing generator	71
3.49: Load angle of generator 200km from kaiga	72
3.50: Speed difference between Kaiga-1 and swing generator	72
3.51: PSS output of Kaiga-1	73
3.52: Speed difference between Kaiga-1 and 2	73
4.1: Schematic diagram of FLC building blocks	76
4.2: seven triangular membership functions	78
4.3: FAM system architecture for two fuzzy antecedents and one consequent	79
4.4: Fuzzy control rule matrix	80
4.5: Generation of the output fuzzy set using correlation minimum encoding	81
4.6: Schematic diagram of the FLPSS	83
4.7: Fuzzy control rule matrix for $\Delta\omega$ and ΔP_c inputs	83
4.8: Fuzzy control rule matrix for $\Delta\omega$ and ΔE_{FD} inputs	84
4.9: FLPSS Simulink block	85
4.10: Load angle of Kaiga-1 for reduced NPC system with FLPSS at machine-1	86
4.11: Load angle of swing generator	87
4.12: Speed difference between Kaiga-1 and swing generator	87
4.13: Speed difference between kaiga-1 and 2	88
4.14: Power output of Kaiga-1	88
4.15: Terminal voltage at Kaiga-1	89
4.16: FLPSS output in PU of field voltage	89
4.17: Load angle at Kaiga-1 with FLPSS for detailed NPC system	90
4.18: Load angle of swing generator	90
4.19: Speed difference between Kaiga-1 and swing generator	91
4.20: Load angle at Kadra Hydro	91
4.21: PSS output at Kaiga-1	92
4.22: Load angle at Kaiga-1 with FLPSS for other 16 generators connected	92
4.23: Load angle of swing generator	93
4.24: Load angle of generator 200km from Kaiga	93
4.25: Speed deviation between Kaiga-1 and Kadra	94

4.26: Speed deviation between Kaiga-1 and 2	94
4.27: Terminal voltage at Kaiga-1	95
A-1: Single line diagram of WSCC 9-bus system	103
B-1: Single line diagram for New England 39-bus system	105

List of Tables: 32

2.1 Eigen value of 3-machine, 9-bus system	32
2.2 Eigen value of 3-machine, 9-bus system with pseudo decentralization	33
2.3 Eigen value of 3-machine, 9-bus system with strip eigen value method	34
2.4 PSS parameters for 3-machine, 9-bus system with pseudo decentralization	34
2.5 Eigen value for 10-machine, 39-bus system	36
2.6 Eigen value for 10-machine, 39-bus system with pseudo decentralization	37
3.1 Eigen value for NPC system without PSS	44
3.2 Eigen value for NPC system with PSS at generator-1	45
A-1 Base case load flow results for WSCC system	103
A-2 Line data for WSCC system	104
A-3 Machine data for WSCC system	104
A-4 Exciter data for WSCC system	104
B-1 Base case load flow for New England system	105
B-2 Line data for New-England system	106
B-3 Machine data for New- England system	107
B-4 AVR data for New-England system	108
C-1 Machine parameters for Kaiga generators	109
C-2 Machine time constants for Kaiga generators	109
C-3 Exciter and AVR parameters for Kaiga generators	109
C-4 Line and transformer data for Kaiga system	110

Abstract

With the increase in the complexity of power system, mostly in the generation, control and transmission levels, stable operation of the system under various conditions is of main concern. Power system is highly non-linear and unpredictable in nature. So stability studies of the system as a whole is very challenging. Proper modeling of dynamics of all the components with sound knowledge of all the constraints is necessary for a detailed study of power system. With reasonable assumptions and simplifications the study can be made easier.

In many cases, instability and eventual loss of synchronism are initiated by some spurious disturbance in the system resulting in oscillatory behaviour that, if not damped, may eventually build up. This is very much a function of the operating condition of the power system, such as strength of the system, generator power output, and Automatic Voltage Regulator (AVR) settings. Oscillations, even if undamped at low frequencies, are undesirable because they limit power transfers on transmission lines, in some cases, may take the generator out of synchronism and induce stress in the mechanical shaft. Power System Stabilizer (PSS) aids in damping these small oscillations via modulation of the generator exciter. The art and science of PSS application has developed considerably over last few decades.

In this thesis the small signal instability problem associated with Kiaga Nuclear Power Plant (NPP) is addressed. The causes for the oscillation are determined and PSS is tuned to damp out these oscillations. An intelligent Fuzzy Logic PSS is also designed, which can be used in place of the existing PSS for proper operation of the system. Other standard methods are also studied and developed for application purposes.

Introduction

1.1 General

Nuclear power generation is identified as one of the major electric power source in future. These power plants are very sensitive to any disturbance (mechanical and electrical) due to various technical and safety reasons. If the exciter and Power System Stabilizer (PSS), any, are not tuned properly, there may be sustained oscillations, which is very dangerous. These oscillations are related to power system stability.

Power system stability is the defined as that property of power system that enables it to remain in a state of operating equilibrium under normal operating conditions and to regain an acceptable state of equilibrium after being subjected to a disturbance. In general stability is a condition of equilibrium between opposing forces. Instability results when a disturbance leads to a sustained imbalance between the opposing forces. In the evaluation of stability the concern is the behaviour of the power system when subjected to a transient disturbance. The disturbances may be small or large. Small disturbances in the form of load changes take place continuously, and the system adjusts itself to the changing conditions. The system must be able to operate satisfactorily under these conditions and successfully supply the maximum load. It must also be capable of surviving numerous disturbances of a severe nature, such as short circuit on a transmission line, loss of a large generator or load, or loss of a tie between two subsystems. The understanding of stability problems is greatly facilitated by the classification of stability into various categories.

The classification can be based upon physical nature/main system parameters such as rotor angle, voltage and frequency. Based on the type of disturbances and time span for which a particular disturbance lasts, it can be further subdivided into various categories as shown in Fig. 1.1.

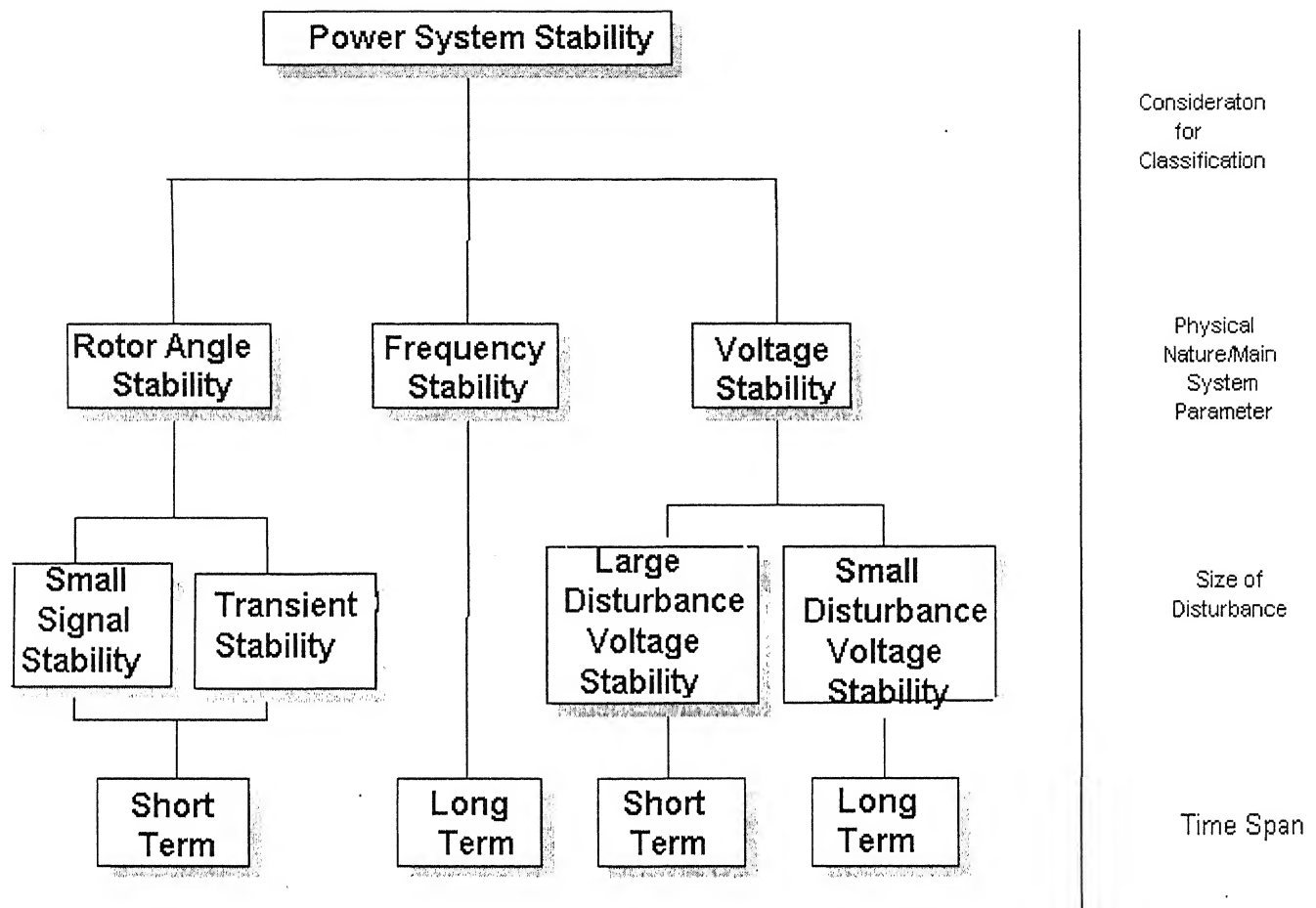


Fig. 1.1: Stability classification

1.2 Rotor Angle Stability

Rotor angle stability is the ability of interconnected synchronous machines to remain in synchronism after being subjected to a disturbance. It depends on the ability to restore equilibrium between electromagnetic torque and mechanical torque of each synchronous machine. If the system is perturbed such as change in load or input, any kind of fault in the system [21], this equilibrium is disturbed, resulting in acceleration or deceleration of the rotors of the machines according to the laws of motion of a rotating body. If one generator temporarily runs faster than another, the angular position of its rotor relative to that of the

slower machine will advance. The resulting additional angular difference transfers part of the load from the slow machine to the fast machine, depending on the power angle relationship [20]. This tends to reduce the speed difference and hence the angular separation. Beyond a certain limit, an increase in angular separation is accompanied by decrease in power transfer; this increases the angular separation further and leads to instability.

For any given situation, the stability of the system depends on whether or not the deviations in angular positions of the rotors results in sufficient restoring torques. When a synchronous machine losses synchronism with the rest of the system, its rotor runs at a higher or lower speed than that required to generate voltage at system frequency. Loss of synchronism can occur between one machine and the rest of the system or between groups of machines. In the later case synchronism may be maintained within each group after its separation from others. The change in electrical torque of a synchronous machine following a perturbation can be expressed into two components:

$$\Delta T_e = K_S \Delta \delta + j K_D \Delta \omega \quad (1.1)$$

where, $K_S \Delta \delta$ is the component of torque change in phase with rotor angle perturbation $\Delta \delta$ and is referred to as the synchronizing torque component. K_S is the synchronizing torque coefficient or stiffness of the system. $T_D \Delta \omega$ is the component or torque in phase with the speed deviation $\Delta \omega$ and is referred to as the damping torque component; T_D is the damping torque coefficient.

Stability depends on the existence of both components of torque for each of synchronous machines. Lack of sufficient synchronizing torque results in instability through an aperiodic drift in rotor angle. On the other hand, lack of sufficient damping torque results in oscillatory instability. For convenience in analysis the rotor angle stability phenomenon can be divided into two categories:

1.2.1 Small Signal (or small-disturbance) Stability

It is the ability of the power system to maintain synchronism under small disturbances. Such disturbances occur continuously on the system because of small

variations in loads and generation. The disturbances are considered sufficiently small for linearization of the system equations to be permissible for purpose of analysis. Instability that may result can be of two forms: (1) steady increase in rotor angle due to lack of sufficient synchronizing torque, or (2) rotor oscillations of increasing amplitude due to lack of sufficient damping torque. The nature of system response to small disturbances depends on a number of factors including the initial operating condition, the transmission system strength and the type of excitation control used. With high gain and continuously acting voltage regulators, the small signal stability problem is one of the ensuring sufficient damping of the system. The high gain regulators improve the steady state stability limit but reduce the damping torque of the system [19]. The stability of the following types of oscillation is of concern

1. Local Modes are associated with the swinging of units at a generating station with respect to the rest of the power system.
2. Inter Area Modes are associated with the swinging of many machines in one part of the system against machines in another part. They are caused by two or more groups of closely coupled machines being connected by weak ties.
3. Control modes are associated with generating units and other controls. Poorly tuned exciters, speed governors, HVDC converters and static var compensators are the usual causes instability of these modes.
4. Torsional Modes are associated with the turbine-governor shaft system rotational components. Instability of torsional modes may be caused by interaction with excitation controls, speed governors, HVDC controls, and series capacitor compensated system.

1.2.2 Transient Stability

It is the ability of the power system to maintain synchronism when subjected to a severe transient disturbance. The resulting system response involves large excursions of generator rotor angles and is influenced by the non-linear power angle relationship. Stability depends on both the initial operating state of the system and the severity of the disturbance. Usually the system is altered so that the post-disturbance steady state operation

differs from that prior to the disturbance. The system is however designed and operated so as to be stable for a selected set of contingencies.

1.3 Voltage Stability and Frequency Stability

It is the ability of power system to maintain steady acceptable voltage at all buses in the system under normal operating conditions and after being subjected to a disturbance. A system enters into a state of voltage instability when a disturbance, increase in load demand, or change in system conditions causes a progressive and uncontrollable drop in voltage. The main factor causing the instability is inability of the power system to meet the demand for reactive power. For purposes of analysis the voltage stability can be classified into two categories, (1) Large disturbance voltage Stability, and (2) Small disturbance voltage stability. Large disturbance voltage stability is concerned with a system's ability to control voltages following large disturbances such as system faults, loss of generation, or circuit contingencies. Small disturbance voltage stability is concerned with a system's ability to control voltages following small perturbations such as incremental change in system load.

Frequency stability is the ability to maintain steady frequency within a nominal range following a disturbance resulting in a significant imbalance between generation and load. Instability that may result occurs in the form of sustained frequency swings leading to tripping of generating units and/or loads. Depends on the ability to restore balance between generation and load of island systems with minimum loss of load and generation. Generally, frequency stability problems are associated with inadequacies in equipment responses, poor coordination of control and protection systems. At present voltage stability and small signal oscillations have appeared as main problem. Increasing steady state stability by high AVR gain is affecting badly the small signal stability.

1.4 State of The Art

With increase in demand and beginning of power markets, the major thrust of interest is in the area of reliable operation of power system. Advancement in VLSI technology and computational facilities has encouraged the utilities to change the old technology. Almost

all the present day generating units are equipped with fast acting voltage regulators. Demello and Concordia [1] have studied the phenomenon of stability as affected by thyristor type excitation system. The basics regarding application of the stabilizing signal to damp the small signal oscillations are given by E.V. Larsen and D.A. Swann [2]. The signal requirements, the potential problems like torsional interaction and noise are addressed in the three part paper [2]. Practical approach to supplementary stabilizing signal from accelerating power is given in [3]. Some alternative method to take care of the mechanical power variations during disturbance are given in [3]. In reference [4], power system stabilizer is applied for enhancement of over all system stability, i.e. not only small signal stability, but also the transient or large signal stability.

All the methods discussed in above references address the problem of PSS tuning based on a Single Machine Infinite Bus (SMIB) analysis, where the generator suffering from oscillations is considered to be connected to a very large system having very high inertia constant. But in practical situations, the controllers of different machines interact with each other during disturbance conditions. So this dynamic interaction has to be considered while tuning the PSS for a particular machine. This leads to analyze the whole stability problem for a multimachine system, where the dynamics of different generators are considered simultaneously. Multimachine PSS tuning considering output feedback and decentralization constraints are studied in [5]-[6]. In reference [7]-[8], the LQR problem is solved for placing the under damped eigen values in a vertical strip. Use of tie line power flow as input for a decentralized controller to stabilize a longitudinal power system is studied in [9]. In 1992 IEEE reviewed the earlier standard for exciter models used for stability studies [10]. This standard also gives detail about the PSS structures used in practice.

With advance in control system, the Conventional PSS (CPSS) can be replaced by intelligent PSS, which can automatically change its parameters as per the situation. In reference [14] Malik et al have coordinated CPSS and Fuzzy Logic PSS (FLPSS). Application of Neural network to prepare the rule base, to tune the FLPSS parameters are given in [13]. In references [15]-[16] Genetic Algorithm (GA) has been applied to optimize the PSS input and output parameters for improvement in system performance.

Implementation of a FLPSS is given in reference [17]. In reference [18], coordination of CPSS and Flexible AC Transmission Systems (FACTS) controller parameters are studied. References [19]-[21] have described the aspect of power system stability in detail. Reference [19] provides ideas regarding modeling of different devices such as generator, exciter, governor system, induction motor, and transformer and transmission lines for stability studies. This also describes PSS tuning for small signal oscillation problems, transient stability analysis, voltage stability analysis and torsional interactions. Reference [20] deals with dynamic stability and control of power systems. The detail modeling of DAE equations describing power system dynamics for both small signal and transient stability analysis is given in [21]. This book also describes the energy function approach for solution of stability problems. In reference [22], fuzzy logic is applied to power system operations, such as Load frequency scheduling, PSS tuning, optimal load flow etc. The practical implementation of Fuzzy logic for all these applications is given in detail. Reference [26] describes application of fuzzy logic to other fields, such as pattern recognition, level control etc.

1.5 Motivation

Kaiga Nuclear Power Plant (NPP) under Nuclear Power Corporation of India Ltd. (NPCIL) has an installed capacity of 2X220 MWe. It is connected to two nearby hydro generators at Kadra and Kudasalli by a single line operating at 220kV, as given in Fig. 1.2.

It is also connected to Guttur 400kV substation with a long line of length 165 km length. One Inter Connecting Transformer (ICT) 220/400 kV is installed at Kaiga and Kaiga-Guttur line operates at 400kV. Earlier this line was operating at 220kV. Both the generators of Kaiga NPP have potential source feed type static exciter [15]. For faster response and to provide higher ceiling voltage during faults, the Automatic Voltage Regulator (AVR) has PID characteristics. The AVR gain and time constant can be varied over wide range of values by selector switches on the field. The generator, exciter, current setting of AVR parameters and other data are given in Appendix-C.

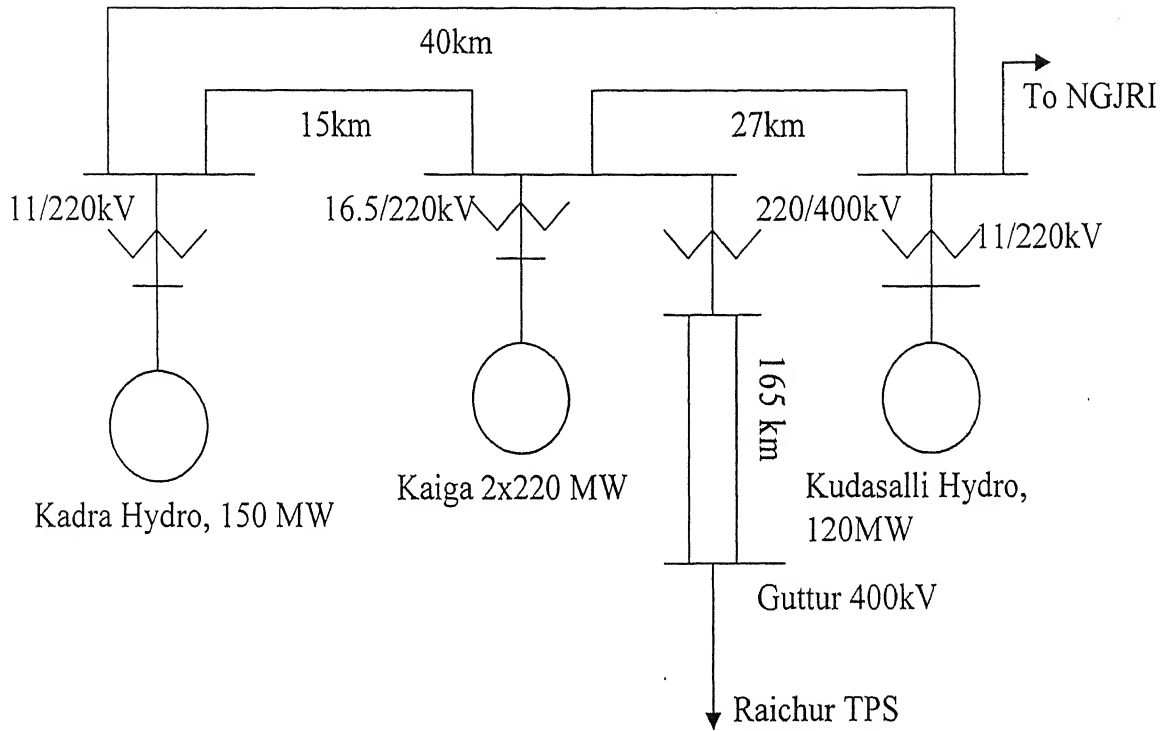


Fig.1.2: Kaiga NPP and nearby generators

The Kaiga generators have experienced severe power oscillations, whenever both generating units are operating and 220kV Kaiga- Kadra and Kaiga-Kudasalli lines are not in operation and power was evacuated through the DC Kaiga-Guttur 220 kV line. The range of observed frequency of oscillation was between 0.8-1.2 Hz. The oscillations, therefore, appear to be in local plant mode. No oscillation was observed in nearby Hydro generators. This indicates that generators at Kaiga are oscillating against a large power system connected through weak transmission line. In view of this it is inferred that PSS on the generators at Kaiga need adjustment to avoid such oscillation. An attempt has been made in this thesis to find out the different reasons for oscillations in the Kaiga generators. Later the existing PSS, which is not functional at present, is tuned to aid in damping these oscillations. All the system data, model and diagram are taken from [27] provided by the manufacturer BHEL.

1.6 Thesis Organization

This thesis has been organized into four parts.

- ❖ Chapter-1 gives a brief idea about system stability. A state of the art in the area of the research work related to stability is described. The problem with Kaiga NPP is defined which is the motivation behind the present work.
- ❖ Chapter-2 discusses the models of different major components of a power system. The differential algebraic equations of the power system are linearized for small signal analysis. Different PSS tuning methods have been described and applied to WSCC 9-bus system and New England 39-bus system.
- ❖ Chapter-3 discusses about the existing AVR and PSS structures at Kaiga NPP. Linearized model of AVR is used along with other DAE equations for eigen value analysis of Kaiga system. Phase and gain plot are found out by an SMIB analysis method. Then PSS is tuned and eigen values were calculated for compensated system.
- ❖ Chapter-4 introduces a new area of PSS design by application of intelligent control system, such as Fuzzy Logic. The basics of FLC design is described in brief. The rule base for different sets of inputs is prescribed. Finally the FLPSS is tuned and system response is observed.

1.7 Paper

1. “*Power System Stabilizer Tuning in Nuclear Power Station: A Case Study of India*”, under preparation for IEEE conference.

Power System Modeling for PSS Tuning

2.1 Introduction

The designing of a large interconnected system to ensure stable operation at minimum cost is a very complex problem. From a control theory point of view, a power system is a very high-order multivariable process, operating in a constantly changing environment. Because of high dimensionality and complexity of the system, it is essential to make simplifying assumptions and to analyze specific problems using the right degree of detail of system representation. This requires a good grasp of the characteristics of the overall system as well as of those of the individual devices. The power system is highly nonlinear and stochastic in nature whose dynamic performance is influenced by a wide array of devices with different response rates and characteristics. Virtually the dynamic behaviour of every major element of the power system has an effect on the system stability. Knowledge of these characteristics is essential for the understanding and study of power system stability. In this chapter, modeling of power system components and power system stabilizers tuning are presented.

2.2 Modeling of Power System Components

For the dynamic study of a system, suitable dynamic model of all the devices should be considered. In case of power system, the dynamics of the system is highly nonlinear because of devices like dynamic loads (mainly induction motor loads), and it is very difficult to predict the system behaviour under all the operating conditions due to varying complexity of the system. In most of the situations, for a change in system conditions, some devices take part to their fullest extent where as some devices have a very little contribution or no contribution at all. Considering this aspect of dynamics we can take these major equipments only with some assumptions to simplify the analysis.

2.2.1 Synchronous Machine

In most of the studies, balanced, symmetrical, three-phase synchronous machine with a field winding and two damper windings on the rotor (2-Axis model or 2.1 model [20]) is considered. Fig. 2.1. shows two-axis (fourth order) model of a synchronous machine with stator transients neglected [21].

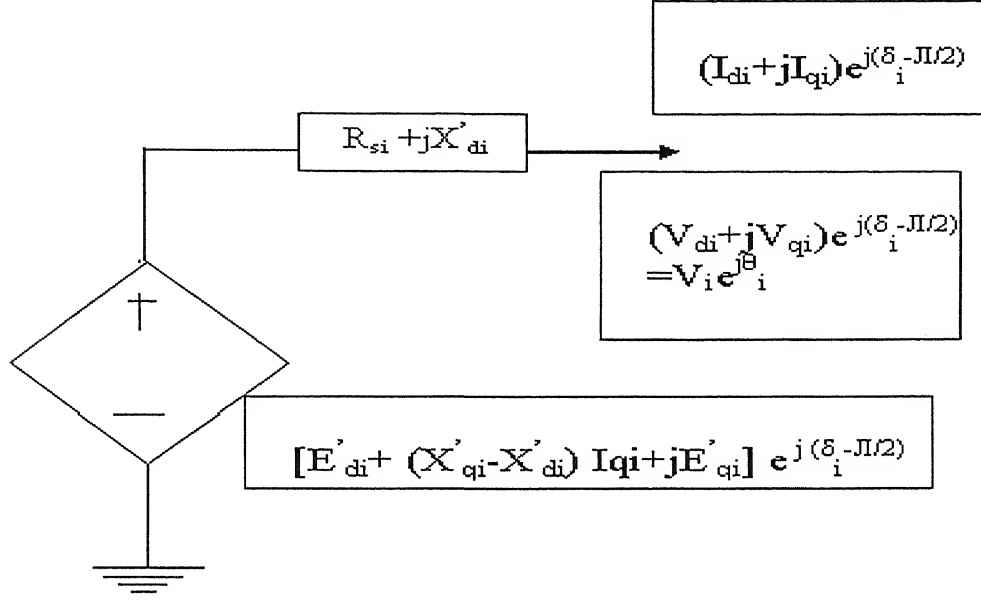


Fig. 2.1: Synchronous machine two-axis model dynamic circuit

The differential equation (in pu) describing the dynamics of m generators of a system is given as:

$$\frac{d\delta_i}{dt} = \omega_i - \omega_s \quad (2.1)$$

$$\frac{d\omega_i}{dt} = \frac{T_{Mi}}{M_i} - \frac{[E'_{qi} - X'_{di}I_{di}]}{M_i}I_{qi} - \frac{[E'_{di} - X'_{qi}I_{qi}]}{M_i}I_{di} - \frac{D_i(\omega_i - \omega_s)}{M_i} \quad (2.2)$$

$$\frac{dE'_{qi}}{dt} = -\frac{E'_{qi}}{T'_{doi}} - \frac{(X_{di} - X'_{di})I_{di}}{T'_{doi}} + \frac{E_{fdi}}{T'_{doi}} \quad (2.3)$$

$$\frac{dE'_{di}}{dt} = -\frac{E'_{di}}{T'_{qoi}} - \frac{(X_{qi} - X'_{qi})I_{qi}}{T'_{qoi}} \quad (2.4)$$

where,

δ = Machine rotor angle with respect to a synchronously rotating frame in degrees

ω = Rotor speed in rad/sec

M = Machine inertia in sec/electrical radian

T_m = Mechanical input torque

E'_q = Voltage across d-axis due to field flux

E'_d = Voltage across q-axis due to damper winding flux across d-axis

I_q = Quadrature axis component of stator current

I_d = Direct axis component component of stator current

X_q = Quadrature axis stator steady state reactance

X_d = Direct axis stator steady state reactance

X'_d = Direct axis stator transient reactance

X'_q = Quadrature axis stator transient reactance

T'_{do} = Direct axis open circuit time constant

T'_{qo} = Quadrature axis open circuit time constant

2.2.2 Exciter Modeling

The physical device that provides the field voltage (E_{fd}) is called exciter. The main function of exciter is to provide sufficient DC power to the field of the synchronous generator for production of field flux linkage. Output of the exciter is nothing but the field voltage of the synchronous machine but proper scaling should be done as the power rating of the two is different [19]. If a synchronous machine is to be useful for a wide range of operating conditions, it should be capable of maintaining constant voltage and frequency. Mechanical input of a machine controls the frequency. For long-term stability studies the dynamics of governor system is to be considered. If it is specified as constant field voltage and mechanical torque input, then it implies that machine does not have voltage and speed (frequency) control.

In steady state, adjustment of field voltage changes the machine terminal voltage. As the field circuit time constant is high (of the order of few seconds), fast control of the field current requires field forcing. Thus exciter should have a high ceiling voltage, which

enables it to operate instantly with voltage levels that are 4 to 5 times the normal value. Depending on the method of power supply to the exciter, the exciters can be categorized as:

- DC excitation system which uses DC generator with brushes and slip rings, driven by main shaft.
- AC excitation system, which uses either an inverted AC generator (brushless) driven off the main shaft with rotating rectifier or an AC generator with a static rectifier to produce DC power.
- Static exciter, such as AC-DC converter in which power is supplied from the synchronous machine or auxiliary power.

E_{fd} normally is not controlled directly, but it is changed through the actuation of the exciter or pilot exciter. The main exciter may have a pilot exciter that provides the means for changing the output of the main exciter. In order to automatically control terminal voltage, a transducer signal must be compared to a reference voltage and amplified to produce the exciter input (V_R). This amplifier comprises the Automatic Voltage Regulator (AVR). The amplifier can be a pilot exciter (another DC generator) or a solid state control. If the voltage input to the AVR amplifier is simply the error voltage produced by the difference between a reference voltage and a conditioned potential transformer connected to the synchronous machine terminals, the closed loop control system may exhibit instabilities. In any standard excitation system this is accomplished through a stabilizing transformer whose input is connected to the output of the exciter and whose output is subtracted from the amplifier input. This feed back stabilization is a part of AVR loop. In case of rotating type of exciters (the first two of the above classification) the relationship between the exciter voltage and current is non-linear because of saturation of the exciter iron. This is taken into account by a proper saturation function which varies as the field voltage E_{fd} represented as $S_E (E_{fd})$ as shown in Fig. 2.2. This function is mainly taken as exponential function [19].

In literature the most commonly used exciter is IEEE - 1 [21] exciter. It essentially represents a DC exciter, with some modifications can also be used for representing static exciter. The regulator output V_R is limited which also imposes limit on E_{fd} . Usually the latter are usually specified and the former can be found from the dynamic equations applying the

steady state conditions. The dynamic equations of IEEE type-1 exciter of i^{th} generator are given as:

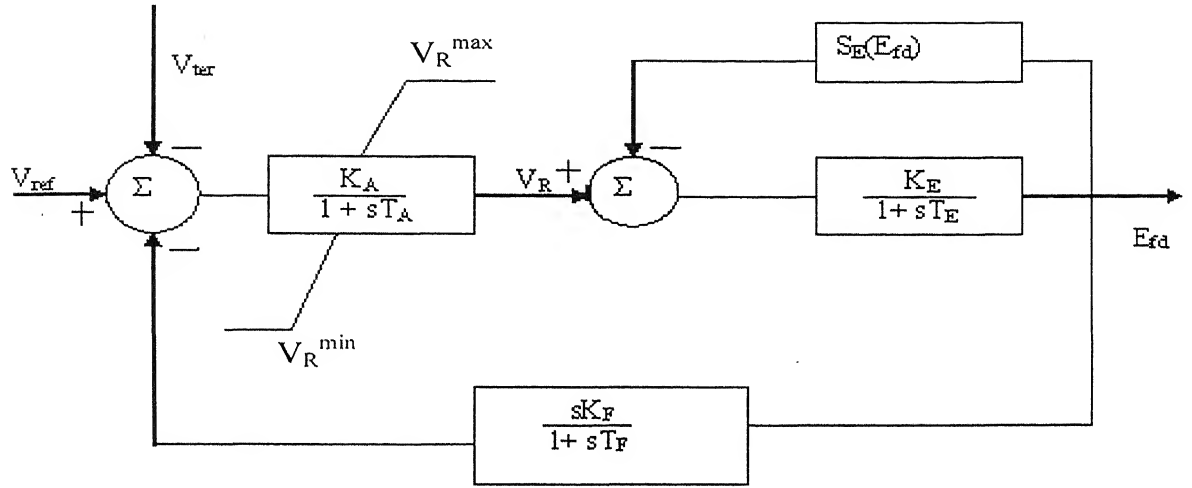


Fig. 2.2: IEEE Type-1 exciter model

$$\frac{dE_{fdi}}{dt} = -\frac{K_{Ei} + S_{Ei}(E_{fdi})E_{fdi}}{T_{Ei}} + \frac{V_{Ri}}{T_{Ei}} \quad (2.5)$$

$$\frac{dV_{Ri}}{dt} = -\frac{V_{Ri}}{T_{Ai}} + \frac{K_{Ai}}{T_{Ai}} R_{fi} - \frac{K_{Ai} K_{Fi}}{T_{Ai} T_{Fi}} E_{fdi} + \frac{K_{Ai}}{T_{Ai}} (V_{refi} - V_i) \quad (2.6)$$

$$\frac{dR_{fi}}{dt} = -\frac{R_{fi}}{T_{Fi}} + \frac{K_{Fi}}{(T_{Fi})^2} E_{fdi} \quad (2.7)$$

where,

T_E = Exciter time constant in Second

K_E = Exciter gain

V_R = Regulator output,

V_R^{max} = Maximum value of regulator output in PU

V_R^{min} = Minimum value of regulator output in PU

T_A = Regulator amplifier time constant

K_A = Regulator gain

R_f = Rate feedback in PU

T_F = Feedback circuit time constant, sec

K_F = Feedback circuit gain

2.3 Complete Differential-Algebraic Equations

The two-axis model equations are rewritten after neglecting the sub-transient reactances and saturation. The turbine and governor dynamics are also neglected resulting in constant T_{Mi} . The limit constraints on V_{Ri} (AVR output) are also deleted, since the objective is to simplify the system for modeling and simulation. A linear damping torque is assumed, that is, $T_{FWi} = D_i (\omega_i - \omega_s)$. The resulting Differential Algebraic Equations (DAE Eqs) for an ***m-machine, n-bus*** system with the IEEE-type I exciters are given as follows:

1. Differential Equations for i^{th} machine is

$$\frac{d\delta_i}{dt} = \omega_i - \omega_s \quad (2.8)$$

$$\frac{d\omega_i}{dt} = \frac{T_{Mi}}{M_i} - \frac{[E_{qi}' - X_{di}' I_{di}]}{M_i} I_{qi} - \frac{[E_{di}' - X_{qi}' I_{qi}]}{M_i} I_{di} - \frac{D_i (\omega_i - \omega_s)}{M_i} \quad (2.9)$$

$$\frac{dE_{qi}'}{dt} = -\frac{E_{qi}'}{T_{doi}'} - \frac{(X_{di} - X_{di}') I_{di}}{T_{doi}'} + \frac{E_{fdi}}{T_{doi}'} \quad (2.10)$$

$$\frac{dE_{di}'}{dt} = -\frac{E_{di}'}{T_{qoi}'} - \frac{(X_{qi} - X_{qi}') I_{qi}}{T_{qoi}'} \quad (2.11)$$

$$\frac{dE_{fdi}}{dt} = -\frac{K_{Ei} + S_{Ei}(E_{fdi}) E_{fdi}}{T_{Ei}} + \frac{V_{Ri}}{T_{Ei}} \quad (2.12)$$

$$\frac{dV_{Ri}}{dt} = -\frac{V_{Ri}}{T_{Ai}} + \frac{K_{Ai}}{T_{Ai}} R_{fi} - \frac{K_{Ai} K_{Fi}}{T_{Ai} T_{Fi}} E_{fdi} + \frac{K_{Ai}}{T_{Ai}} (V_{refi} - V_i) \quad (2.13)$$

$$\frac{dR_{fi}}{dt} = -\frac{R_{fi}}{T_{Fi}} + \frac{K_{Fi}}{(T_{Fi})^2} E_{fdi} \quad (2.14)$$

2. Algebraic Equations

The algebraic equations consist of the stator algebraic equations and network equations. The stator algebraic equations directly follow from Fig. 2.1, applying Kirchhoff's Voltage Law (KVL). A phasor diagram pertaining to universal rotating frame and local machine is given in Fig. 2.3.

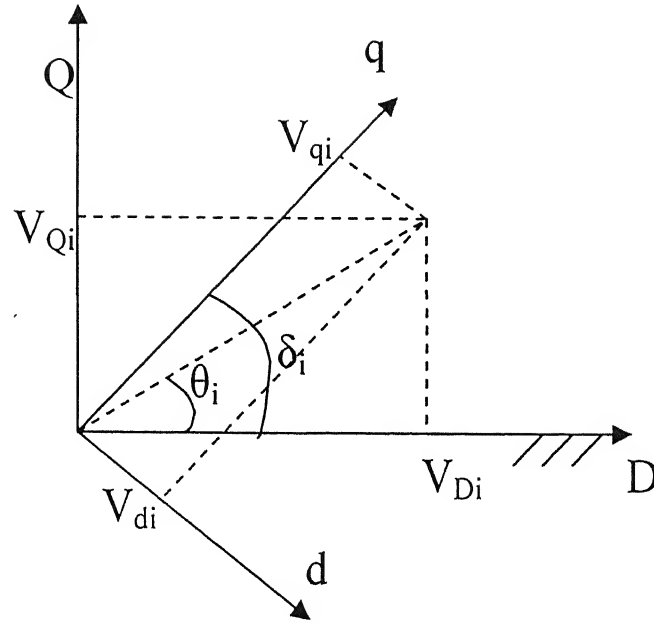


Fig 2.3: Phasor diagram for universal rotating frame

(a) Stator Algebraic Equations for i^{th} machine, it is

$$E'_{di} - V_i \sin(\delta_i - \theta_i) - R_{Si} I_{di} - X'_{qi} I_{qi} = 0$$

$$E'_{qi} - V_i \cos(\delta_i - \theta_i) - R_{Si} I_{qi} - X'_{di} I_{di} = 0 \quad (2.15)$$

(b) Network Equations

Network equations corresponding to Fig. 2.4 are given as

For Generator buses:

$$V_i e^{j\theta} (I_{di} - jI_{qi}) e^{-j(\delta_i - \pi/2)} + P_{Li}(V_i) + jQ_{Li}(V_i) = \sum_{k=1}^n V_i V_k Y_{ik} e^{j(\theta_i - \theta_k - \alpha_{ik})} \quad (2.16)$$

$$i=1, \dots, m$$

For load Buses:

$$P_{Li}(V_i) + jQ_{Li}(V_i) = \sum_{k=1}^n V_i V_k Y_{ik} e^{j(\theta_i - \theta_k - \alpha_{ik})} \quad (2.17)$$

$$i=m+1, \dots, n$$

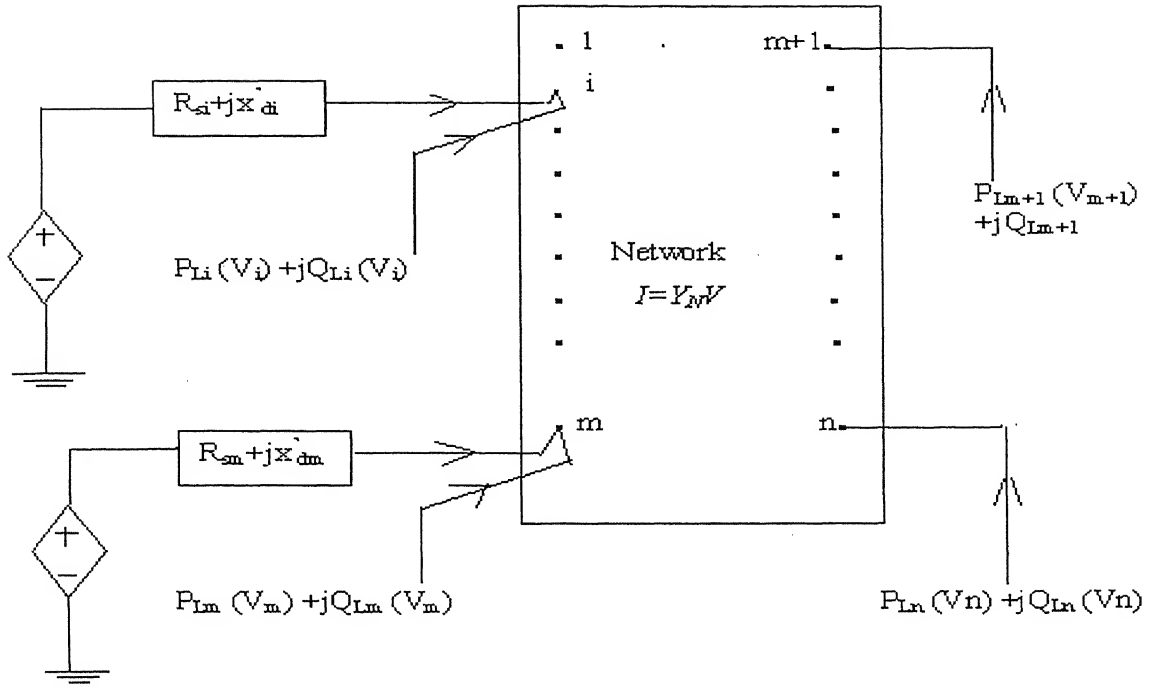


Fig 2.4: Interconnection of synchronous machine dynamic circuit and the rest of the network

In eq. (2.17) $V_i e^{j\theta_i} (I_{di} - jI_{qi}) e^{-j(\delta_i - \pi/2)} = P_{Gi} + jQ_{Gi}$ is the complex power “injected” into bus i due to generator. So Eq. (2.16) and (2.17) are only the real and reactive power balance equations at all the n -buses. Power balance equation at the generator buses shows the interaction of the state variables.

Functionally the differential equations Eqs (2.8) - (2.14), together with stator algebraic equation, Eq.(2.15). and the network equations Eqs. (2.16)- (2.17) form a set of differential algebraic equations (DAE) of the form:

$$\dot{x} = f(x, y, u) \quad (2.18)$$

$$0 = g(x, y) \quad (2.19)$$

With, $x = [x_1', x_2', \dots, x_m']^T$ as the state vector, where $x_i = [E_{qi}', E_{di}', \delta_i, \omega_i, E_{fdi}', R_{fi}', V_{Ri}']$, $y = [I_{d-q}', V', \theta']^T$ as the set of algebraic variables where $I_{d-q} = [I_{d1}', I_{q1}', \dots, I_{dm}', I_{qm}']$, and $V = [V_1, \dots, V_n]^T$, $\theta = [\theta_1, \dots, \theta_n]^T$.

As the network and stator transients are neglected, the current variables are of less important. For stability analysis, they are expressed in terms of the state and network variables. Either polar form or rectangular form can be used [21]. The network equations (2.16) and (2.17) are written in power balance form. They can also be expressed in current

balance form ($I=Y_N V$ where Y_N is $N \times N$ admittance matrix of the network). In transient stability analysis Y_N is reduced from the standard load flow admittance matrix to take into account the machine internal reactance, and also the loads are represented as constant admittance type and included in reduced admittance matrix. This reduces the computational time and simplifies the analysis [21].

2.4 System Linearization

Linearized analysis of multi machine power system is necessary for the study of both steady state and voltage stability. The DAE equations Eqs. (2.8)- (2.19) are linearized for analysis of low frequency oscillatory stability of the system. Two kinds of analysis are possible, viz

(1) A multi machine linearized analysis that computes the eigen values and also finds those machines that contribute to a particular eigen value (participation factor analysis[]). Both local and inter area oscillations can be studied in such a framework.

(2) A Single Machine Infinite Bus (SMIB) system case that investigates only local oscillations.

Considering the participation of the generators in the oscillatory modes the site for PSS installations can be determined. The linearized analysis of the system is the basis for the designing of PSS for the machines [2].

Considering Eqs (2.18) and (2.19), the vector y includes both the I_{d-q} and V vectors. Thus, Eq (2.18) is of dimension $7m$, and Eq (2.19) is of dimension $2(n+m)$. To show explicitly the traditional load-flow equations and the other algebraic equations, y is partitioned as

$$Y = [I_{d-q}^T \theta_1 V_1 \dots \dots V_m | \theta_2 \dots \dots \theta_n V_{m+1} \dots \dots V_n]^T$$

$$= [y_a^T | y_b^T]^T \quad (2.20)$$

Here, the vector y_b corresponds to the load-flow variables and the vector y_a correspond to the other algebraic variables. Bus 1 is taken as the slack bus and buses 2,, m are the PV buses and $m+1, \dots \dots, n$ are PQ buses. The dimension of x is $7m$. Linearizing Eq(2.18) about a steady state operating point gives

$$\Delta \dot{x} = A\Delta x + B\Delta y + E\Delta u \quad (2.21)$$

$$0 = C\Delta x + D\Delta y \quad (2.22)$$

where,

$$\begin{aligned} A &= \left[\frac{\delta f}{\delta x} \right]_{(x_0, y_0, u_0)} & B &= \left[\frac{\delta f}{\delta y} \right]_{(x_0, y_0, u_0)} & C &= \left[\frac{\delta f}{\delta x} \right]_{(x_0, y_0, u_0)} \\ D &= \left[\frac{\delta g}{\delta y} \right]_{(x_0, y_0, u_0)} & E &= \left[\frac{\delta f}{\delta u} \right]_{(x_0, y_0, u_0)} \end{aligned} \quad (2.23)$$

The DAE equations can be expressed as

$$\begin{bmatrix} \Delta \dot{x} \\ 0 \end{bmatrix} = \begin{bmatrix} A & B \\ C & D \end{bmatrix} \begin{bmatrix} \Delta x \\ \Delta y \end{bmatrix} + \begin{bmatrix} E \\ 0 \end{bmatrix} \Delta u \quad (2.24)$$

Matrix D is called the network algebraic jacobian [20], the system matrix (A_{sys}) is obtained after rearranging the algebraic variables [20].

$$\Delta \dot{x} = A_{sys} \Delta x + E \Delta u \quad (2.25)$$

where,

$$A_{sys} = A - BD^{-1}C \quad (2.26)$$

The jacobian matrix gives the eigen values of the system for a small disturbance about the steady state operating point. The system is unstable if some of the eigen values lie in the right half of s-plane. For a weak system with increase in loading, the eigen values move towards the right half of s-plane [2], and after a particular critical value of loading the system becomes unstable. Also in some cases, the eigen value analysis shows that though the system is stable at steady state but for small disturbances the system starts oscillations. Oscillations in a system are undesirable as it affects the power transfer limit and also some cases sustained oscillation may lead to system instability. These small frequency oscillations are mainly because of fast acting voltage regulators and weak transmission lines (long lines). PSS is, thus, provided to damp out the oscillations in the system as described in chapter-1.

2.5 Power System Stability and Power System Stabilizer

Power System Stabilizer (PSS) is a supplementary control device to extend stability limits by modulating generator excitation to provide damping to the oscillations of synchronous machine rotors relative to one another. These oscillations of concern typically occur in the frequency range of approximately 0.2 to 2.5 Hz [19-21], and insufficient damping of these oscillations may limit the ability to transmit power. To provide damping, the stabilizer must produce a component of electrical torque on the rotor which is in phase with speed deviation [2]. For this PSS uses the as input the auxiliary signals which are derived from generator speed or electrical power output or field voltage etc [20]. The art and science of applying power system stabilizers have developed considerably, which involve the use of various tuning procedures and input signals, and learning to deal with practical problems such as noise and interaction with turbine generator shaft torsional modes of oscillation [2]. The implementation details differ depending upon the stabilizer input signal employed. However, for any input signal the stabilizer must compensate for the gain and phase characteristics of the excitation system, the generator and the power system which collectively determine the transfer function from the stabilizer output to the component of electrical torque which can be modulated by excitation control [19]. This transfer function which can be denoted as $GEP(s)$ is strongly influenced by voltage regulator gain, generator power level, and AC system strength.

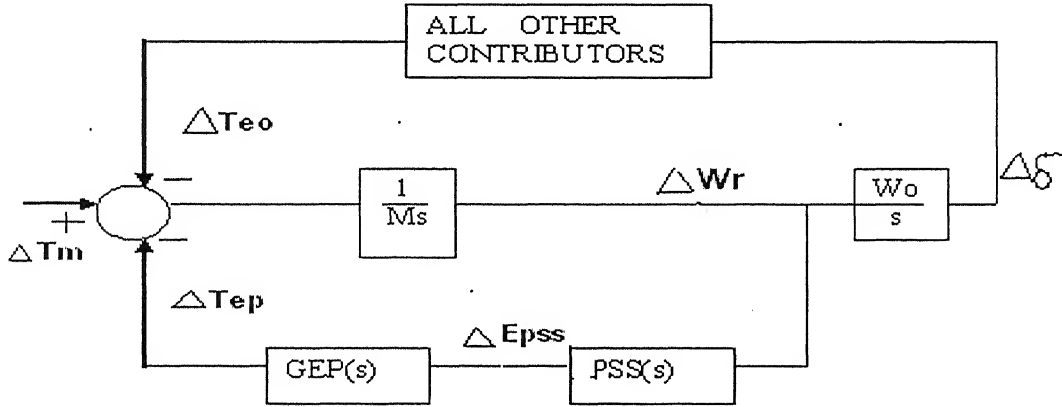


Fig. 2.5: Stabilizer with speed input-system block diagram

The block diagram in Fig. 2.5 illustrates, in terms of a few basic small-signal transfer function blocks, the relationship between the applied torque on the turbine-generator shaft

and the resulting generator rotor speed, ω_G and rotor angular displacement δ . The electrical torque may be considered to have two components, (a) that which is produced by the power system stabilizer solely by modulation of the generator flux, T_{ep} , and (b) that which results from all other sources including shaft motion, T_{eo} . The functional block relationship between speed and torque is shown for a stabilizer employing speed as an input signal. The contribution of torque due to the stabilizer path is given by:

$$\frac{\Delta T_{ep}}{\Delta \omega_G} = PSS_{\omega}(s) * GEP(s)$$

The transfer function $GEP(s)$ represents the characteristics of the Generator, the Exciter, and the Power system. The variation of $GEP(s)$ with exciter gain, generator loading, and ac system strength plays a dominant role in power system stabilizer tuning requirements and performance. The basic characteristics of this plant which are significant to stabilizer applications are as follows [2]:

- The phase characteristics of $GEP(s)$ are nearly identical to phase characteristics of closed loop voltage regulator.
- The gain of $GEP(s)$ increases with generator load.
- The gain of $GEP(s)$ increases as the ac system becomes stronger. This effect is amplified with high gain regulator.

A properly tuned PSS must provide the necessary positive damping torque over a wide range of operating condition and disturbance to cancel the negative torque introduced by various sources [1]. The overall excitation control system (Exciter, AVR, PSS and other Limiters) is designed so as to [4]

- Maximize the damping of the local plant mode as well as the inter area mode oscillations without compromising the stability of other modes.
- Enhance the system transient stability.
- Minimize the consequences of excitation system malfunction due to component failures.

2.6 PSS Structure

The block diagram of PSS, which is commonly used for analysis purposes, is given in Fig. 2.6. The PSS can be single input type or dual input type [10]. In case of dual input type, the blocks of PSS remain same for both of the inputs, only block parameters vary. The function of each block is given below.

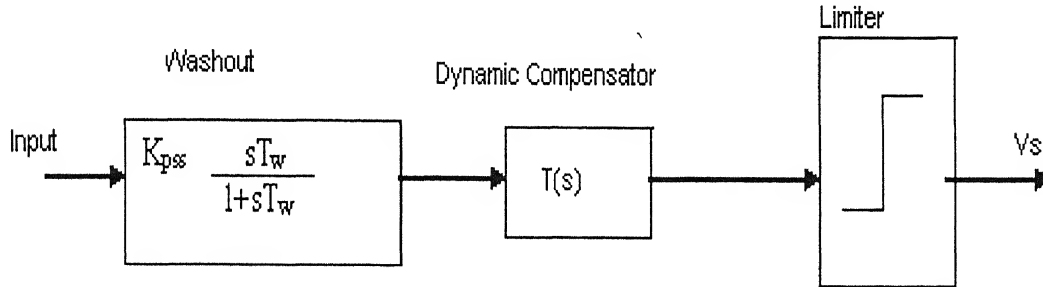


Fig. 2.6: PSS block diagram

1. Washout Circuit

The washout circuit is provided to eliminate steady state bias in the output of PSS, which will modify the generator terminal voltage. The PSS is expected to respond only to transient variations in the input signal and not the DC offsets in the signal. This is achieved by subtracting from it the low frequency component of the signal obtained by passing the signal through a low pass filter.

The washout circuit acts essentially as a high pass filter and it must pass all frequencies that are of interest. If only the local modes are of interest, the time constant T_w can be chosen in the range of 1 to 2 second. However if interarea modes are also to be damped, then T_w can be chosen in the range of 10 to 20 second. There is noticeable improvement in first swing stability when T_w is increased from 1.5 to 10.

2. Dynamic Compensator

The dynamic compensator used in practice is made up of multiple stages lead-lag compensators. A two stage lead-lag compensator has the following transfer function.

$$T(s) = \frac{K s (1 + sT_1)(1 + sT_2)}{(1 + sT_3)(1 + sT_4)} \quad (2.27)$$

where K_S is the gain of PSS. The time constants T_1 to T_4 are chosen to provide a phase lead to the signal in the range of frequencies that are of interest (0.1 to 3 Hz). With static exciters, only one lead-lag stage may be necessary. In general, the dynamic compensator can be chosen with the following transfer function.

$$T(s) = \frac{K_S N(s)}{D(s)} \quad (2.28)$$

where,

$$\begin{aligned} N(s) &= 1 + a_1s + a_2s^2 + \dots + a_ns^n \\ D(s) &= 1 + b_1s + b_2s^2 + \dots + b_ps^p \end{aligned} \quad (2.29)$$

The zeros of $D(s)$ should lie in the left half of s-plane. They can be complex or real. Some of the zeros of $N(s)$ can lie in the right half of s-plane making it a non-minimum phase system. For design purposes, PSS transfer function is approximated to $T(s)$, the transfer function of the dynamic compensator. The effect of washout filter can be neglected in the design, but must be considered in evaluating performance of PSS under various operating conditions.

3. Limiter

The output of the PSS must be limited to prevent the PSS action to encounter the action of AVR. For example, when load rejection takes place, the AVR acts to reduce the terminal voltage whereas PSS action calls for higher value of terminal voltage. It may even be desirable to block the PSS action in case of load rejection. The negative limit of PSS output is of importance during the back swing of rotor. The AVR action is required to maintain the voltage after angular separation has increased PSS action in the negative direction must be curtailed more than that in the positive direction. Ontario hydro uses a -0.05 p.u as the low limit and 0.1 to 0.3 as the higher limit [2].

4. Control Input

The most commonly used and the obvious choice is deviation in the rotor angular speed. However, for practical implementations other signals such as bus frequency, electrical power, acceleration power and field voltage etc are also used [2]-[4].

2.7 Multi Machine PSS Tuning

In case of PSS tuning considering SMIB model, the dynamic interaction between generators is not considered. This approach is sufficient when local mode of oscillation is of major concern. But when both local and inter area modes are considered, SMIB methods may not be sufficient. In usual practice PSS is tuned for local oscillations and when it is put into operation, the parameters are again adjusted depending on the oscillations with respect to other generators [21]. In case of multi machine PSS tuning methods, dynamic interactions between the generators are considered. This method is also called as coordinated calculation of PSS parameters. It is not necessary that all the machines will have the PSS; this method can also be applied when some of the generators are tuned for PSS depending upon the participation in oscillations.

2.7.1 Co-ordination of Power System Stabilizer Parameters

This is called co-ordination method because the PSS parameters for all the machines are determined simultaneously. For a PSS with two lead-lag stages the PSS transfer function $G_{pss}(s)$ for a single input signal is given as

$$G_{pss}(s) = \frac{K_i(1+sT_i)(1+sT_j)}{(1+sT_2)(1+sT_4)} \quad (2.30)$$

where i and j are defined according to the signal used as input to the stabilizer, time constants T_2 and T_4 are assumed known, and the washout time constant T_w will be considered in all cases to be equal to 10.0 second. The right hand side of (2.30) can be written as

$$G_{PSS}(s) = d + \frac{\beta_1 s + \beta_0}{s^2 + \alpha_1 s + \alpha_0} \quad (2.31)$$

where,

$$\alpha_1 = \frac{T_3 + T_4}{T_2 T_4}; \alpha_0 = \frac{1}{T_2 T_4}; d = \frac{K_i T_i T_j}{T_2 T_4}$$

$$\beta_0 = \frac{K_i}{T_2 T_4} (1 - \frac{T_i T_j}{T_2 T_4}) ; \beta_1 = \frac{K_i}{T_2 T_4} [T_i + T_j - \frac{T_i T_j}{T_2 T_4} (T_2 + T_4)] \quad (2.32)$$

An adequate state space representation for $G_{PSS}(s)$ can be obtained by using the observable canonical form as

$$\dot{X}_c = A_c x_c + B_c u_c \quad (2.33)$$

$$y_c = C_c x_c + D_c u_c \quad (2.34)$$

where

$$A_c = \begin{bmatrix} 0 & -\alpha_0 \\ 1 & -\alpha_1 \end{bmatrix}, B_c = \begin{bmatrix} \beta_0 \\ \beta_1 \end{bmatrix}, C_c = [0 \ 1], D_c = d \quad (2.35)$$

For the machine with a dual input PSS, $G_{pss}(s)$ will be a 1 x 2 transfer function matrix of the form:

$$G_{PSS}(s) = [G_1(s) \ G_2(s)] \quad (2.36)$$

Where $G_1(s)$ and $G_2(s)$ have the structure as given in equation (2.31). The time constants T_2 and T_4 are considered to be the same for both signals. This means that matrices A_c and C_c will be the same. Matrices B_c and D_c on the other hand, are augmented with a new column corresponding to the added input signal.

2.7.2 Determination of Coordinated PSS Parameters

In literature many methods are available for simultaneous tuning of PSSs. In this thesis two methods are used for this purpose.

2.7.2.1 Determination via Structurally Constrained Optimal Control [5], [6]

PSS parameters can be obtained by using optimal controller design approach for a large power system. But these methods suffer from the disadvantage of needing the measurement and transmission of a large number of variables. This is a serious drawback concerning practical aspects. Again it can not be designed as a state feedback controller as all the states are not measurable especially in the case of power system. Constraints like output feedback (only measurable states are used) and decentralization (only local states are used) are of particular interest.

The PSS design problem consists of determining the parameters of the $G_{PSS}(s)$ transfer function so that eigen values of the compensated system are sufficiently stable. With T_2 and T_4 known, the only parameters which remain to be calculated are the PSS gain K_i and the lead-lag time parameters T_i and T_j .

Let the linear state space model of the power system without compensation is given as [5], [19]-[21]:

$$\dot{x} = A x + B u \quad (2.37)$$

$$y = C x \quad (2.38)$$

Compensating the system with the controller given by the Eq. (2.33) and (2.34) in feedback connections implies that $u_c = y$ and $u = y_c$. The resulting composite system is then represented as:

$$\dot{x} = (A + B D_c C) x + B C_c x_c \quad (2.39)$$

$$\dot{x}_c = (A + B D_c C) x + B C_c x_c \quad (2.40)$$

Defining $X_a \equiv [x^T, x_c^T]^T$ as the augmented state vector, Eqs (2.37) – (2.40) become

$$\dot{x}_a = \begin{bmatrix} A + B D_c C & B C_c \\ B C_c C & A_c \end{bmatrix} x_a \quad (2.41)$$

If in addition, we define a 3 x 1 augmented control vector u_a , it can be easily verified that Eq.2.23 can be rewritten as

$$\dot{x}_a = (A_a - B_a G_a C_a) x_a = A_c x_a \quad (2.42)$$

where,

$$A_a = \begin{bmatrix} A & B C_c \\ 0 & A_c \end{bmatrix}, B_a = \begin{bmatrix} B & 0 \\ 0 & I \end{bmatrix}, C_a = [C \quad 0] \quad (2.43)$$

$$G_a^T = \begin{bmatrix} -D_c^T & -B_c^T \end{bmatrix}$$

From the above equations, following informations can be inferred

- Matrices A_a , B_a , and C_a are completely known as these consist terms T_2 and T_4 . The unknown parameters (β_0 , β_1 and d , which depend on K_i , T_i and T_j) appear only in matrix G_a .
- Eq. (2.24) exhibits the form of a *constant-output feedback problem*, where the (fictitious) process to be compensated is described by matrices A_a , B_a , and C_a , and G_a is a constant output feedback matrix to be determined so that $u_a = -G_a y_a$, where $y_a = C_a x_a$.
- Several methods can be used to determine the output feedback matrix G_a , such as pole placement via output feedback or optimal output feedback, the later approach is preferred.
- Some practical aspects of the multi machine problem impose further constraints on the control strategies. In fact, the conventional PSSs use signals derived from locally measurable quantities such as rotor speed, AC bus frequency or electric power. The use of cross feedback among the distinct machines, although theoretically desirable, poses practical difficulties. In a typical power system exhibiting dynamic stability problems, the power plants may be located hundreds of kilometers apart from each other. But the approach to process the information from different subsystems in order to tune PSS requires fairly sophisticated data transmission and coordination schemes. However, conventional PSS without using any cross-feedback can be tuned yielding good damping for all the modes. In order to achieve that, proper structural constraints like output feedback and decentralization are considered.

With the system to be controlled given by Eqs.(2.37) –(2.38) , the objective is to determine the control strategy that minimizes the quadratic performance index:

$$j(x_a, u_a) = \frac{1}{2} \int (x_a^T Q x_a + u_a^T R u_a) dt \quad (2.44)$$

where the positive semidefinite matrix Q and the positive definite matrix R are state and input weighting matrices respectively. This is the so-called linear quadratic regulator (LQR) problem [] and its well known solution is given by the state feedback strategy:

$$u_a^* = -K^* x_a \quad (2.45)$$

where, $K^* = R^{-1} B_a^T P$, and P is the solution of the Algebraic Riccati Equation (ARE)

$$A_a^T P + P A_a - P B_a R^{-1} B_a^T P + Q = 0 \quad (2.46)$$

The above solution takes into account the whole system dynamics, as described, but it is again impractical concerning power system applications, since it prescribes feedback of all the state parameters to the entire input terminal.

Applying the output feedback constraint, the control strategy can be expressed as:

$$u_a = -G_a y_a = -G_a C_a x_a \quad (2.47)$$

That is, only the measured outputs are used to synthesize the system input. Comparing this with Eq. (2.45) by imposing the output feedback constraint on the conventional feedback strategy is tantamount the following equation for G_a :

$$K^* = G_a C_a \quad (2.48)$$

Since above equation implies that $C_a^T G_a^T = K^{*T}$, matrix G_a^T can be obtained by using the concept of matrix pseudo inverse, applied to matrix C_a^T . It can, thus, be easily shown that the output feedback gain matrix is given by

$$G_a = K^* C_a^T (C_a C_a^T)^{-1} \quad (2.49)$$

As K matrix is not a full matrix, the pseudo inverse is taken, for which, this method is called “Pseudo decentralization method”

Now applying the decentralization constraint that is only the local states are fed back to the local inputs. It is easy to see that the decentralization constraint imposes a block diagonal structure on the state feedback matrix K . Therefore, the decentralized can be expressed as:

$$K\text{-Block diagonal } \{K_1 K_2 K_3 \dots K_N\} = 0 \quad (2.50)$$

The generalized ARE considering both the constraints (output feedback and decentralization) is given as

$$A_a^T P + P A_a - P B_a R^{-1} B_a^T P + Q + L^T R L = 0 \quad (2.51)$$

where L matrix takes into account the two constraints and determined using in iterative process. The multiplying factors selection is quite arbitrary so also selection of weighting matrices Q and R . Initially P is calculated by solving the generalized ARE and using this value, K is calculated. From K matrix, G_a is calculated. Knowing the G_a matrix the block diagonal elements give the PSS settings, K_i , T_i and T_j

2.7.2.2 Determination by Strip Eigen Value Assignment Method [7], [8]

The problem with the pseudo decentralization method is that the weighting matrices Q and R are selected arbitrarily. In some literature [6], they are taken as identity matrices. In this case, the PSS gives good damping for a particular operating condition only. But for some other loading conditions the PSS puts adverse effect on the eigen values, some become negative also. Proper weighting matrix selection takes a large time which is not suitable for real time application. Some literatures [6] have taken R as an identity matrix and values of diagonal elements of Q depending upon the damping of that particular mode. Here we have tried with giving weight to all the modes arbitrarily which leads to an optimal setting for many operating conditions.

In the strip eigen value assignment method there is no need to define the Q matrix at any stage. A linear quadratic controller is designed such that the optimal closed-loop system has eigen values lie within a vertical strip in complex s-plane [8]. The desired position of eigen values is obtained without any convergence problem.

Let (A, B) be the pair of the open-loop system matrices in the system Eq. (2.37) and $h(\geq 0)$ represents the prescribed degree of relative stability. Then the closed loop system matrix $A_c = A - BR^{-1}B^T P$ has all the eigen values lying on the left side of the $-h$ vertical line as shown in Fig. 2.7 where matrix P is the solution of ARE

$$(A + hI_n)^T P + P (A + hI_n) - P B R^{-1} B^T P + Q = 0_n \quad (2.52)$$

With $Q = 0_n$, the unstable modes of $A + hI_n$ are shifted to their mirror image positions with respect to $-h$ vertical line, which are the eigenvalues of the closed loop system matrix A_c .

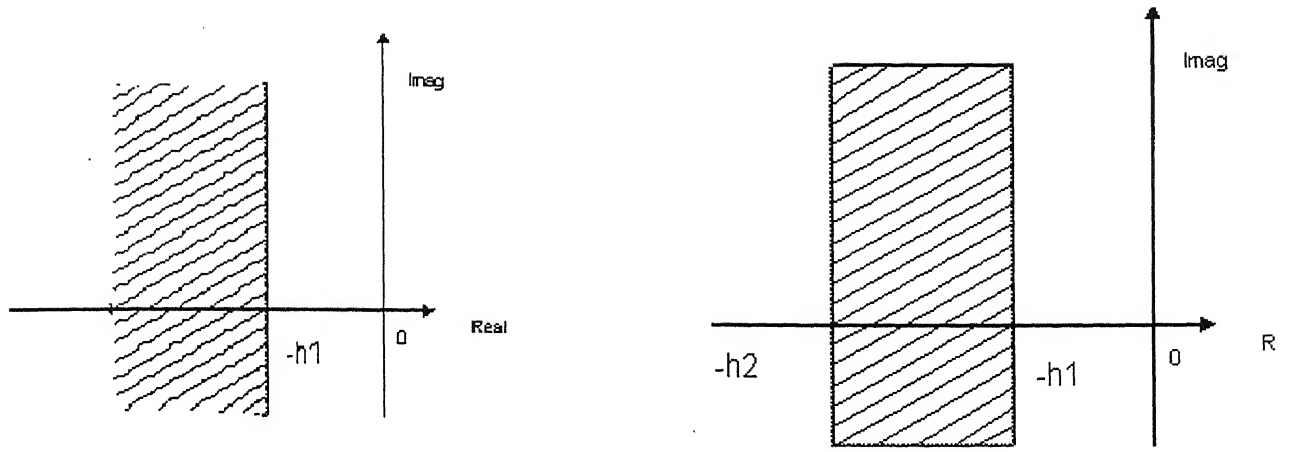


Fig. 2.7: (a) single vertical line

(b) vertical strip

Assume that h_1 and h_2 are two positive real values to determine an open vertical strip of $[-h_2, -h_1]$ on the negative real axis as shown in Fig. 2.7 and given as an $n \times n$ matrix $A_1 = A + h_1 I$. The control law is changed to be

$$u(t) = -\rho Fx(t) \quad (2.53)$$

With the feedback gain $F = R^{-1}B^T P$. The matrix P is the solution of the following modified ARE:

$$A_1^T P + P A_1 - P B R^{-1} B^T P = 0_n \quad (2.54)$$

The gain ρ is selected by

$$\rho = 0.5 + \frac{h_2 - h_1}{2 \text{tr}(A_1)} = 0.5 + \frac{h_2 - h_1}{\text{tr}(B \cdot F)} \quad (2.55)$$

where trace (A_1) are the eigen values of A_1 in the right half of the complex s-plane.

The final closed loop system consists of a set of eigen values which lie inside the vertical strip of $[-h_2, -h_1]$. Here we can assume the matrix R to be a unity matrix. Thus solving the ARE does not require Q matrix.

2.8 Results and Discussions

The pseudo decentralization method and the strip eigen value placement method have been implemented on WSCC 3-machine, 9-bus system and New England 39-bus system.

Though, the objective is to tune PSS for NPC system, the standard systems were tested for the verification of proposed methods. The line diagram and the system data are given in appendix[1]. MATLAB® is used for all the analysis purposes

Initially the base case parameters were found out for the given operating and loading conditions. After linearization of the DAE equations around the base case points the eigen values were calculated using the code developed in MATLAB®. Other parameters such as damping ratio, frequency of damped and undamped oscillations, and the participation factors were calculated. Participation factors decide the location of PSS. Then PSS was considered and the new eigen values were calculated. The zero eigen values appearing in the analysis are called as redundant eigen values. This is because there is no infinite bus, so the angles are relative angles and the machine inherent damping is taken as zero [19], [21].

2.8.1 WSCC 9-bus System

WSCC system consists of three generators. Bus 1 is considered as infinite or swing bus for all the calculations. The generators are equipped with rotating type exciters. The rate stabilizer, AVR amplifier and exciter were considered in detail with the exponential saturation function [19]. The participation factor analysis shows that generator two and three are participating maximum in the critical mode shown in Table 2.1. The position of eigen values in s-plane are shown in Fig. 2.1. So PSS were placed at generators 2 and 3. The eigen value after inclusion of PSS shows improvement in system damping. Table 2.2 shows the eigen values after placing PSS at generators 2 and 3 using pseudo decentralization method. The eigen values with strip pole placement method after putting PSS at generators 2 and 3 is given in Table 2.3. As the objective is only to test the proposed method non-linear simulation was not done for the WSCC system. Both Pseudo decentralization and strip eigen value assignment methods are tested. Figs 2.10 and 2.11 shows the eigen values computed using strip eigen value placement method and pseudo decentralization method. It can be observed that with pseudo decentralization method the minimum damping ratio is 0.0531 and with strip eigen value method 0.0985. Table 2.4 shows the parameters of PSS obtained by using pseudo decentralization method with speed deviation as input to PSS (single input PSS).

Table 2.1: Eigen values of 3-machine 9-bus system

Eigen values	Damping ratio	Frequency of oscillation in Hz
0.0000	0.0000	0
0.0000	0.0000	0
$-0.4488 \pm 0.5773i$	0.6137	0.1164
$-0.4326 \pm 0.7762i$	0.4868	0.1414
$-0.4424 \pm 1.2030i$	0.3451	0.2040
-3.2258	1.0000	0.5134
-3.5139	1.0000	0.5593
-4.9221	1.0000	0.7834
$-0.2084 \pm 7.5727i$	0.0275	1.2057
$-5.0877 \pm 7.7705i$	0.5478	1.4782
$-5.1683 \pm 7.8736i$	0.5478	1.4990
$-5.1839 \pm 7.9161i$	0.5478	1.5060
$-0.8377 \pm 11.4903i$	0.0727	1.8336

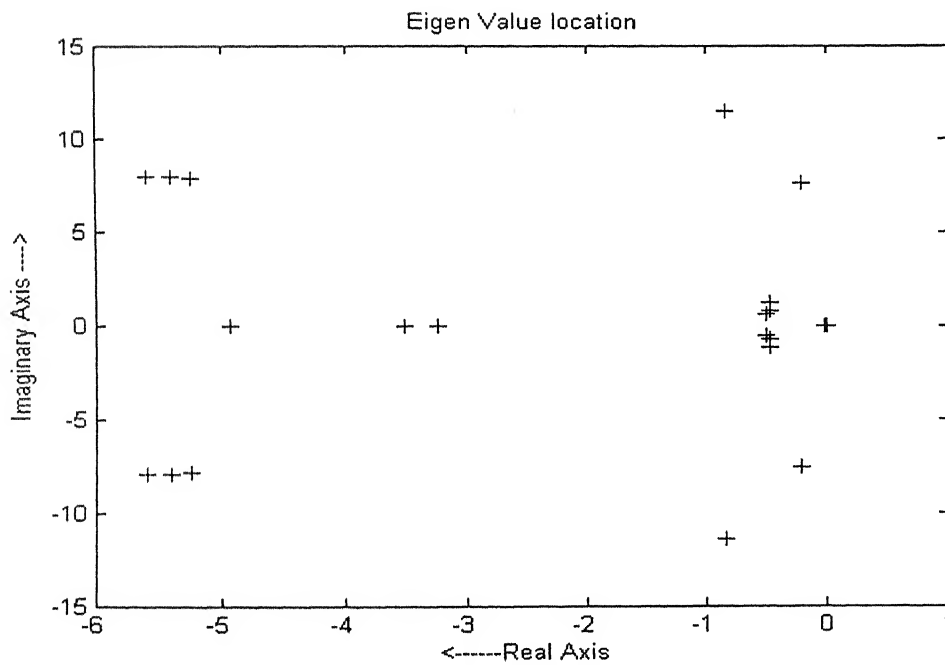


Fig. 2.8: Eigen values for 3 machine 9 bus system

Table 2.2: Eigen Values with PSS at two machines (Pseudo decentralization method)

Eigen Values	Damping Ratio	Frequency of Oscillation in Hz
0.0000	0	0.0000
$-0.3204 \pm 0.0628i$	0.9813	0.0520
-0.5000	1.0000	0.0796
-0.5000	1.0000	0.0796
$-0.4274 \pm 0.6561i$	0.5458	0.1246
$-0.4441 \pm 0.8028i$	0.4841	0.1460
-1.0000	1.000	0.1592
-1.0000	1.000	0.1592
-1.0772	1.000	0.1714
$-0.2689 \pm 1.2073i$	0.2174	0.1969
-3.2258	1.0000	0.5134
-3.5128	1.0000	0.5591
-4.9187	1.0000	0.7828
$-0.4029 \pm 7.5742i$	0.0531	1.2072
$-4.9446 \pm 7.6568i$	0.5425	1.4506
$-5.1376 \pm 7.9085i$	0.5448	1.5010
$-5.2122 \pm 7.8677i$	0.5523	1.5020
$-0.8651 \pm 11.5079i$	0.0750	1.8367

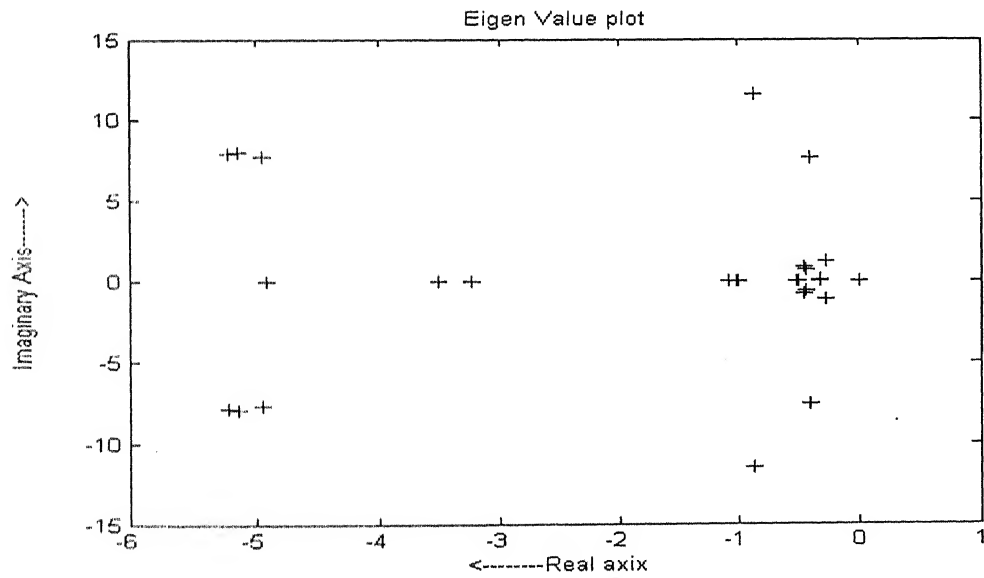


Fig. 2.9: Eigen Values for 3 machine 9 bus system with Pseudo decentralization method

Table 2.3 Eigen value for 3- machine 9-bus system with strip eigen value placement method

Eigen Value	Damping ratio	Frequency of Oscillation in Hz
$-0.4845 \pm 0.5454i$	0.6641	0.1161
$-0.4548 \pm 0.7154i$	0.5365	0.1349
$-0.4628 \pm 1.1545i$	0.3721	0.1980
$-1.7056 \pm 0.6927i$	0.9265	0.2930
-3.2258	1.0000	0.5134
-3.4975	1.0000	0.5567
-4.9032	1.0000	0.7804
$-1.5568 \pm 7.6398i$	0.1997	1.2409
$-5.2324 \pm 7.8321i$	0.5555	1.4991
$-5.4004 \pm 7.9179i$	0.5635	1.5254
$-5.5650 \pm 7.9491i$	0.5735	1.5444
$-1.1365 \pm 11.4838i$	0.0985	1.8366

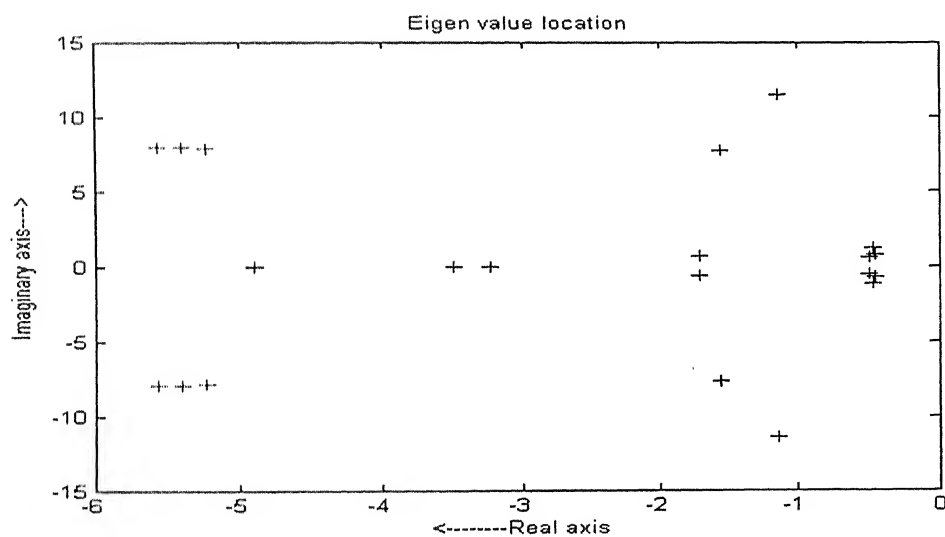


Fig. 2.10: Eigen Value of 3 machine 9-bus system with strip eigen value placement

Table 2.4 PSS parameters for 3 machine 9-bus system with pseudo decentralization

Machine No.	K	T_1	T_2	T_3	T_4
2	2.213	0.1525	0.0525	0.05913	0.05
3	1.49	0.4765	0.05	0.0210	0.05

2.8.2 New England 39-bus system

The New England system consists of 10 machines and again the generators are equipped with DC exciters. The machine at bus 1 is considered an infinite generator for all the analysis. The open loop analysis (Table 2.5) shows that, there are three critical modes (modes with damping ratio < 0.05). Fig. 2.12 shows the eigen values for open loop case. Though the generators 3 and 7 do not participated in the oscillations corresponding to these modes, PSS was assumed in all the 9 generators except the 1st generator. The strip eigen value placement method can not be applied to this system as it has got some limitations for bigger systems. A dual input PSS was considered. The parameters after inclusion of PSS are given in Table 2.6. It shows marked improvement in the eigen values. Fig. 2.12 shows the eigen value location after inclusion of PSS. The minimum damping ratio after inclusion of PSS is 0.0528. The improvement from previously developed method is that Q matrix was assigned values depending on the participation of the generators in the oscillations [19].

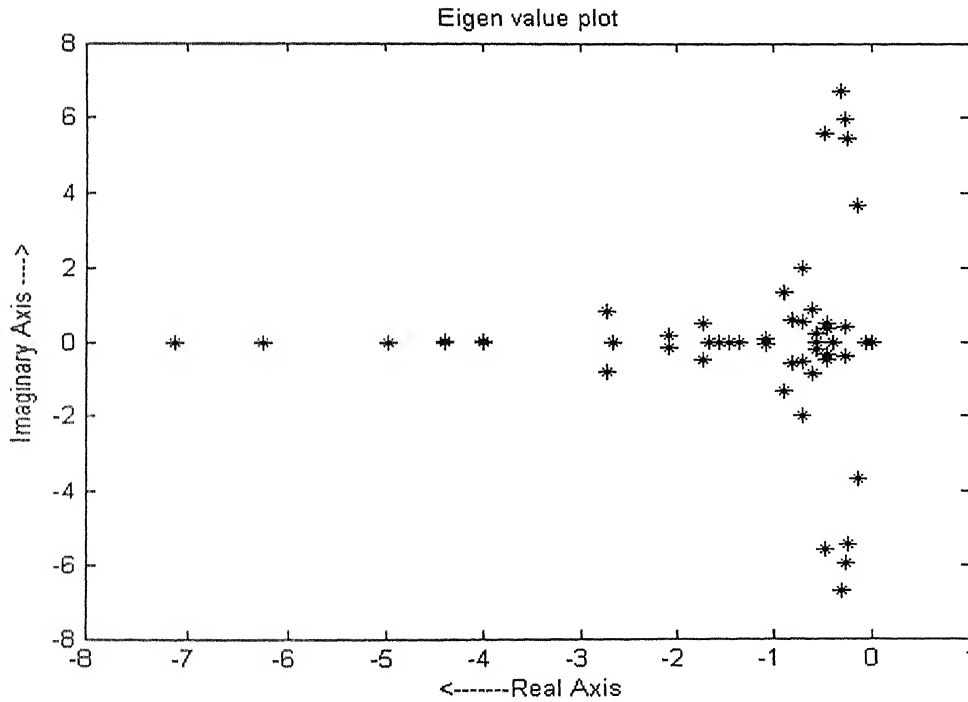


Fig. 2.11: Eigen values for 10 machine 39-bus New England system

Table 2.5 Eigen values of 10 machine 39 bus system

Eigen Value (1.0e+002 *)	Damping ratio	Frequency (Hz)	Eigen Value (1.0e+002 *)	Damping ratio	Frequency (Hz)
0.0000	0	0.0000	-0.0449	1.0000	0.7150
-0.0000	0	0.0006	-0.0507	1.0000	0.8063
-0.0040	1.0000	0.0636	-0.0020 ± 0.0548i	0.0367	0.8728
-0.0027 ± 0.0041i	0.5481	0.0785	-0.0046 ± 0.0559i	0.0814	0.8922
-0.0057	1.0000	0.0914	-0.0026 ± 0.0599i	0.0441	0.9538
-0.0057 ± 0.0018i	0.9556	0.0949	-0.0629	1.0000	1.0007
-0.0047 ± 0.0037i	0.7809	0.0949	-0.0041 ± 0.0667i	0.0610	1.0630
-0.0047 ± 0.0049i	0.6895	0.1080	-0.0708	1.0000	1.1264
-0.0071 ± 0.0053i	0.8041	0.1415	-0.0035 ± 0.0720i	0.0479	1.1472
-0.0083 ± 0.0059i	0.8145	0.1622	-0.0745	1.0000	1.1855
-0.0060 ± 0.0089i	0.5596	0.1717	-0.0048 ± 0.0778i	0.0619	1.2410
-0.0109 ± 0.0006i	0.9985	0.1734	-0.0068 ± 0.0847i	0.0795	1.3523
-0.0138	1.0000	0.2204	-0.0057 ± 0.0857i	0.0662	1.3663
-0.0144	1.0000	0.2295	-0.1558	1.0000	2.4789
-0.0156	1.0000	0.2485	-0.1573	1.0000	2.5043
-0.0089 ± 0.0129i	0.5688	0.2501	-0.1576	1.0000	2.5076
-0.0166	1.0000	0.2639	-0.1759	1.0000	2.7999
-0.0178 ± 0.0048i	0.9656	0.2933	-0.4827	1.0000	7.6822
-0.0205 ± 0.0017i	0.9965	0.3268	-0.4845	1.0000	7.7104
-0.0066 ± 0.0198i	0.3151	0.3322	-0.4915	1.0000	7.8221
-0.0259	1.0000	0.4117	-0.4926	1.0000	7.8395
-0.0271 ± 0.0083i	0.9559	0.4511	-0.4931	1.0000	7.8471
-0.0019 ± 0.0369i	0.0522	0.5886	-0.4990	1.0000	7.9418
-0.0443	1.0000	0.7049	-1.1688	1.0000	18.6023

Table 2.6 Eigen values of New England 39-bus system with Pseudo decentralization

Eigen Value (1.0e+002*)	Damping Ratio	Frequency in Hz	Eigenvalue (1.0e+002*)	Damping Ratio	Frequency in Hz
0.0000	0	0	-0.0446	1.0000	0.7101
-0.0023	1.0000	0.0361	-0.0498	1.0000	0.7919
-0.0040	1.0000	0.0631	-0.0044 ± 0.0555i	0.0793	0.8865
-0.0026 ± 0.0041i	0.5364	0.0782	-0.0058 ± 0.0569i	0.1018	0.9097
-0.0058	1.0000	0.0921	-0.0035 ± 0.0601i	0.0579	0.9575
-0.0054 ± 0.0025i	0.9083	0.0951	-0.0636	1.0000	1.0124
-0.0046 ± 0.0040i	0.7551	0.0970	-0.0057 ± 0.0675i	0.0837	1.0779
-0.0047 ± 0.0052i	0.6680	0.1122	-0.0711	1.0000	1.1320
-0.0069 ± 0.0053i	0.7920	0.1387	-0.0038 ± 0.0722i	0.0528	1.1500
-0.0062 ± 0.0086i	0.5858	0.1691	-0.0743	1.0000	1.1828
-0.0108	1.0000	0.1712	-0.0049 ± 0.0779i	0.0626	1.2416
-0.0074 ± 0.0081i	0.6734	0.1749	-0.0079 ± 0.0847i	0.0923	1.3546
-0.0117	1.0000	0.1861	-0.0073 ± 0.0866i	0.0836	1.3828
-0.0123	1.0000	0.1960	-0.1573 ± 0.0001i	1.0000	2.5035
-0.0142 ± 0.0005i	0.9995	0.2259	-0.1580	1.0000	2.5146
-0.0157 ± 0.0002i	0.9999	0.2504	-0.1758	1.0000	2.7985
-0.0049 ± 0.0162i	0.2902	0.2699	-0.2000	1.0000	3.1831
-0.0193	1.0000	0.3070	-0.2000 ± 0.0000i	1.0000	3.1831
-0.0199 ± 0.0022i	0.9937	0.3193	-0.2000 ± 0.0000i	1.0000	3.1831
-0.0207 ± 0.0081i	0.9310	0.3543	-0.2000	1.0000	3.1831
-0.0250	1.0000	0.3972	-0.2000	1.0000	3.1831
-0.0028 ± 0.0281i	0.1001	0.4491	-0.2000	1.0000	3.1832
-0.0400	1.0000	0.6361	-0.2000	1.0000	3.1835
-0.0400 ± 0.0000i	1.0000	0.6366	-0.2001	1.0000	3.1847
-0.0400	1.0000	0.6366	-0.4840	1.0000	7.7024
-0.0400 ± 0.0000i	1.0000	0.6367	-0.4856	1.0000	7.7293
-0.0400 ± 0.0000i	1.0000	0.6367	-0.4920	1.0000	7.8298
-0.0401	1.0000	0.6383	-0.4926	1.0000	7.8400
-0.0405	1.0000	0.6449	-0.4931	1.0000	7.8478
-0.0083 ± 0.0414i	0.1970	0.6724	-0.4990	1.0000	7.9421
-0.0423	1.0000	0.6733	-1.1688	1.0000	18.6025

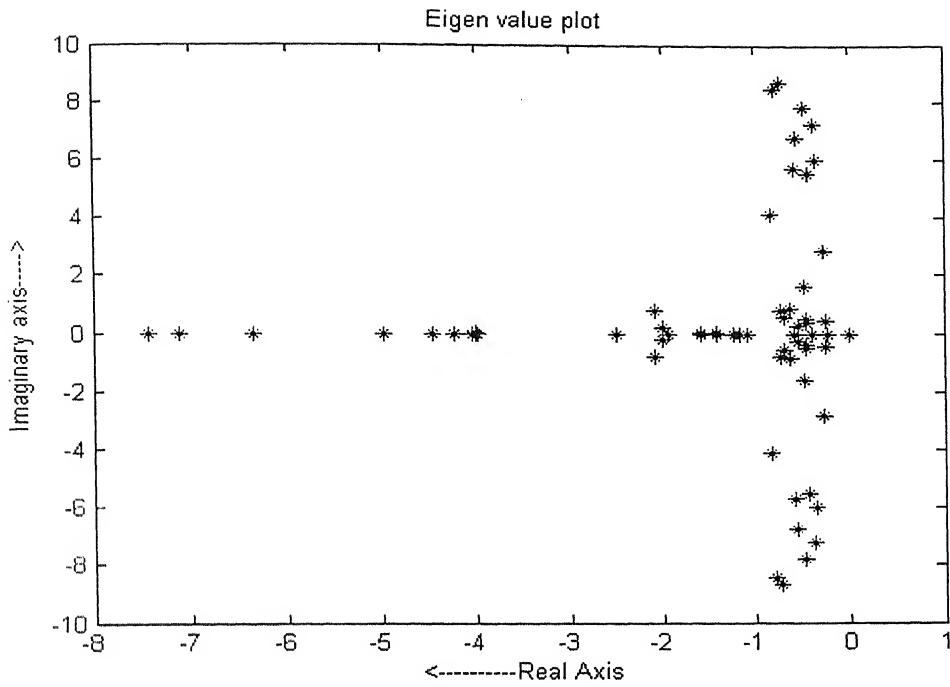


Fig. 2.12: Eigen Value for 10 m/c 39 bus system with Pseudo Decentralization

2.9 Conclusion

The methods described in this chapter can be invariably used for PSS tuning in case of multi machine environment. But still the analysis is not complete. Before doing multi machine PSS tuning we must first perform the SMIB analysis, because a lot of literatures are available in this respect and till date PSS tuned through SMIB are operating well. But the truth is that, we should consider the dynamics among all the generators, this will reduce the burden of doing trial and error methods in the field while practically incorporating the PSS. Again strip eigen value method and pseudo decentralization method are capable of shifting the under damped eigen values (Eigen values with $\zeta < 0.05$) to the safe damping region. But strip eigen value placement has got inherent disadvantage of application to small system only. The selection of the weighting matrices is still a hit and trial method. In some cases we take them as identity matrices [6], and in some cases we are giving weightage depending on its participation in system oscillating modes. Depending on the operating conditions also these matrices has to be changed which is practically very difficult to achieve. This process is also an arbitrary method. Some robust intelligent PSS has to be found out, which will be simpler and easy to implement.

PSS Tuning for Kaiga Nuclear Power Plant

3.1 Introduction

Kaiga nuclear power plant has *static busfed* type of exciter, which gets power from an auxiliary transformer. The basic function of AVR is to control the firing angle of the exciter. So AVR output is fed to the exciter gate circuit. From the AVR output to the main field of generator a linear circuit is considered [19] i.e. the rectifier dynamics are neglected. For fast operation during disturbance the AVR regulator is provided with PID characteristics which do not need a rate feedback [19]. Also it is provided with high ceiling voltages for field forcing. AVR time constant and gain can be varied by selector switches in the plant. Fig. 3.1 shows the block diagram of AVR. The current settings and range of values are given in Appendix-C.

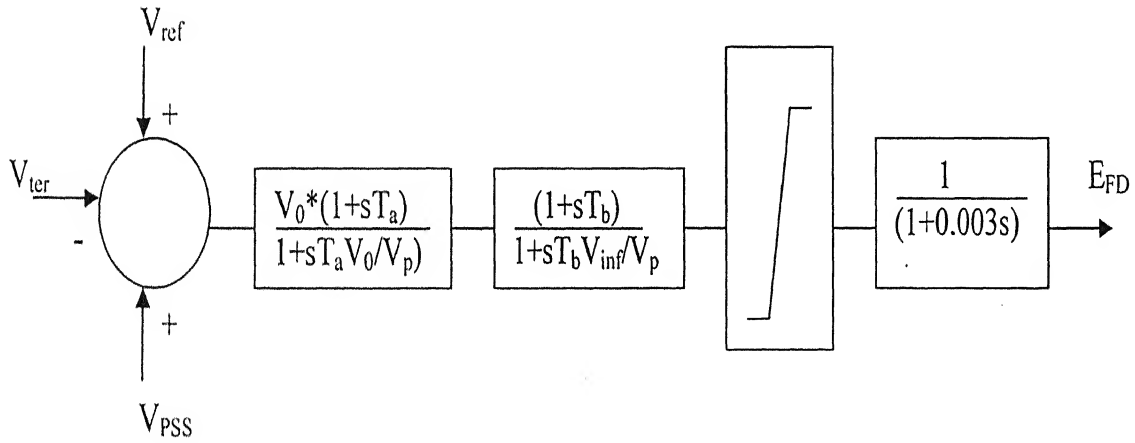


Fig.3.1: AVR block diagram

3.2 Exciter and AVR Dynamic Equations for Kaiga NPP

Kaiga AVR has no feedback stabilization (rate feed back) and the PID amplifier has equal number of poles and zeros, this is reduced in the form of observable canonical form [6]. There is no saturation as the exciter is static type. The limits are not considered for linear modeling. Fig.3.2 shows the simplified AVR block diagram. The initial conditions for steady state load flow were calculated from the dynamic equations.

The method is similar to that discussed in the section 2.6.1. From the Fig. 3.1, the output y_c is the same as V_R (fig.2.2). Error voltage ($V_{ter} - V_{ref}$) is the control input u_c ,

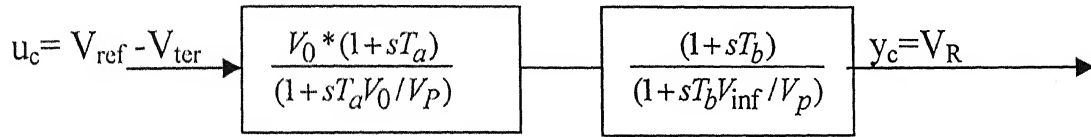


Fig. 3.2: Simplified AVR block Diagram

The PID transfer function is given as

$$G(s) = \frac{K_s (1 + sT_i) (1 + sT_j)}{(1 + sT_2) (1 + sT_4)} \quad (3.1)$$

The state space model in observable canonical form can be written as

$$\begin{bmatrix} \dot{x}_1 \\ \dot{x}_2 \end{bmatrix} = \begin{bmatrix} 0 & -\alpha_0 \\ 1 & -\alpha_1 \end{bmatrix} \begin{bmatrix} x_1 \\ x_2 \end{bmatrix} + \begin{bmatrix} \beta_0 \\ \beta_1 \end{bmatrix} u_c \quad (3.2)$$

$$y_c = \begin{bmatrix} 0 & 1 \end{bmatrix} \begin{bmatrix} x_1 \\ x_2 \end{bmatrix} + d u_c \quad (3.3)$$

α_0 , α_1 , β_0 , β_1 , and d in terms of K_s , T_b , T_j , T_2 , and T_4 are given in Eq (2.32). y_c in terms of the actual parameters are given as, $y_c = V_R$, $u_c = V_{ref} - V_{ter}$. The initial conditions can be calculated by equating derivative terms to zero at steady state [20]. These equations are linearized and included for further analysis.

3.2.1 PSS Block Diagram at Kaiga NPP

Kaiga NPP has got a dual input PSS as shown in Fig.3.3. Electrical power deviation and speed deviation or frequency deviation are the two inputs. The power and frequency transducers sense the actual values. After weighting and washout stage, deviation in electrical power and deviation in frequency signals are obtained. Depending on the power deviation, gain K_3 is decided. In this case, for power deviation less than 15% of rated value, K_3 varies as a quadratic function of ΔP , which implies that PSS is not fully utilized. For ΔP greater than 15% of rated value, K_3 is 1 that is PSS is fully utilized. For tuning the PSS, lead-lag block are not necessary to be tuned. Properly weighted (multiplied with K_3) frequency or speed deviation signal is added to negative of the weighted power deviation signal gives final PSS output. For proper phase compensation so that final torque due to PSS is in phase with the speed deviation signal, K_1 and K_2 are to be determined. The range of the parameters is given in Appendix-C

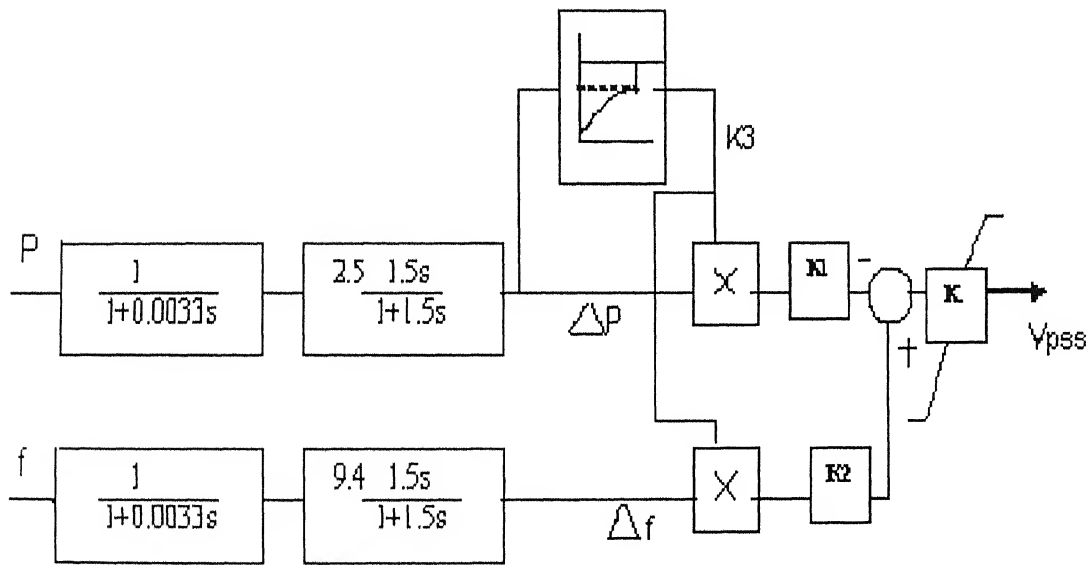


Fig. 3.3: PSS block diagram of Kaiga NPP

3.3 SMIB Analysis and PSS Tuning

The SMIB approach is used for tuning of Kaiga PSS. The reason behind this is, nearby hydro units are facing no problem when there is oscillation at Kaiga, so they do not have immediate plans to go for PSS tuning. The second reason can be attributed to the non-

availability of exact data of those generators. Even though there are different multi machine PSS tuning methods, SMIB method is still preferred as the other developed methods are very difficult to implement [21].

3.3.1 Phase Plot

The single machine equivalent was obtained from the existing data for the two machines. The voltage and MVA base were changed. The two nearby generators were assumed as constant impedance loads injecting power to the system [21] as opposed to the normal loads. One infinite bus was assumed at Guttur connected to Kaiga over the double circuit line of 165 km length. After static load flow analysis, the loads were changed to equivalent admittance knowing the voltage magnitude at their terminals. Then Thevinin equivalent was calculated at the terminals of Kaiga, transfer reactance was calculated between the single machine equivalent and assumed infinite system. The constants K1-K6 [1], [10] were calculated. The transfer function for Generator, Exciter and Power system, $GEP(s)$ [2] was found out. This is nothing but the transfer function from the PSS input point to the output of exciter as in the Heffron-Phillips model [19]. Phase plot which is given in Fig 3.5 and Gain plot which is given in Fig.3.6 were obtained for the system at different frequencies. This gives the amount of phase compensation required by the PSS output so that the final torque produced due to this will be in phase with the speed deviation [2].

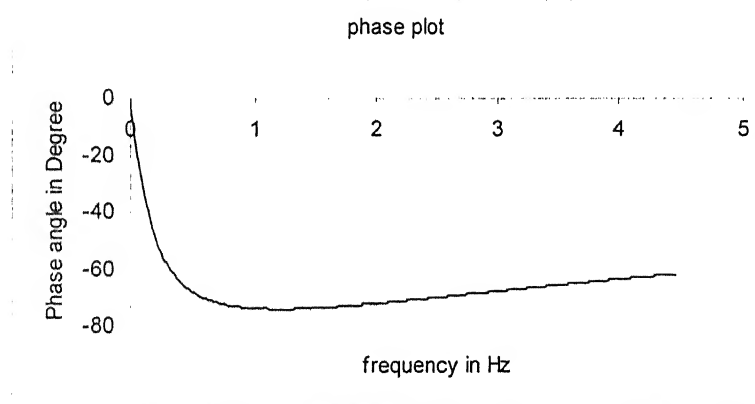


Fig.3.4: Phase plot for kaiga NPP

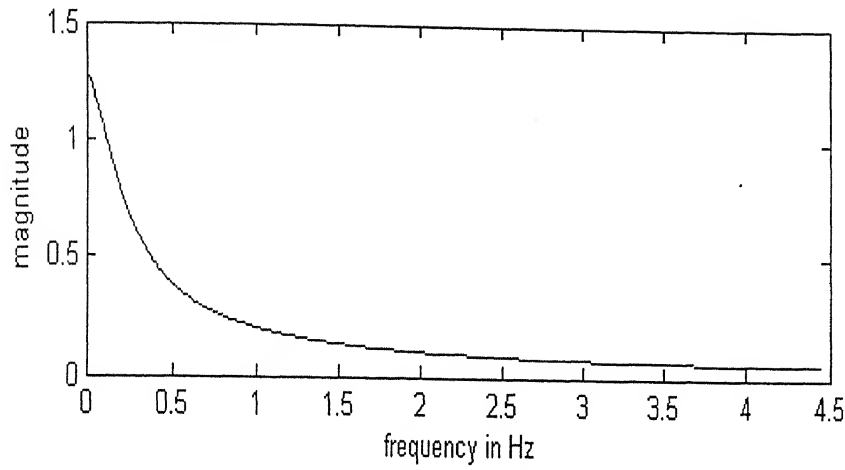


Fig. 3.5: Gain Plot for Kaiga NPP

3.3.2 Eigen Value Analysis

The linearized model as developed in 2.4 is replaced with Kaiga AVR and exciter. The Inter Connecting Transformer (ICT) is considered as a part of the network for eigen value analysis. The two nearby hydro generators are considered as two loads (of 90 MW each) for this analysis. As they are small in size and do not oscillate when Kaiga generators are oscillating, the SMIB analysis gives enough idea about the system behaviour for small disturbances. The base case load flow is run and the system is linearized. The eigen value analysis is performed and given in Table 3.1. The minimum damping ratio of the system is found to be 0.0102. Fig. 3.6 shows the eigen values in s-plane. Two critical modes are existing in the open loop case (without PSS) which proves the insufficient damping for the existing system. Participation factor analysis shows that Kaiga generators are participating maximum in the oscillatory modes corresponding to speed and load angle deviation ($\Delta\omega$ and $\Delta\delta$). The frequency of oscillation comes out to be in the range of local mode [19]. So it proves that Kaiga generators are oscillating with respect to a strong system connected over a long transmission line. No intraplant mode of oscillation is observed. The oscillation pattern changes for different loading and AVR setting conditions. So the cause of oscillation can be attributed to the improper setting of the AVR as after inclusion of ICT also there is no major improvement in the eigen values. Normally inclusion of ICT solves the problem of generator connected to rest of the system with weak line ($X_e > 0.5$ PU, including transformer reactance). The zero eigen values appearing in the analysis are redundant eigen values as discussed in section 2.7.

3.3.3 PSS Tuning

The PSS provided by BHEL has no lead-lag block as the conventional PSS has. So the methods used for tuning PSS are not used here. The tuning is done completely through MATLAB[®] SIMULINK which is explained in the next section. The PSS has options for either frequency or speed input. Here we have used the direct speed input. Frequency input PSS is for weak to medium transmission systems [2]. As the phase plot shows that there is considerable phase lag in the range of frequency of interest, only local mode is addressed. The eigen value analysis confirms the oscillations at local mode and poor damping of the oscillations. As there is no inter area mode of oscillations SMIB analysis is sufficient even though this aspect also needs attention [21]. K_1 and K_2 values are the important parameters, which can only be varied. Other parameters such as the transducer time constant, washout filter time constant and final gain are fixed values. Appendix [3]. After inclusion of PSS the system eigen values are given in Table 3.2. From Table 3.2 the minimum system damping is 0.0729. This shows the improvement in the system damping. Fig. 3.7 shows the system eigen values after PSS is included in the linearized analysis.

Table3.1 Eigen value analysis without PSS

Eigen Value(1.0e+002 *)	Damping ratio	Frequency in Hz
0.0000	0	0.0000
-0.0000	1.0000	0.0000
-0.0054 ± 0.0067i	0.6308	0.1371
-0.0119	1.0000	0.1895
-0.0108 ± 0.0059i	0.8766	0.1952
-0.0264	1.0000	0.4202
-0.0408	1.0000	0.6488
-0.0479	1.0000	0.7617
-0.0006 ± 0.0498i	0.0102	0.7920
-0.0623	1.0000	0.9923
-0.0045 ± 0.0674i	0.0666	1.0752
-0.3054	1.0000	4.8610
-0.3139	1.0000	4.9966
-0.3165	1.0000	5.0369
-8.3033	1.0000	132.1519
-8.3223	1.0000	132.4530
-8.3282	1.0000	132.5470

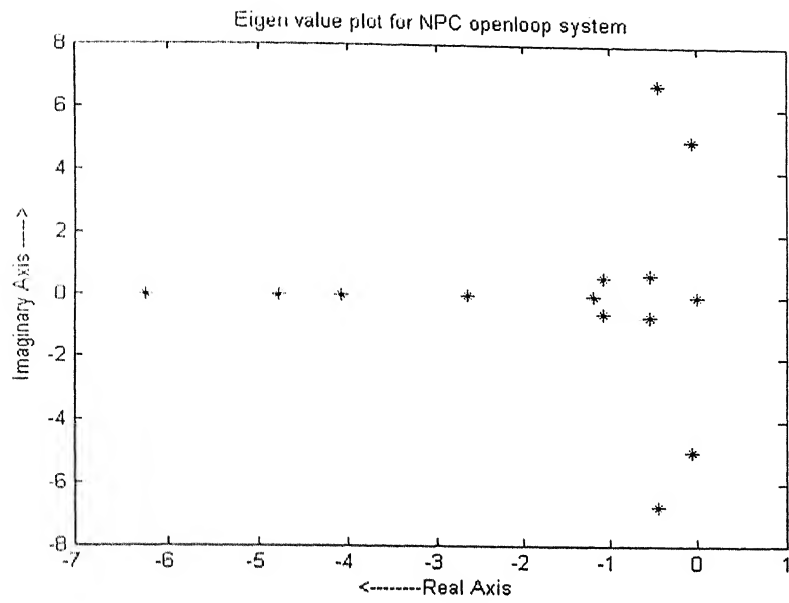


Fig. 3.6: Eigen value without PSS

Table 3.2 Eigen Value Analysis with PSS on 1st Machine at Kaiga NPP

Eigen Value(1.0e+002 *)	Damping ratio	Frequency in Hz
0.0000	0	0.0000
-0.000	1.0000	0.0000
-0.0017	1.0000	0.0266
-0.0055 ± 0.0069i	0.6234	0.1412
-0.0096	1.0000	0.1533
-0.0139	1.0000	0.2205
-0.0245	1.0000	0.3901
-0.0249	1.0000	0.3960
-0.0492	1.0000	0.7827
-0.0041 ± 0.0560i	0.0729	0.8943
-0.0637	1.0000	1.0140
-0.0356 ± 0.2072i	0.1694	3.3456
-0.3081	1.0000	4.9034
-0.3164	1.0000	5.0361
-0.3232	1.0000	5.1440
-8.2554	1.0000	131.3884
-8.3124	1.0000	132.2964
-8.3281	1.0000	132.5456

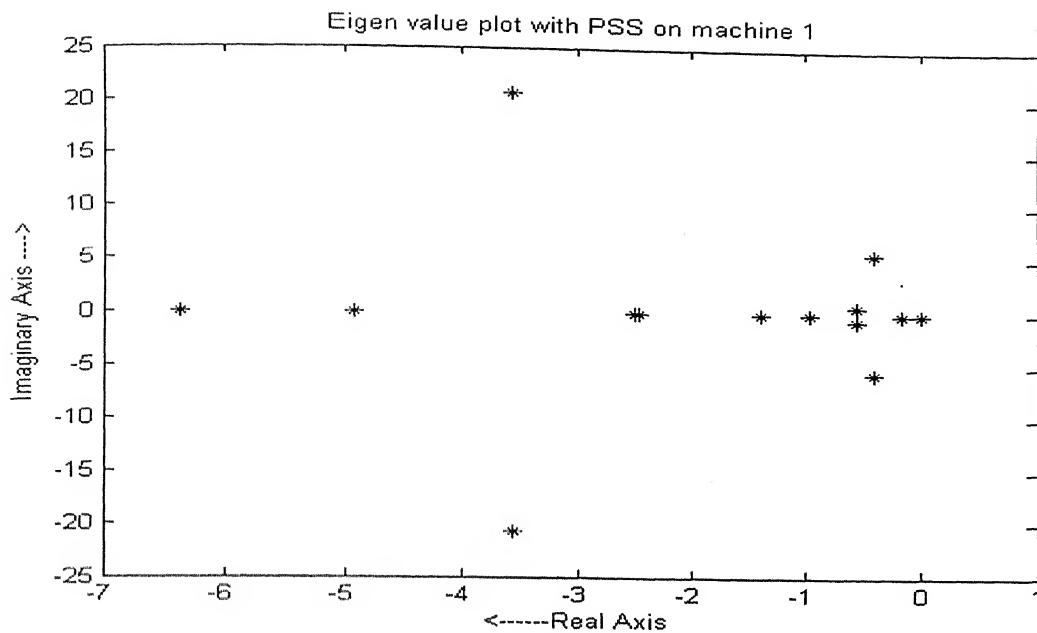


Fig 3.7: Eigen value locations with PSS on generator-1

3.4 Simulink Models for NPC System

Non-linear Simulation is required for the transient stability analysis of the system. For this, Simulink[®] model is used. It uses the generator model as described in section 2.2 with transient saliency neglected (i.e. $X'_{q} = X'_{d}$). Other detail system data are given in Appendix-3. Swing bus is designed with a generator having very high Inertia constant and large capacity so that rotor dynamics can be neglected.

Simulink model of Fig. 3.8 shows the reduced model of NPC system, where the nearby hydro generators are considered as loads of 180MW. A large value of load is also assumed at the swing bus end. The AVR, exciter and PSS simulink models (Fig. 3.9, Fig. 3.10, and Fig. 3.11) used are similar to those supplied by the manufacturer. Fig 3.12 shows the detail NPC system model. The two nearby generators are considered and one of them is equipped with IEEE-1 exciter. The NPC system model is further expanded by considering 16 other generators to make the system more practical (Fig. 3.18). Some of these generators are equipped with exciters and others have constant field voltage. Internal subsystem diagram for one machine is shown in Fig. 3.14. Kaiga generators are equipped with IEEE-1 exciter which is shown in Fig. 3.15, for a comparative study purpose.

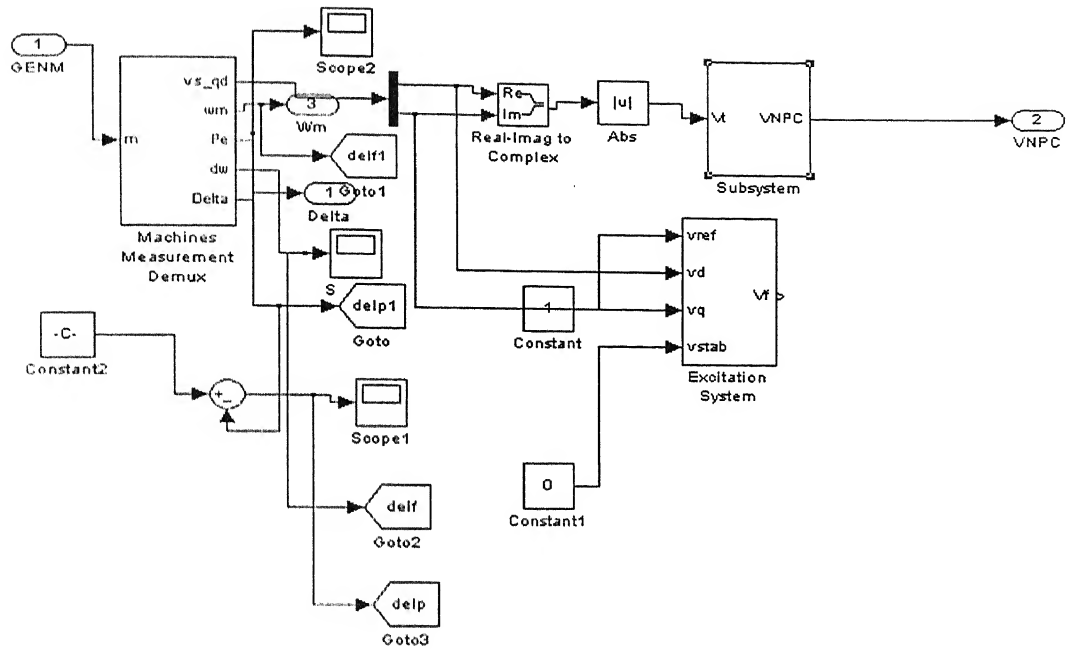


Fig.3.9: Exciter and AVR signal collection diagram

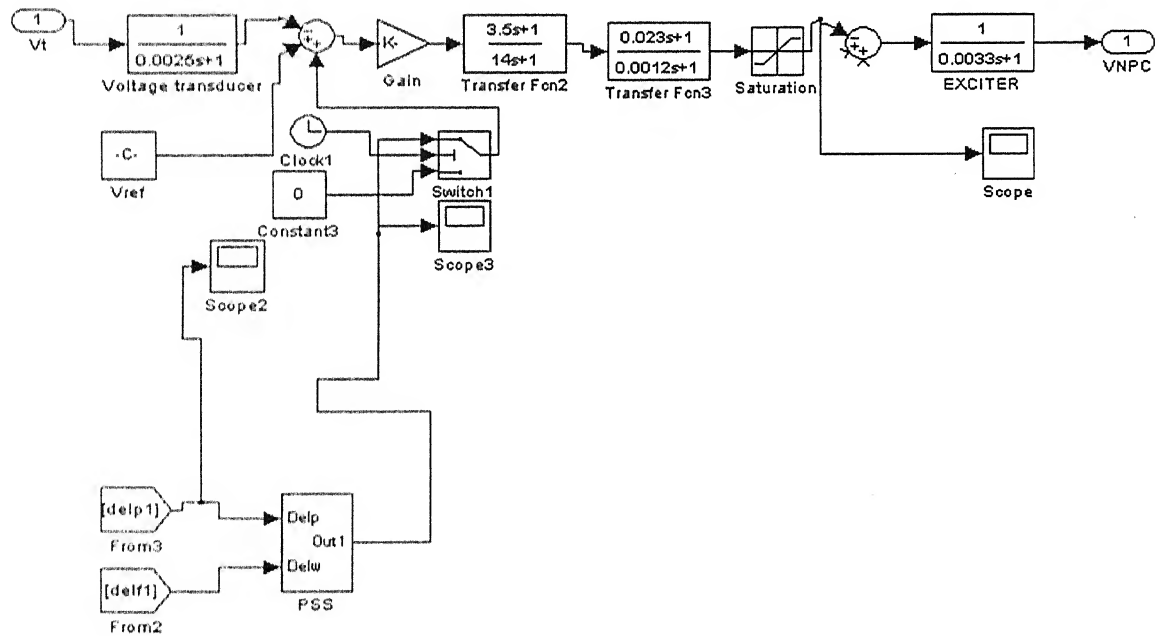


Fig. 3.10: Exciter and AVR simulink model

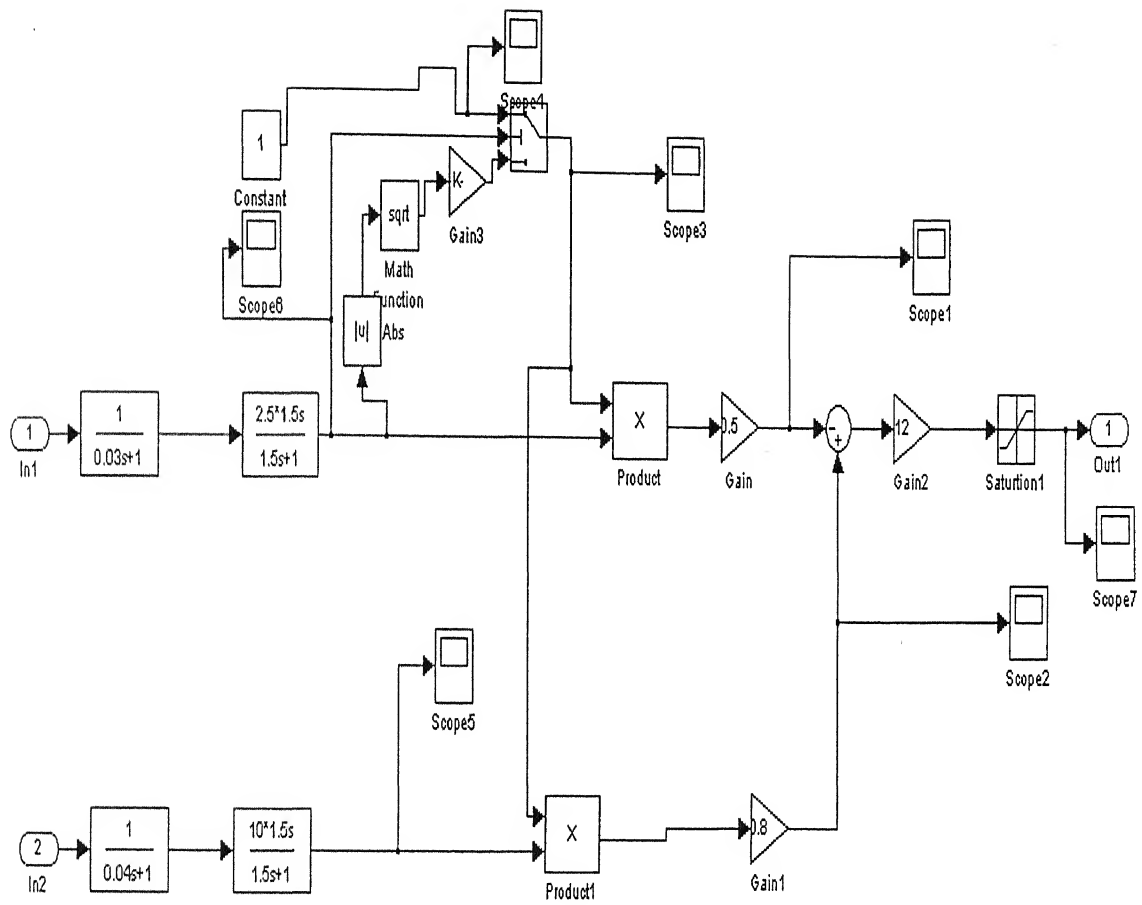


Fig. 3.11: Simulink model for PSS

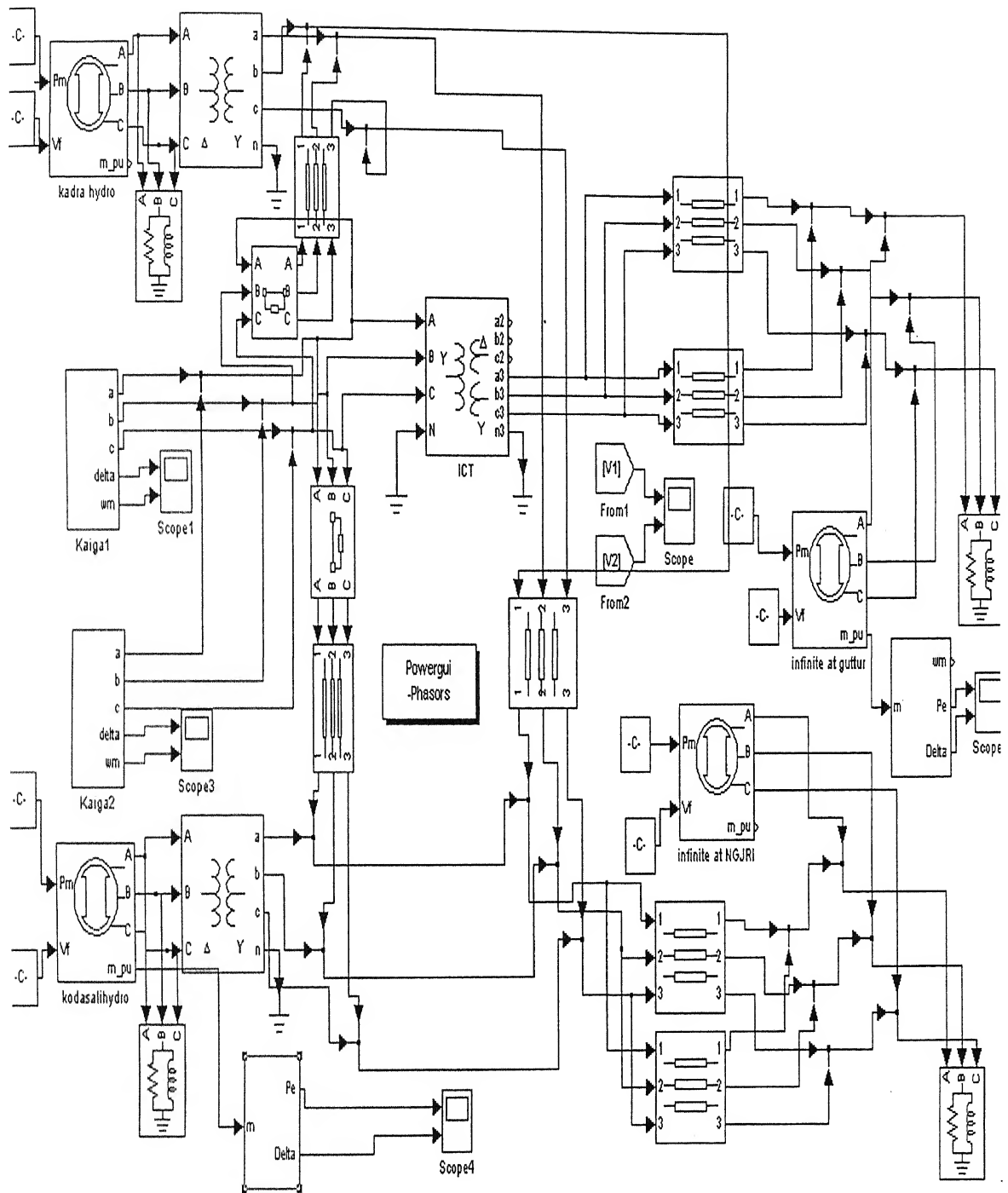


Fig. 3.12: Detail model of NPC system

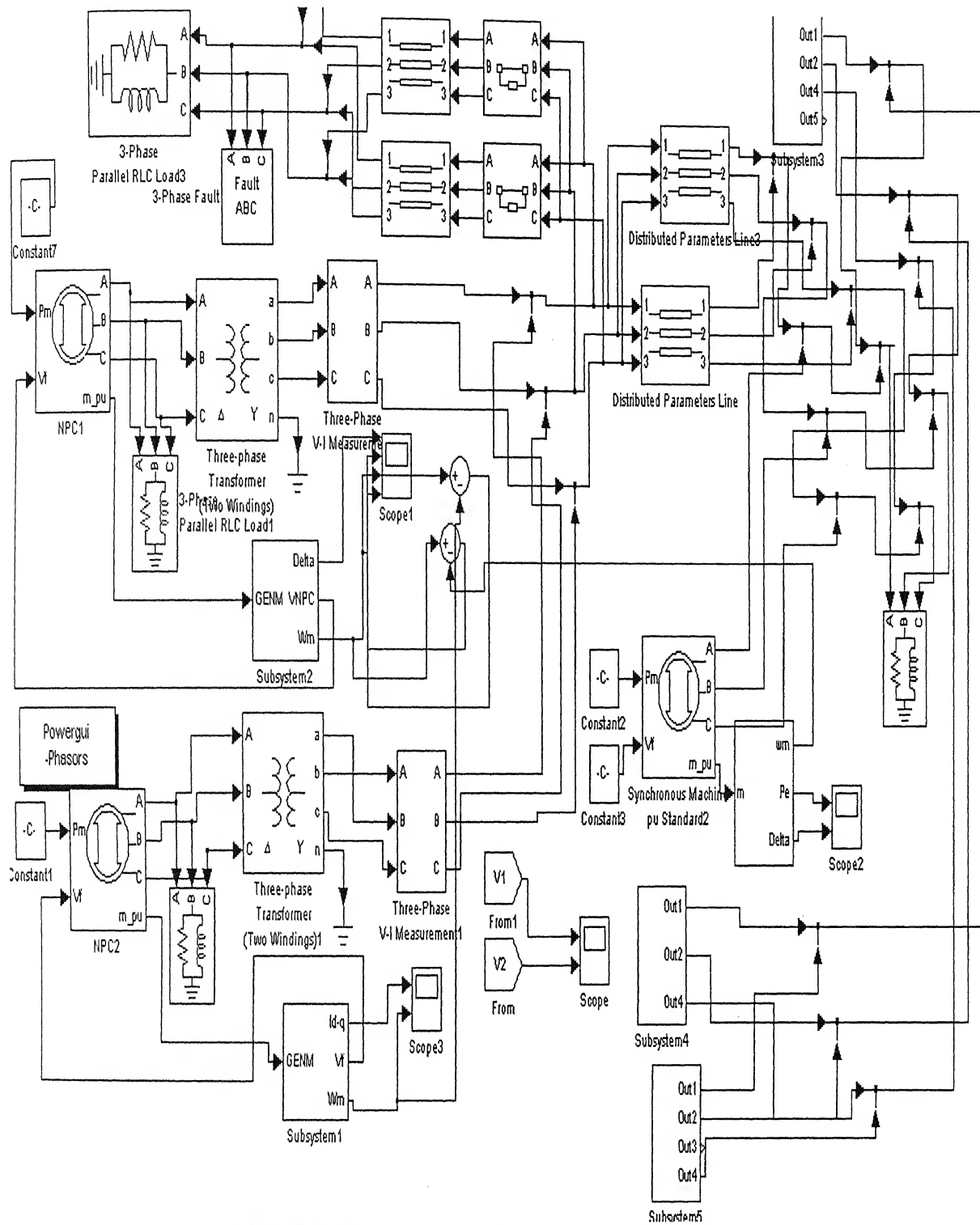


Fig.3.13 Kaiga system with 16 other generators

दुस्रोत्तम काशीनाथ केलकर पुस्तकालय
भारतीय प्रौद्योगिकी संस्थान कानपुर
संख्यांक क्र० A...152052...

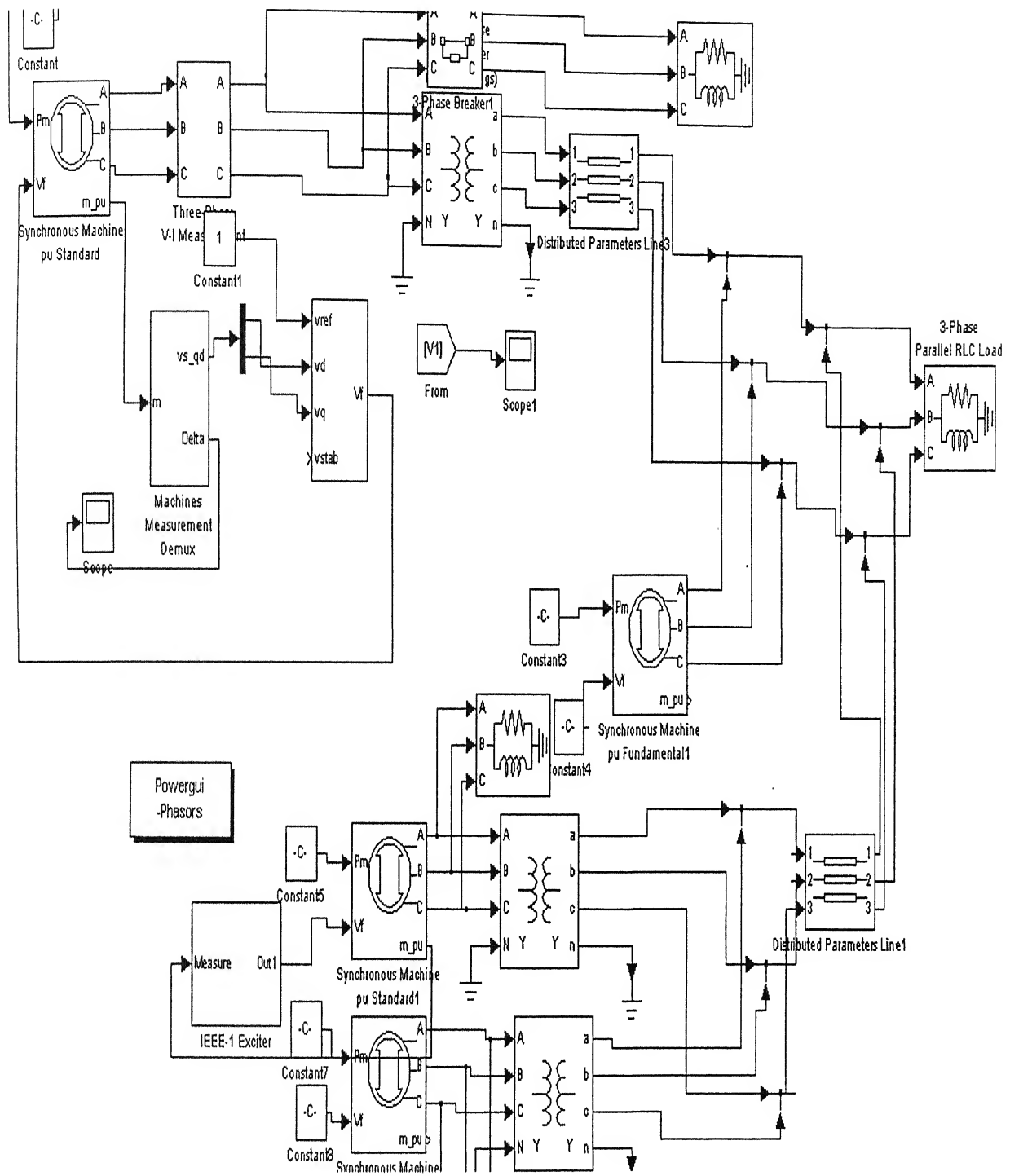


Fig.3.14: Kaiga system with IEEE-1 exciter

3.5 Simulation and Results

Using Graphical User Interface (GUI) block, the initial steady states and load flow is performed. This is necessary to start the simulation from steady state. A line is tripped at 30 sec for all the simulations. Kaiga-1 and Kaiga-2 are rated at 200MW and 215 MW respectively. Following cases were studied.

- (a) NPC reduced system without PSS
- (b) NPC reduced system with PSS at generator-1
- (c) Detailed NPC system without PSS
- (d) Detailed NPC system with PSS at generator-1
- (e) Reduced NPC system with 16 other generators
- (f) Reduced NPC system with 16 other generators and PSS at Kaiga-1

3.5.1 NPC Reduced System without PSS

The time constant ratio T_1/T_2 is set to 0.5 and the simulation is performed with a fault initiated at 30 second. The load angle and power variations are shown in Fig. 3.15 and Fig. 3.16, respectively. The speed deviation between the both Kaiga generators is plotted in Fig. 3.17 whereas speed deviation between Kaiga and slack bus (bus-1) is shown in Fig. 3.18. The swing generator load angle and Kaiga bus voltage are also oscillating which can be seen from Fig. 3.19 and Fig. 3.20 respectively. The frequency of oscillation is observed as 1.2 Hz which is quite similar to the result of eigen value analysis. By changing the T_1/T_2 ratio to 0.25, the system oscillations are getting damped after few cycles which can be seen from the Figs. 3.21 to 3.24. From Figs. 3.21 to 3.24 it can be observed that oscillation is damped out after more than 15 second.

3.5.2 NPC Reduced System with PSS at Generator-1

PSS signal is given to the AVR summing point of gen-1, the time constant ratio T_1/T_2 is set to 0.5, and PSS settings $K_1=0.4$, $K_2=0.5$. Simulation is performed with a fault initiated at 30 second. The load angle and power variations are shown in Fig. 3.25 and Fig. 3.30 respectively. The speed deviation between the both Kaiga generators is plotted in Fig. 3.26 whereas speed deviation between Kaiga and slack bus (bus-1) is shown in Fig. 3.27. The

swing generator and Kaiga bus voltage are shown in Fig. 3.28 and Fig. 3.29 respectively. It can be observed that there is very little oscillation in system parameters.

3.5.3 Detailed NPC System without PSS

The two nearby hydro generators were connected to the Kiaga generators. The exciter parameters of Kadra hydro are assumed suitable values [15]. The time constant ratio T_i/T_2 at Kaiga-1 is set to 0.5 and the simulation is performed with a fault initiated at 30 second. The load angle of Kaiga-1 and Kudasalli hydro are shown in Fig. 3.31 and Fig. 3.33 respectively. The speed deviation between the both Kaiga generators is plotted in Fig. 3.34 whereas speed deviation between Kaiga and Kadra is shown in Fig. 3.32. The frequency of oscillation is observed as around 1.2 Hz which is quiet similar to the result of eigen value analysis. . From Figs. 3. 31 to 3. 34 it can be observed that oscillation is not damped out.

3.5.4 Detailed NPC System with PSS at Generator-1

PSS signal is given to the AVR summing point of gen-1, the time constant ratio T_i/T_2 is set to 0.5, and PSS settings $K_1=0.5$, $K_2=0.8$. The simulation is performed with a fault initiated at 30 second. The load angle of Kaiga-1 and Kadra hydro are shown Fig. 3.35 and Fig. 3.37 respectively. The speed deviation between the both Kaiga generators is plotted in Fig. 3.36 whereas speed deviation between Kaiga and Kadra is shown in Fig. 3.38. The PSS output and Kaiga-1 bus voltage are shown in Fig. 3 .39 and Fig. 3.40 respectively. It can be observed that there is very little oscillation in system parameters.

3.5.5 Reduced NPC System with 16 Other Generators

To make the system more practical 16 other generators are connected at the swing bus end. Some of these generators have exciter on them. The time constant ratio T_i/T_2 is set to 0.5 and the simulation is performed. Following a three phase fault and subsequent opening of line connecting Kaiga and the nearby load, Kaiga-1 and 2 start oscillations. The load angle variations of generator-1, generator at 200km from Kaiga, and swing generator are shown in Fig. 3.41, Fig. 3.42 and Fig. 3.45 respectively. The speed deviation between the both Kaiga generators is plotted in Fig. 3.43 whereas speed deviation between Kaiga and slack bus (bus-1) is shown in Fig. 3.46. Bus voltage at Kaiga-1 is also oscillating which can

bee seen from Fig. 3.44. From Figs. 3.41 to 3.46 it can be observed that oscillation is damped out after more than 25 second.

3.5.6 Reduced NPC System with PSS at Kaiga-1

PSS signal is given to the AVR summing point of gen-1, the time constant ratio T_i/T_2 is set to 0.5, and PSS settings $K_1=0.2$, $K_2=0.3$. The simulation is performed with a fault initiated at 30 second. The load angle of Kaiga-1, generator at 200km from Kaiga and swing generator are shown Fig. 3.47, Fig. 3.48 and Fig. 3.49 respectively. The speed deviation between the both Kaiga generators is plotted in Fig. 3.52 whereas speed deviation between Kaiga and is shown in Fig. 3.50. The PSS output at Kaiga-1 is shown in Fig 3.51. It can be observed that there is very little oscillation in system parameters.

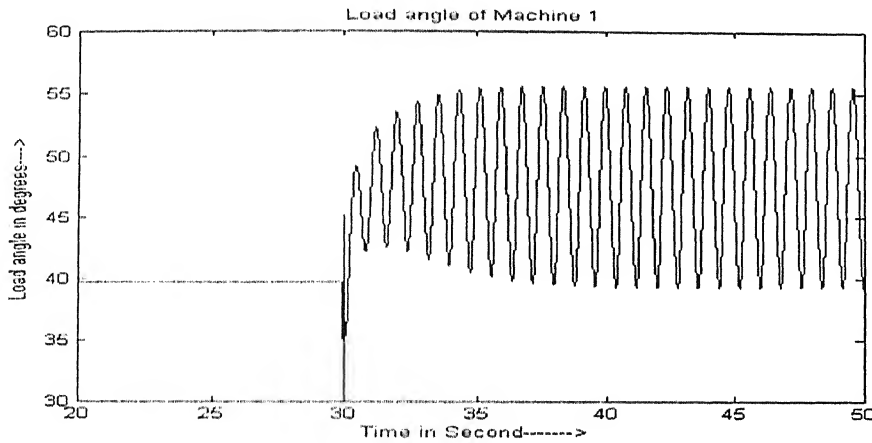


Fig 3.15: Load angle oscillation of machine-1 at Kaiga for reduced NPC system

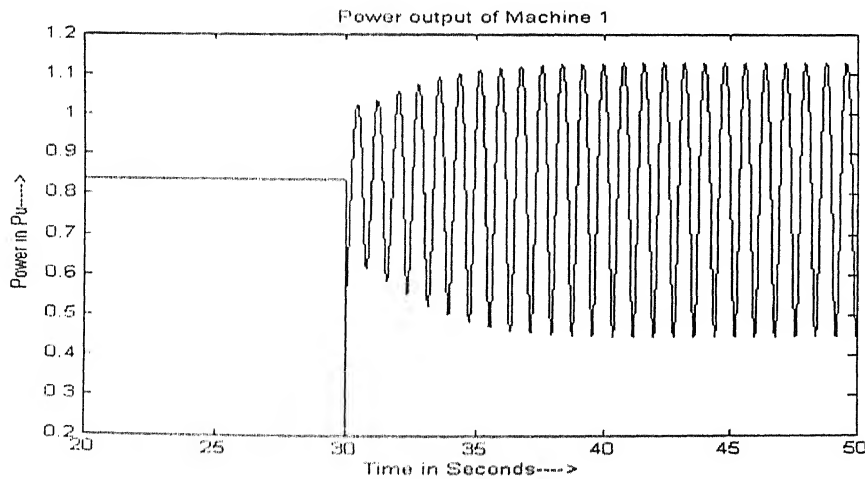


Fig.3.16: Power output of machine 1 at Kaiga

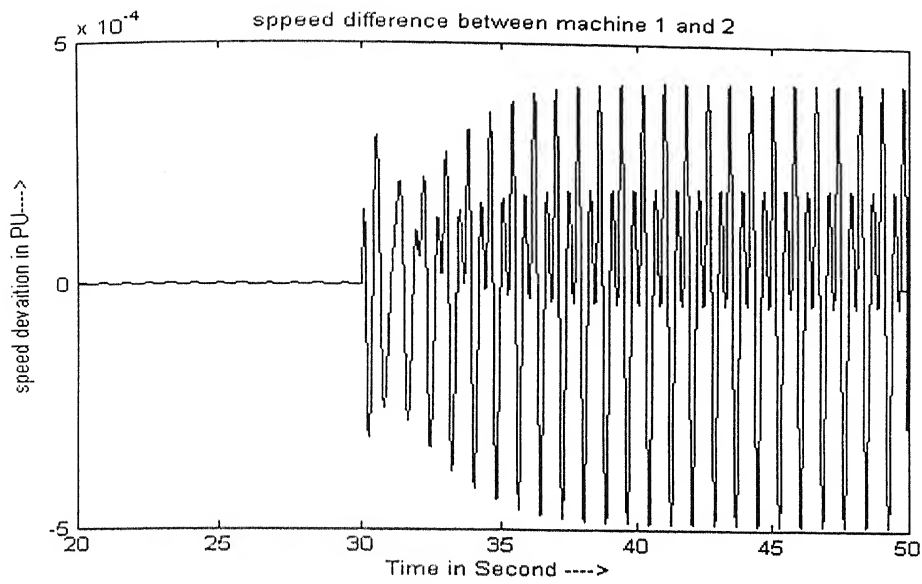


Fig.3.17: Speed difference between Kaiga-1 and 2

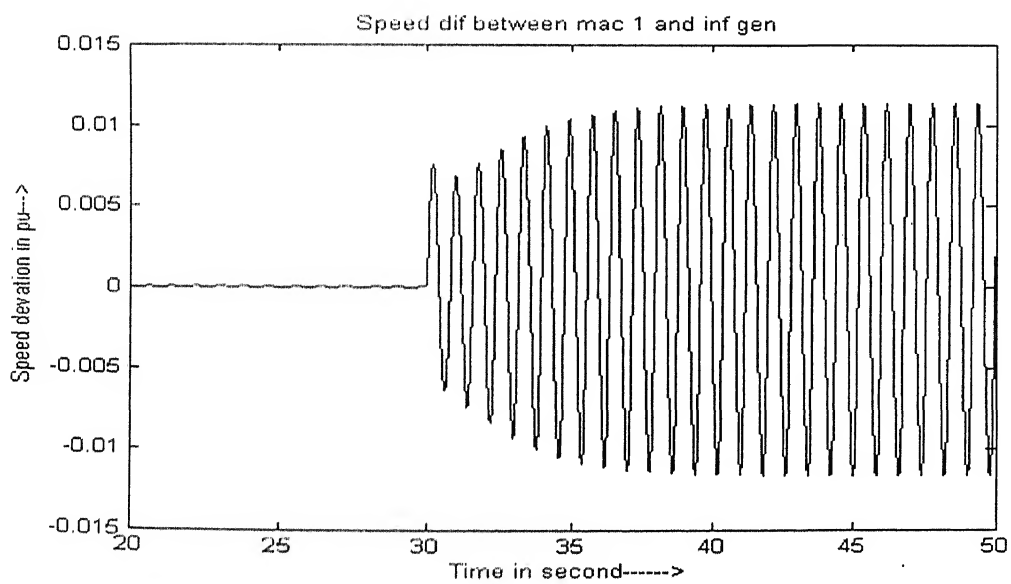


Fig. 3.18: Speed difference between Kaiga-1 and swing generator

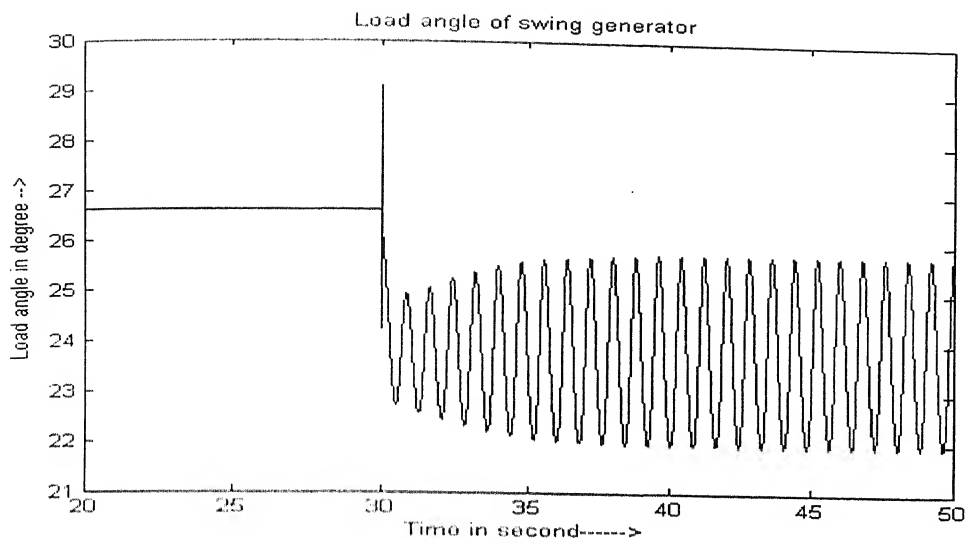


Fig. 3.19: Load angle of swing generator

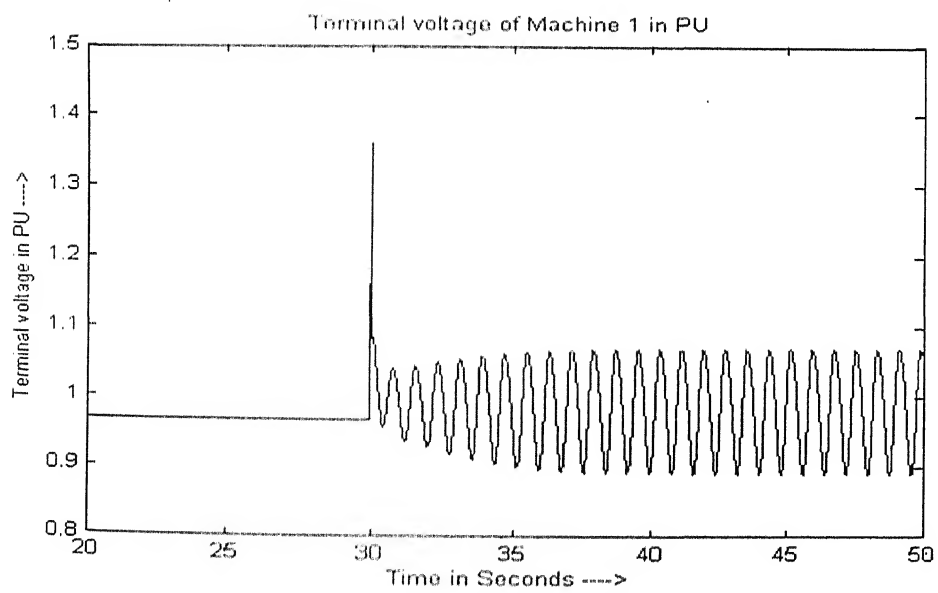


Fig. 3.20 Terminal voltage of Kaiga-1

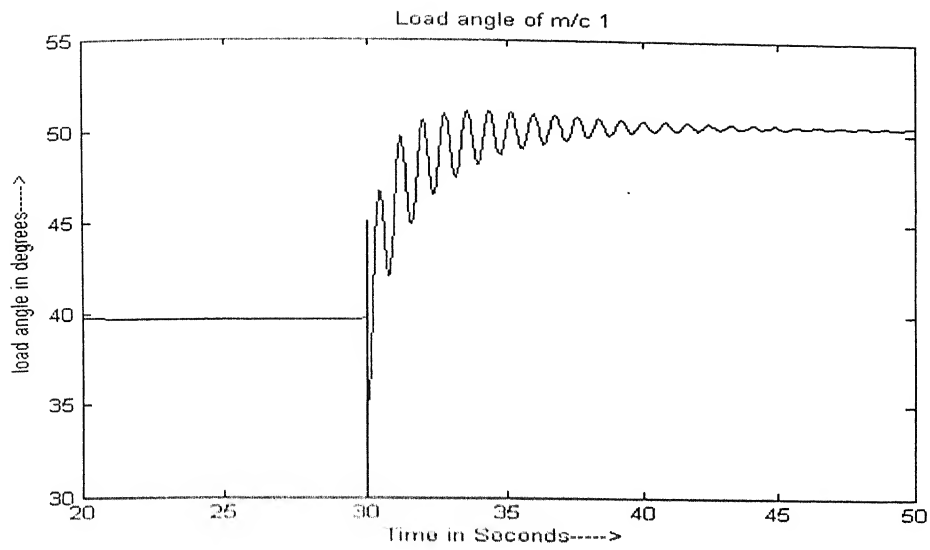


Fig. 3.21: Load angle of Kaiga-1 for reduced NPC system with $T_1/T_2 = 0.25$

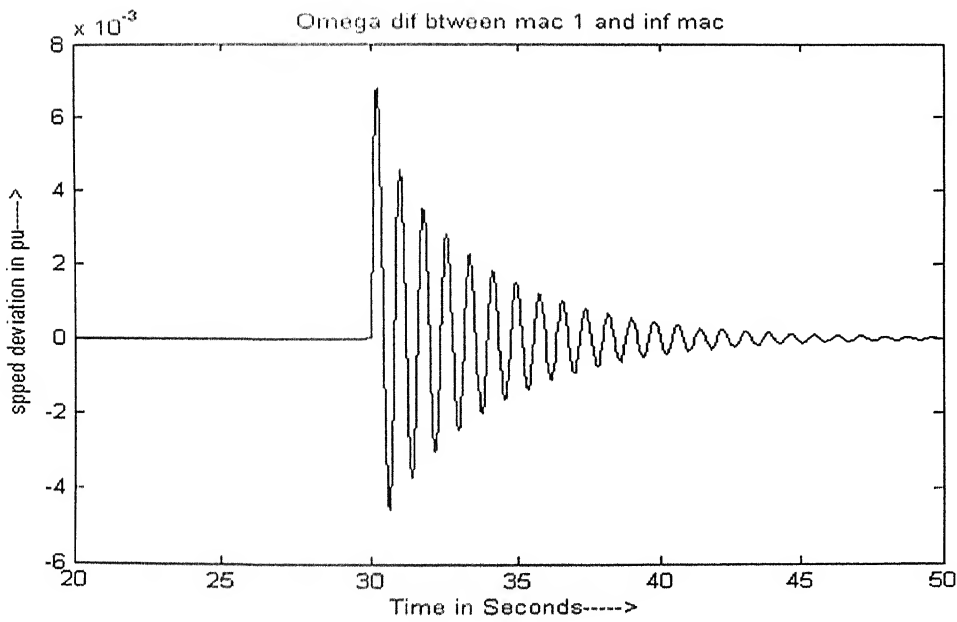


Fig. 3.22: Speed difference between kaiga-1 and swing machine

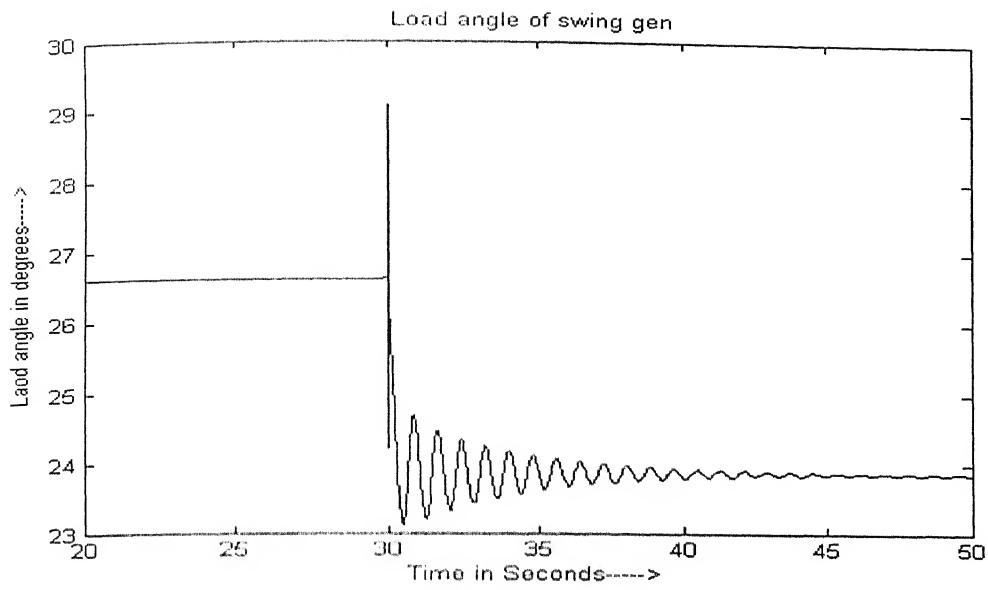


Fig. 3.23: Load angle of swing generator

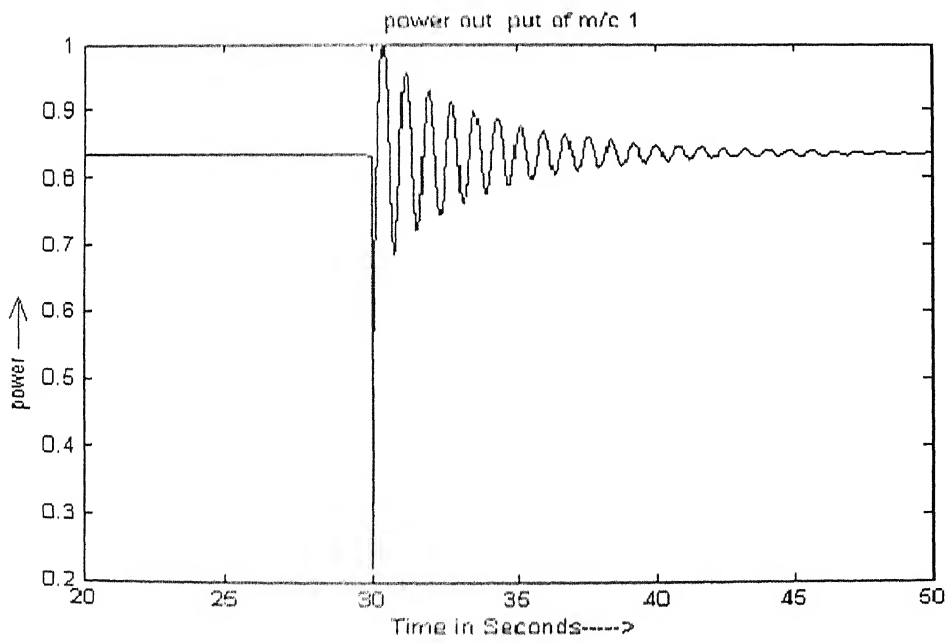


Fig. 3.24: Power output of Kaiga-1

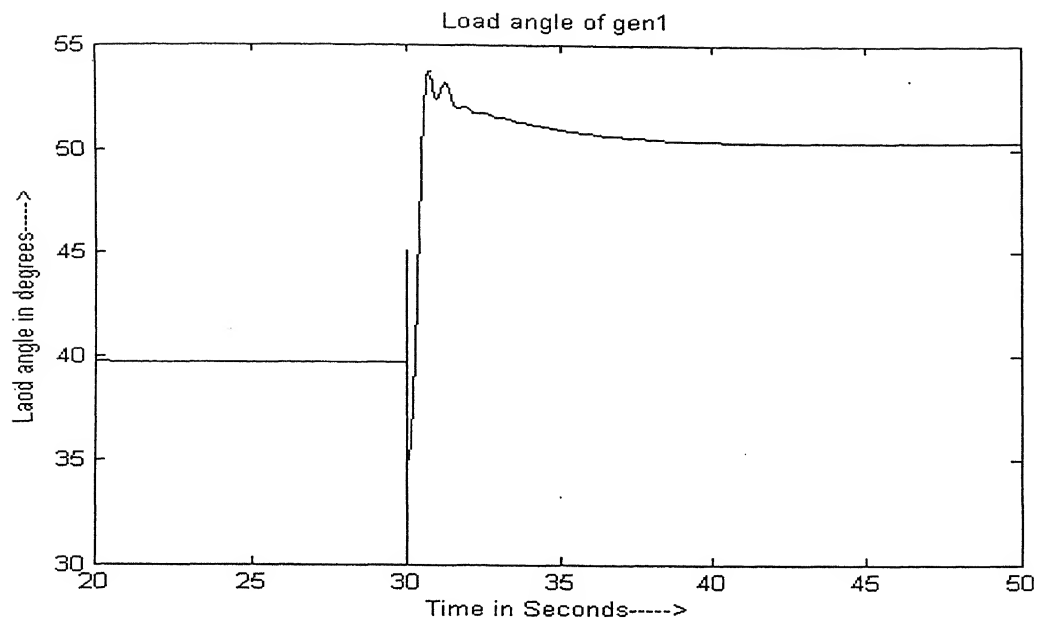


Fig. 3.25: Load angle of Kaiga-1, with PSS for reduced NPC system

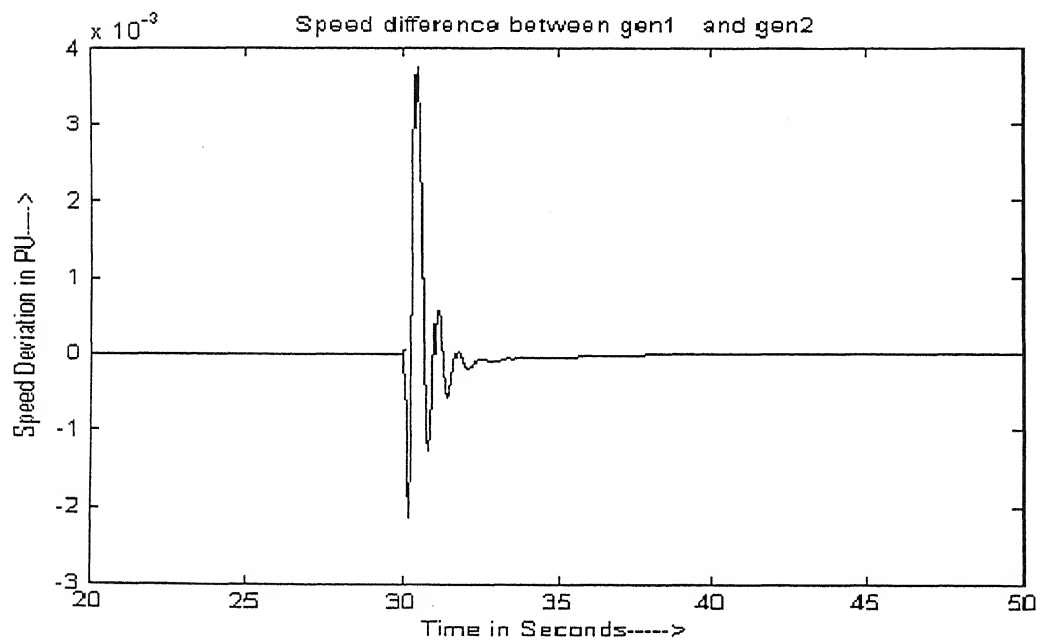


Fig. 3.26: Speed difference between Kaiga-1 and 2

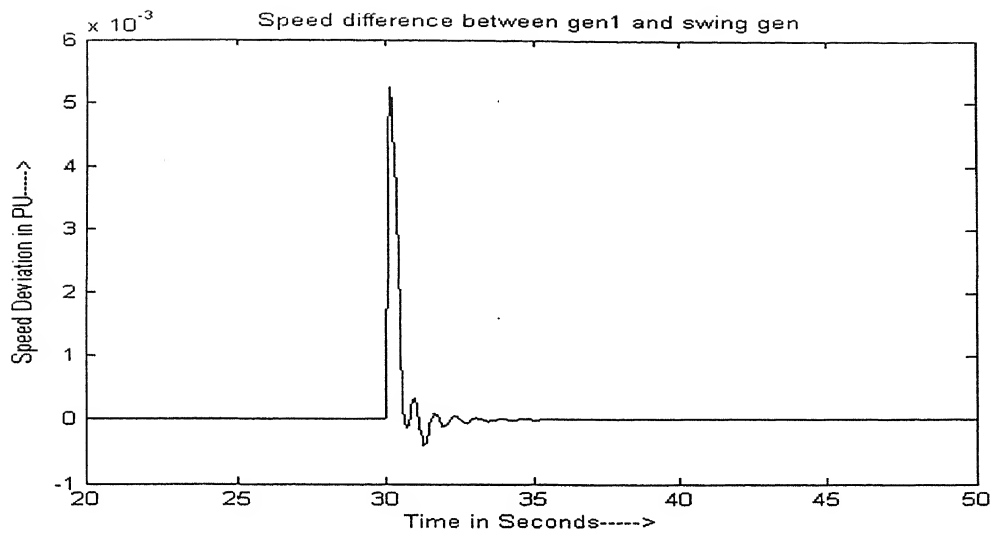


Fig. 3.27: Speed difference between Kaiga-1 and swing generator

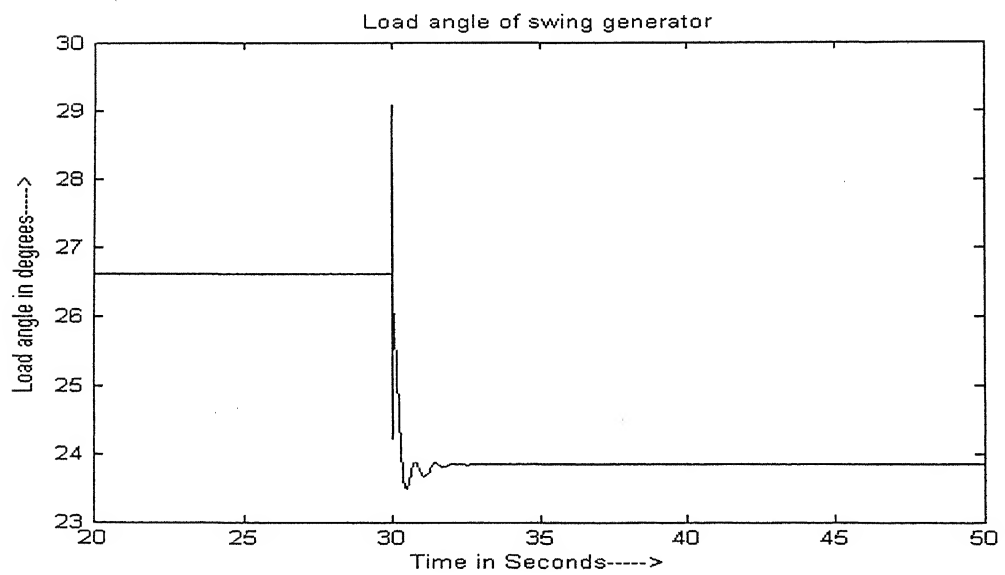


Fig. 3.28: Load angle of swing generator

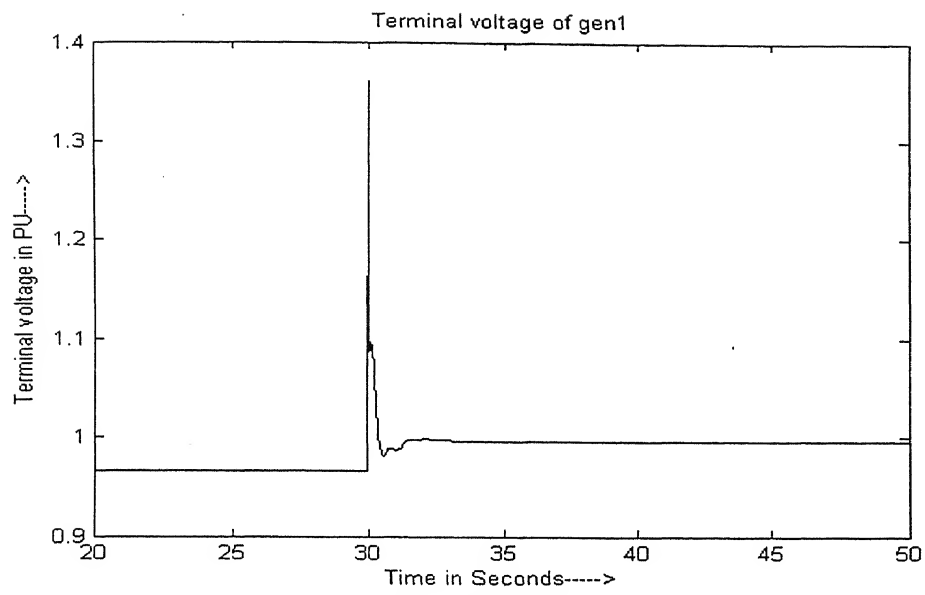


Fig. 3.29: Terminal voltage at Kaiga-1

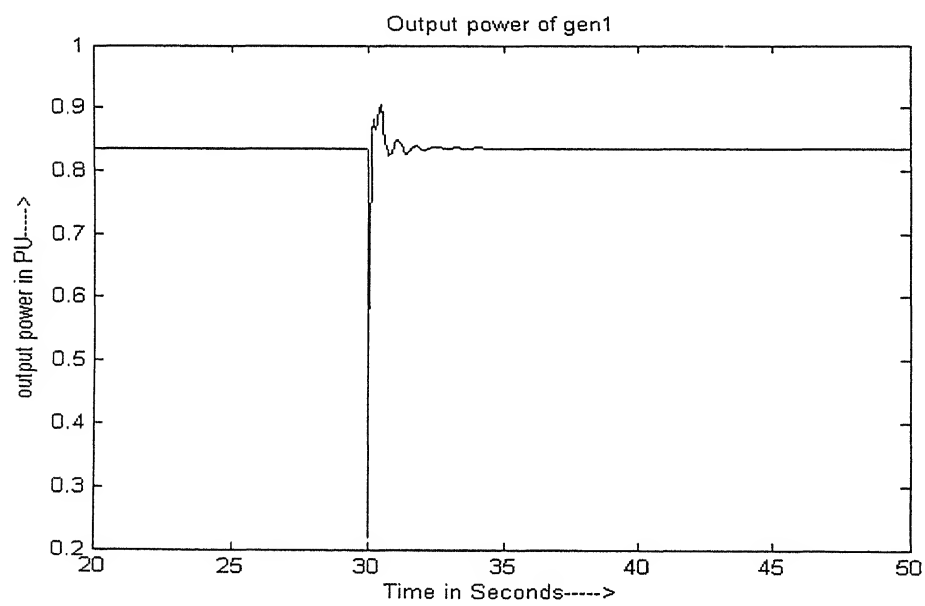


Fig. 3.30: Power output of Kaiga-1

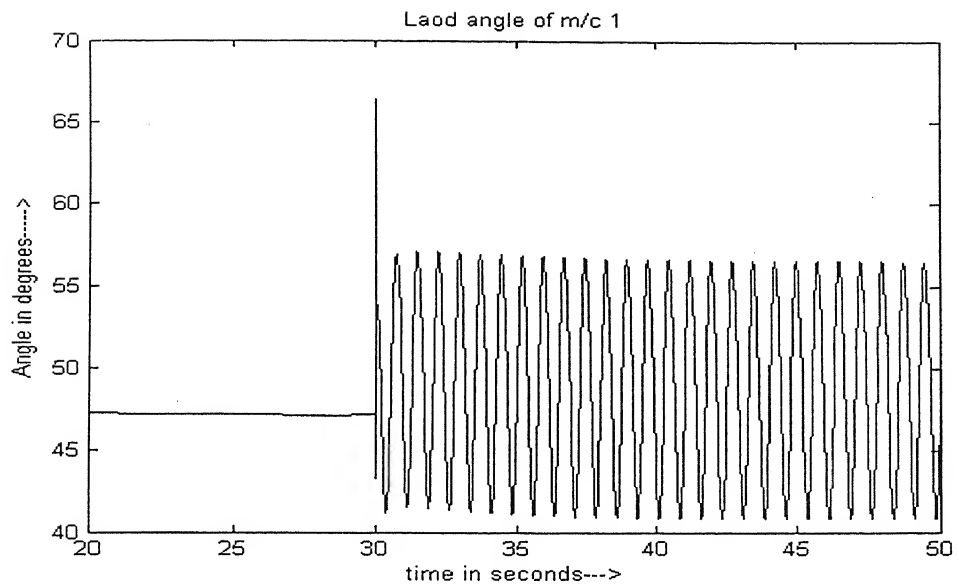


Fig. 3.31: Load angle of Kaiga-1 in detail model without PSS, for detailed NPC system

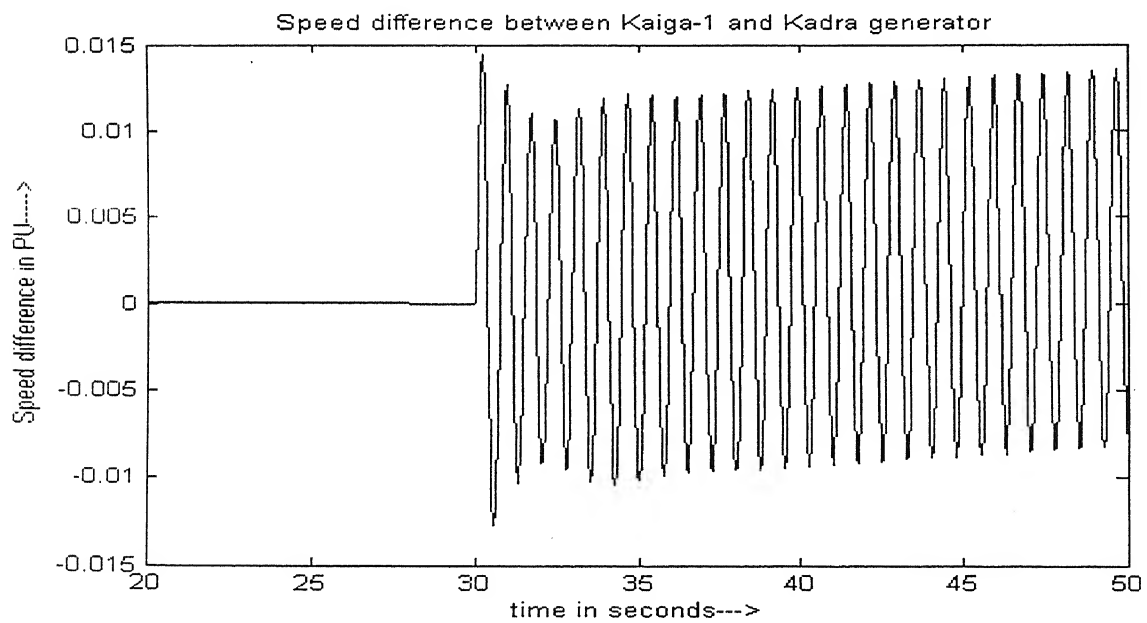


Fig. 3.32: Speed difference between Kaiga-1 and Kadra hydro

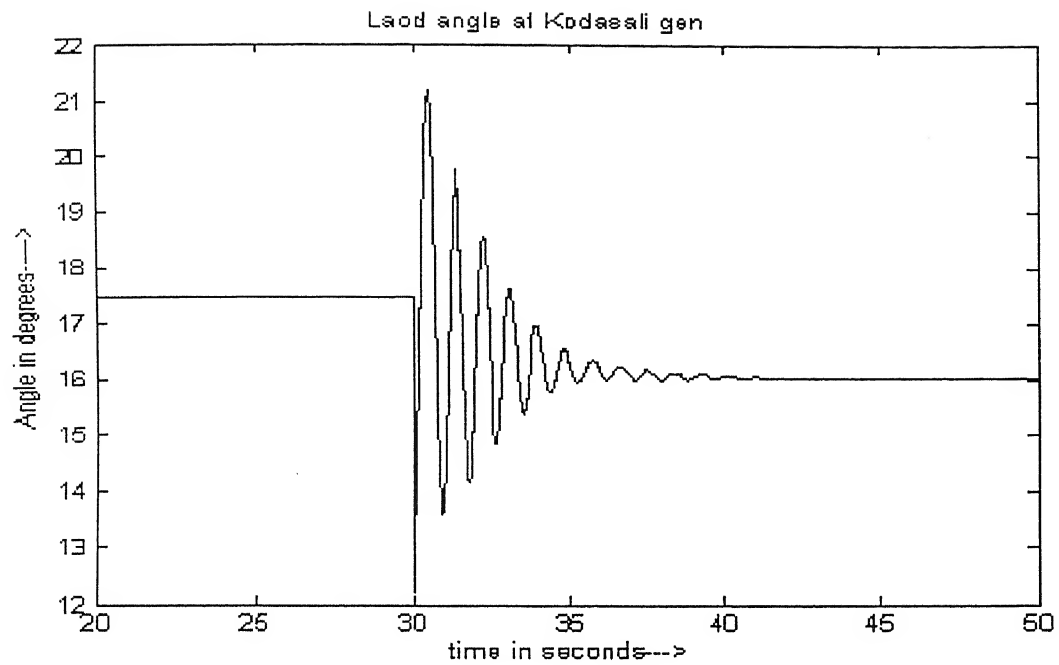


Fig. 3.33: Load angle at Kodasali Hydro

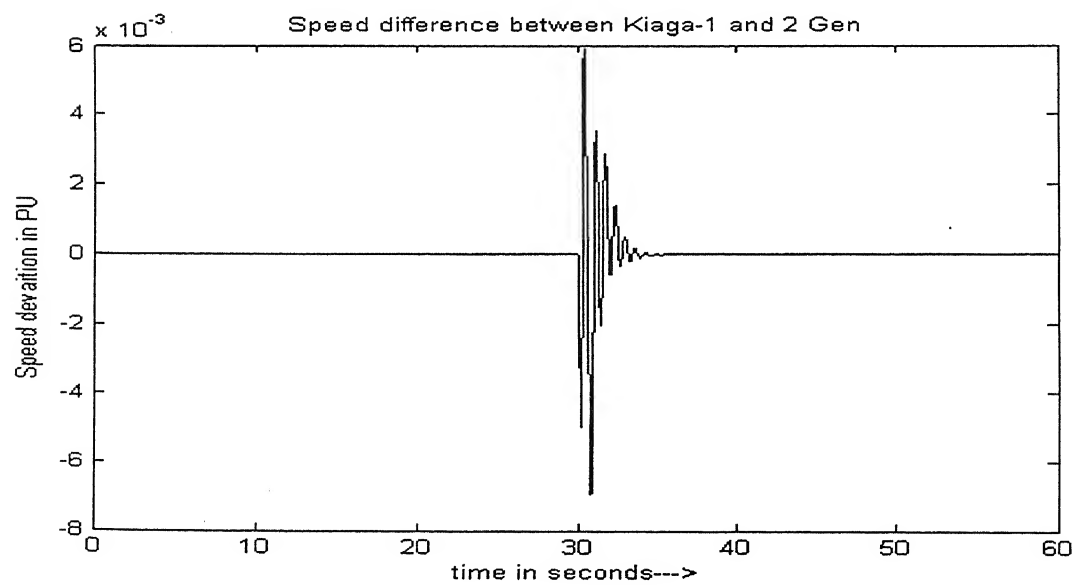


Fig. 3.34: Speed difference between Kaiga-1 and 2

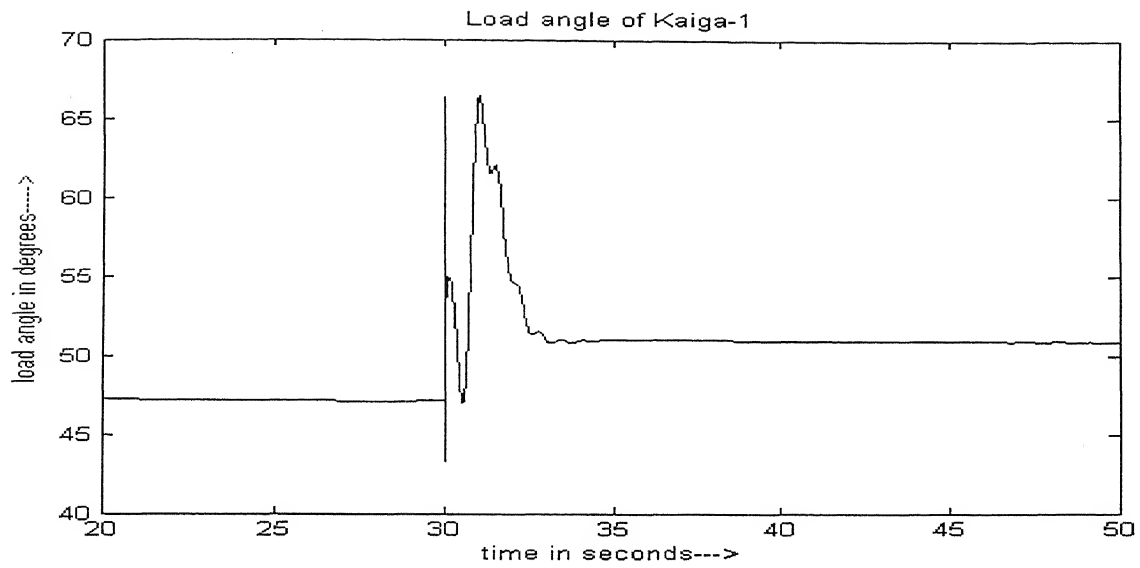


Fig. 3.35: Load angle of Kaiga-1, for detailed NPC system with PSS at Kiaga-1

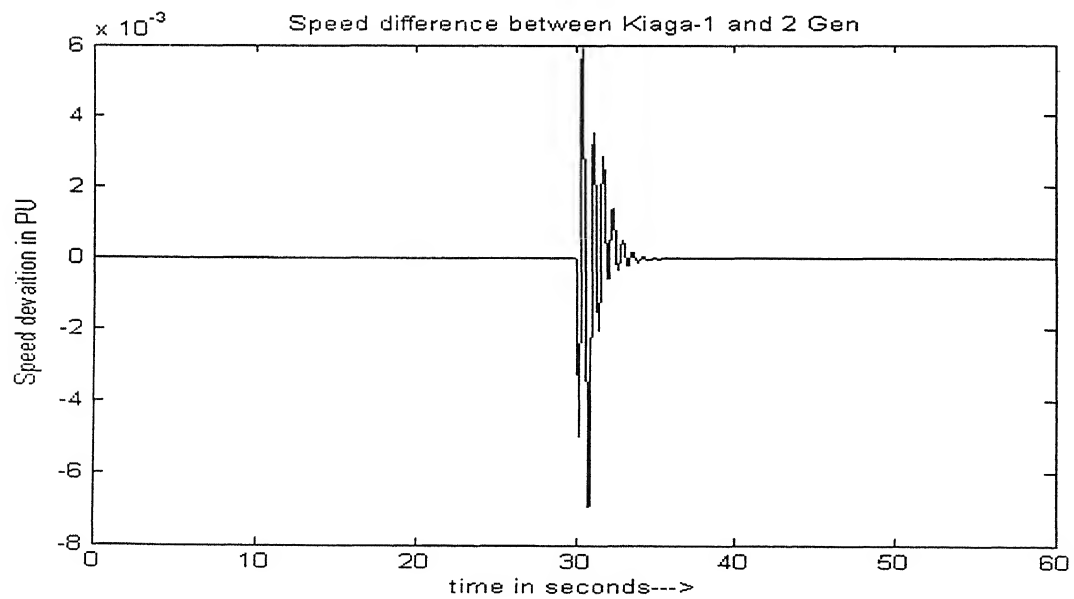


Fig. 3.36 Speed difference between Kaiga-1 and 2

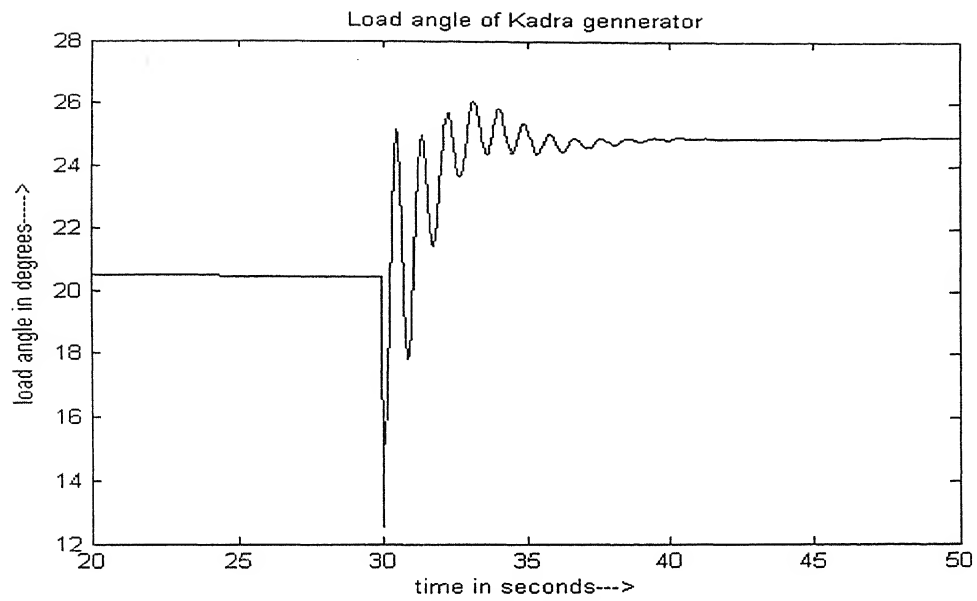


Fig. 3.37: Load angle at Kadra hydro

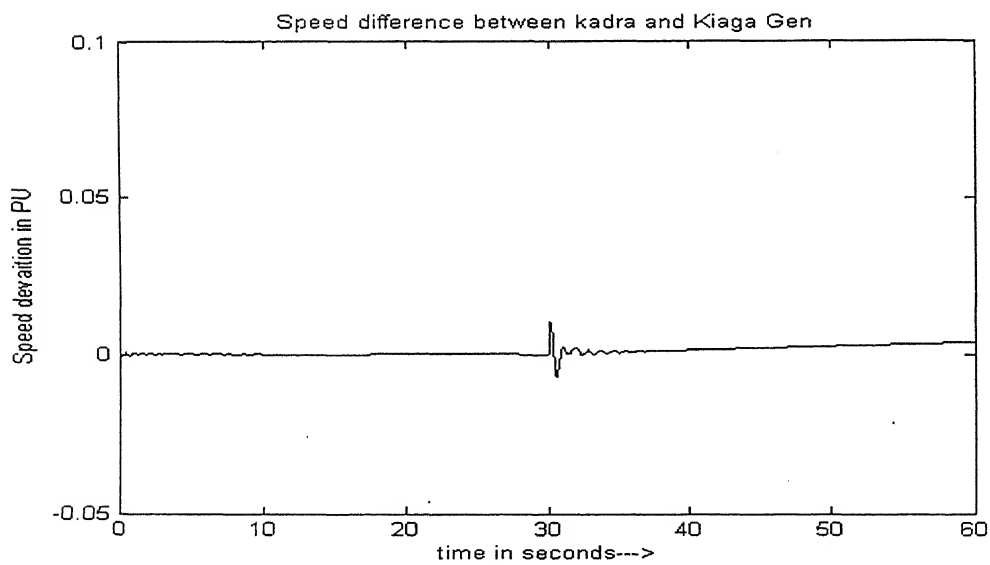


Fig. 3.38 Speed difference between Kaiga-1 and Kadra

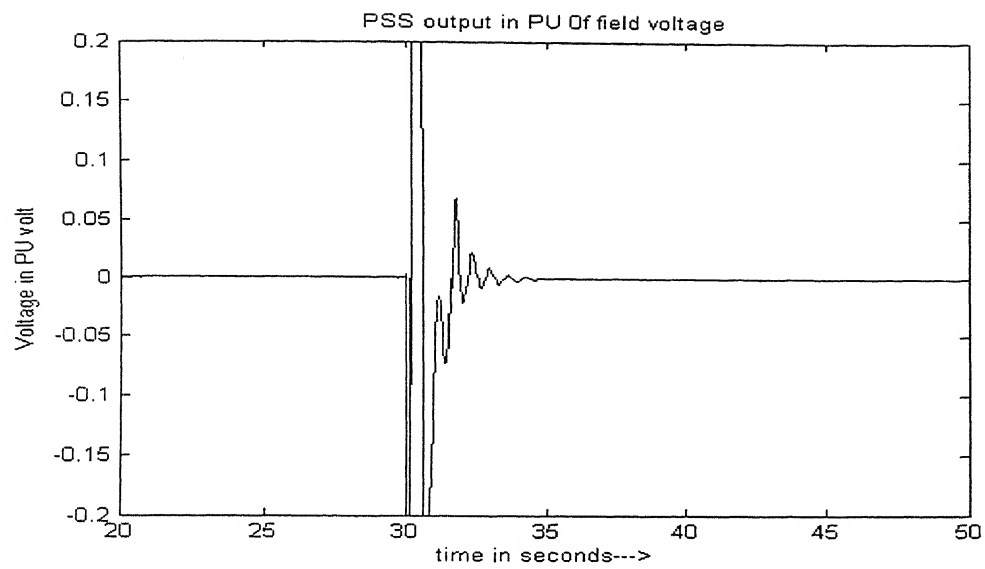


Fig. 3.39: PSS output at Kaiga-1

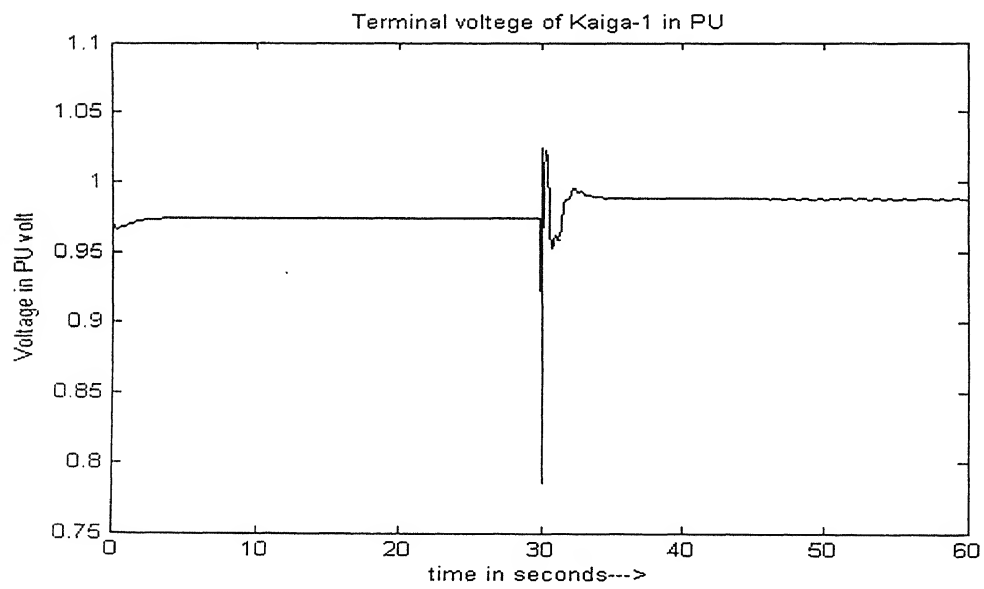


Fig. 3.40: Terminal voltage at Kaiga-1

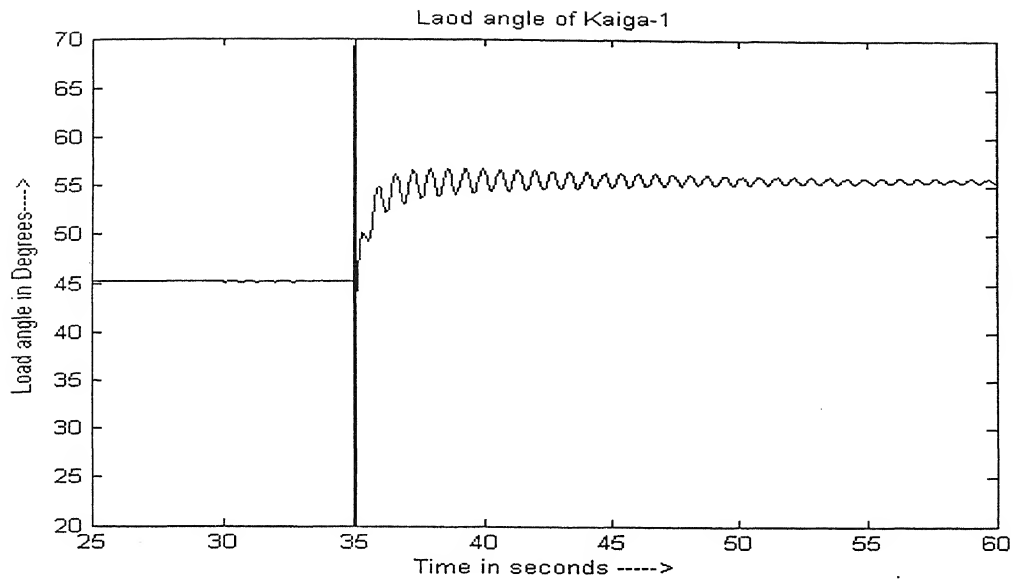


Fig. 3.41: Load angle at Kaiga-1 with a three phase fault cleared in 3 cycles, for Kaiga generator with 16 other generators

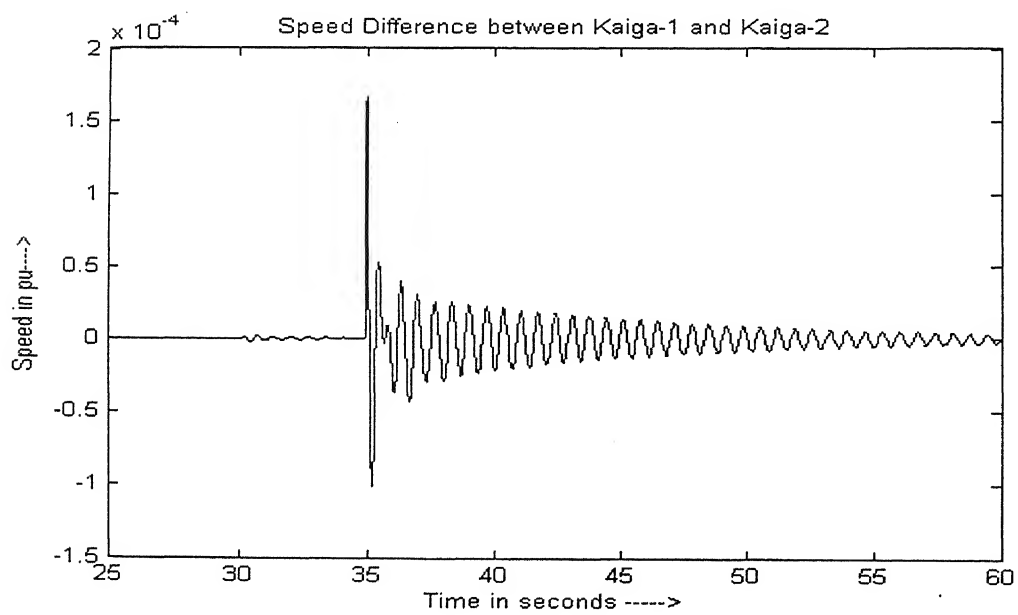


Fig. 3.42: Speed difference between kaiga-1 and 2

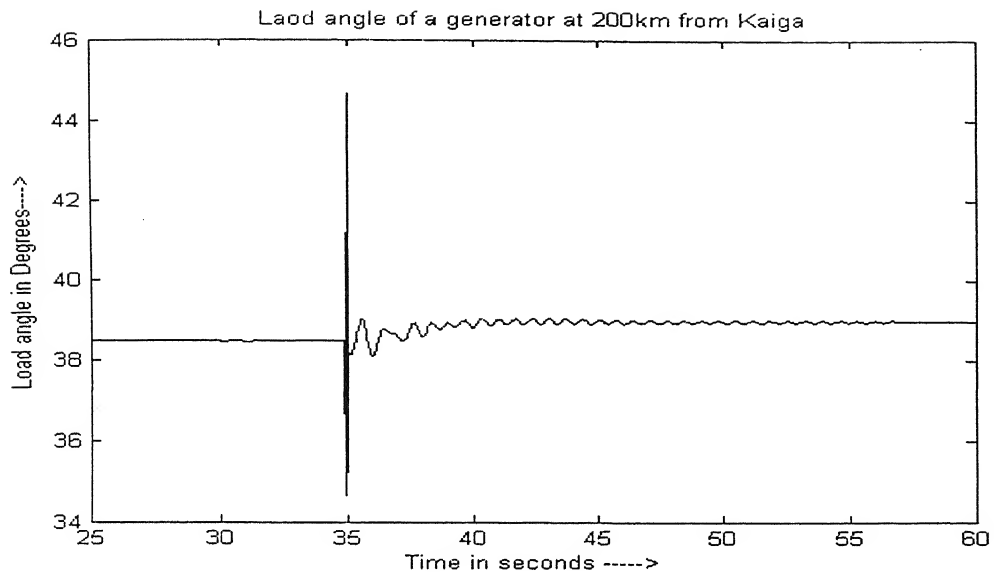


Fig. 3.43: Load angle of generator 200km from Kaiga

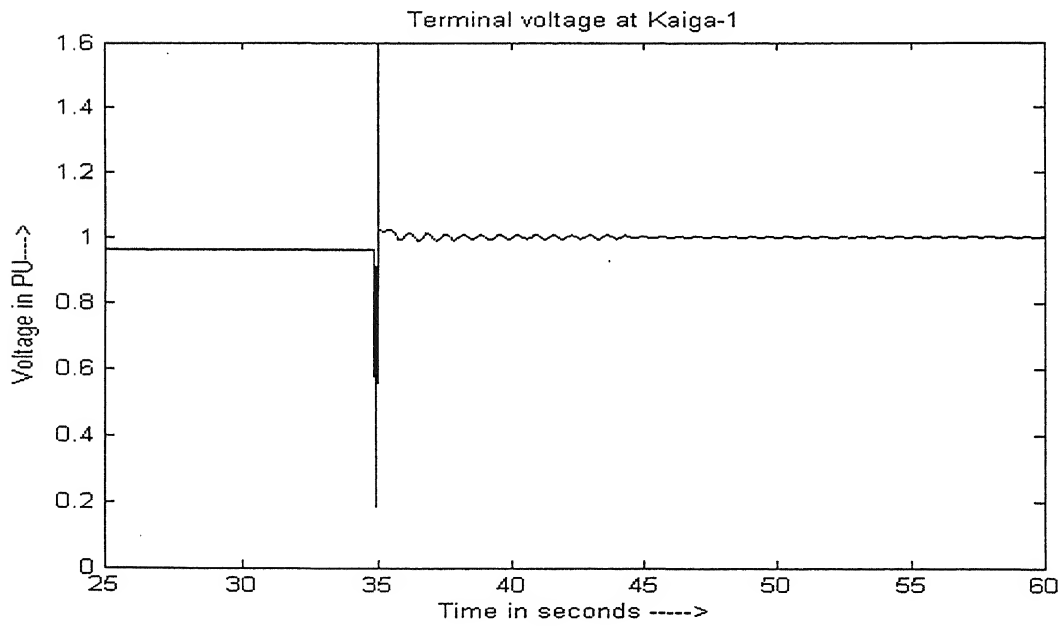


Fig . 3.44: Terminal voltage at Kaiga-1

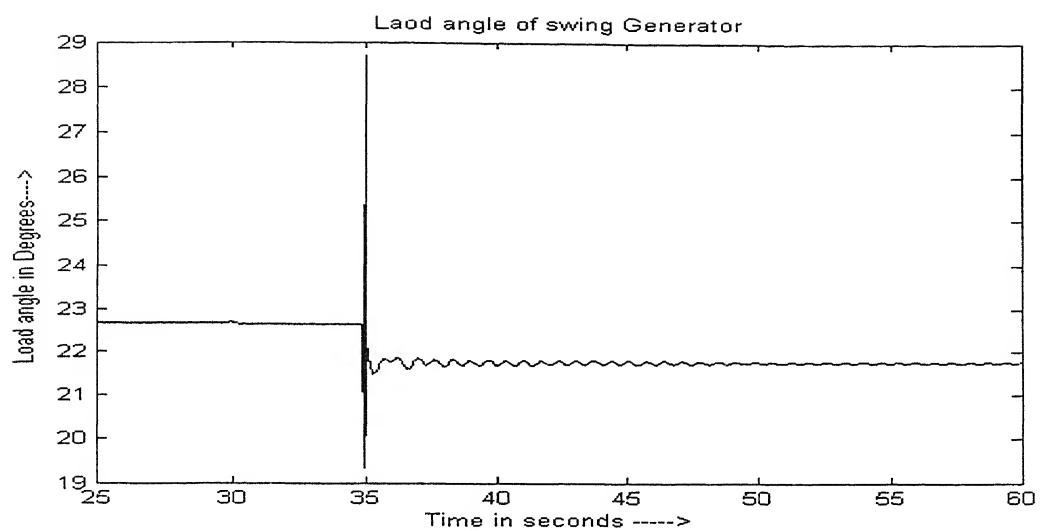


Fig. 3.45: Load angle of swing generator

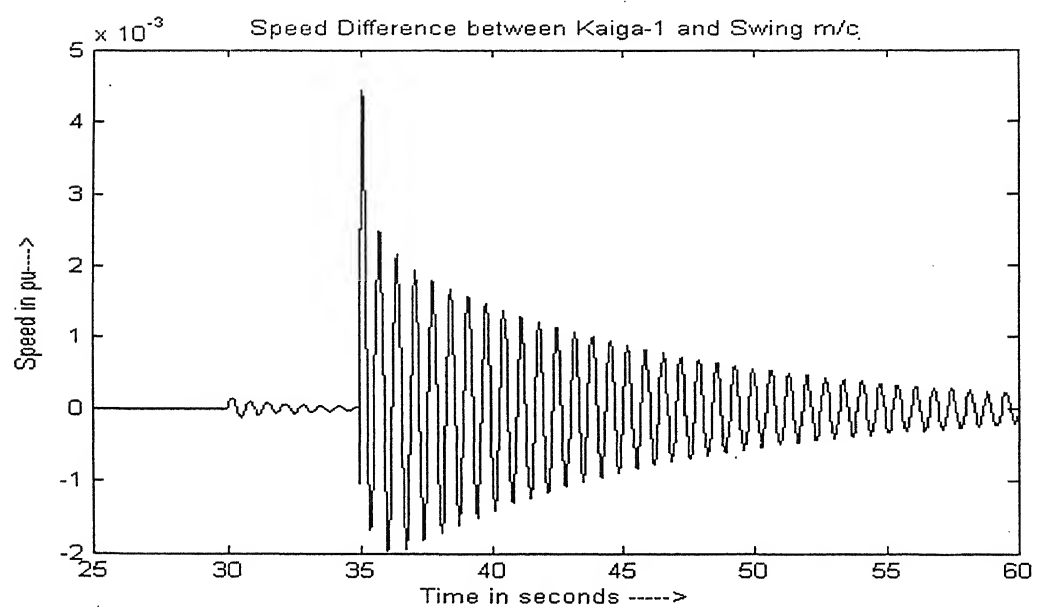


Fig. 3.46: Speed difference between Kaiga-1 and infinite generator

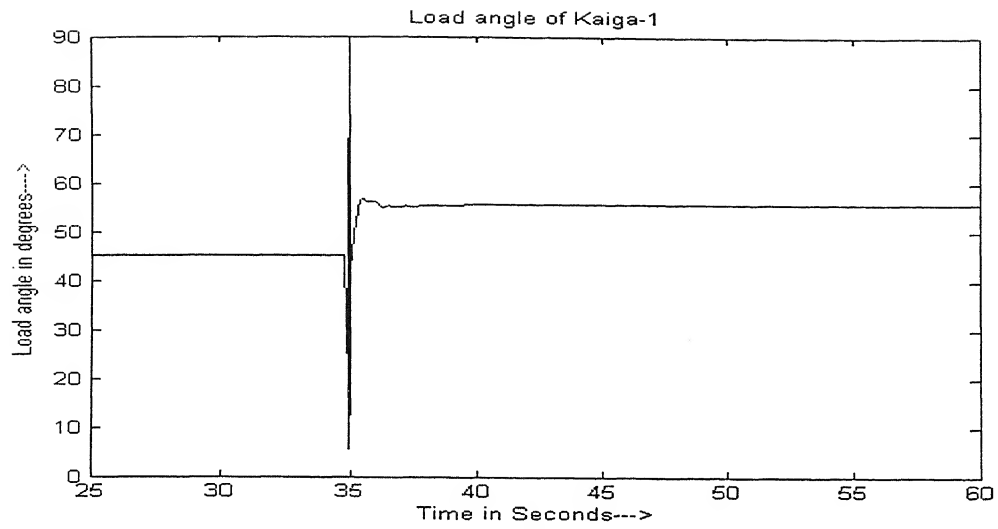


Fig. 3.47 Load angle of Kaiga-1, for Kaiga system with 16 other generators

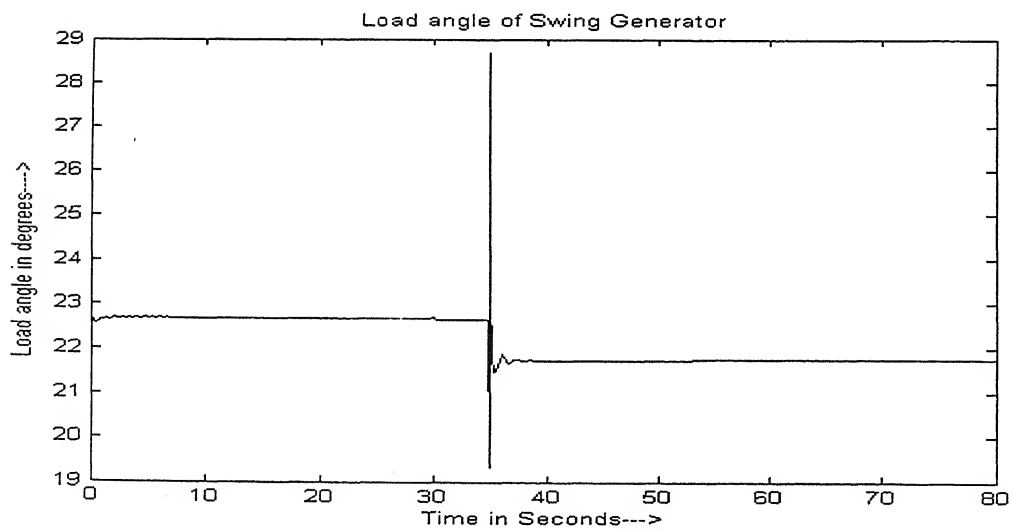


Fig. 3.48: Load angle of swing generator

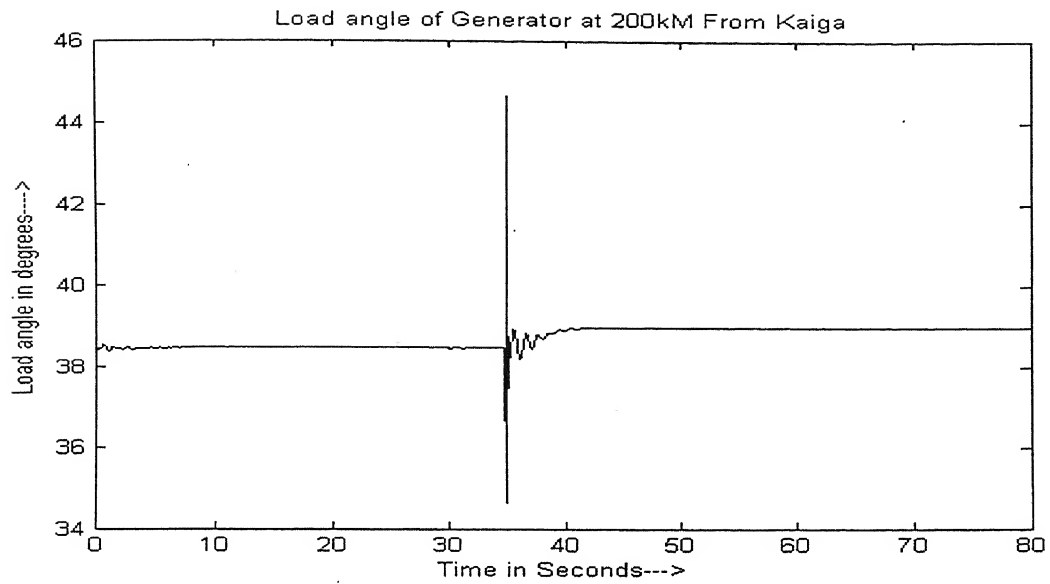


Fig. 3.49: Load angle of generator 200km from Kaiga

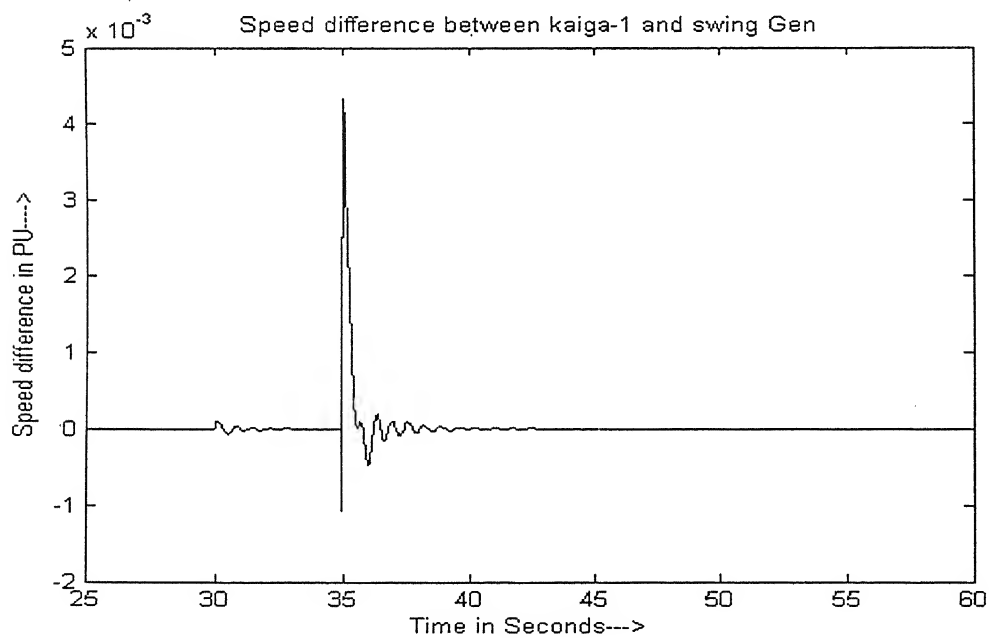


Fig. 3.50: Speed difference between Kaiga-1 and swing generator

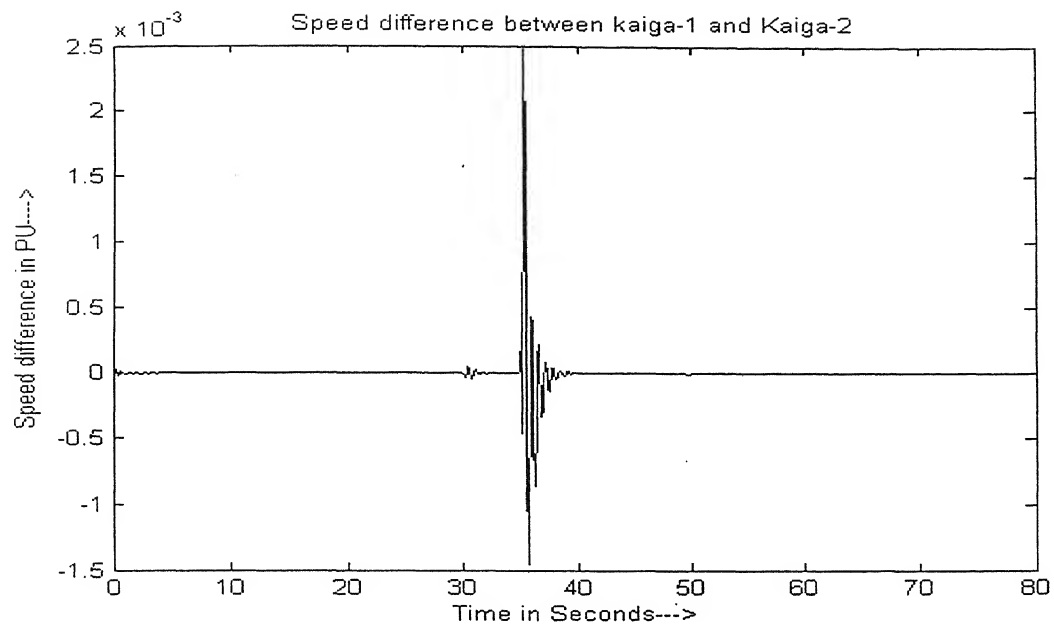


Fig. 3.51: PSS output of Kaiga-1

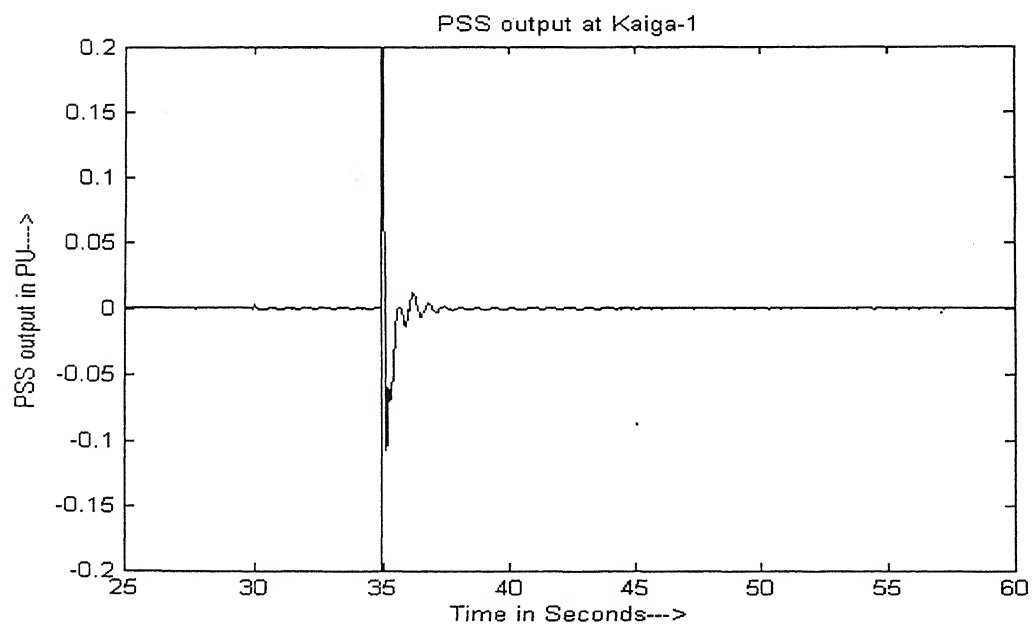


Fig. 3.52: Speed difference between kaiga-1 and 2

3.6 Conclusion

Kaiga generators are working satisfactorily when there is no trip of Kaiga- Kadra and Kaiga- Kudasalli lines. But when both of the two lines trip, there is sustained oscillation of about 1.2 Hz. This is also verified by simulation studies. When the ratio T_i/T_2 is 0.5 there are sustained oscillations. But for the ratio of 0.25, with same loading conditions, the oscillations die out rapidly. The PSS tuned is shifting the eigen values to the safe damping region there by improving the system dynamic performance. This is also proved through non-linear simulation. The determining factors of PSS performance i.e. K_1 and K_2 changes while the system configuration is altered by incorporating the ICT or adding a new line etc. So again an intelligent PSS has to be considered for the system.

Fuzzy Logic Based PSS Design

4.1 Introduction

Conventional PSSs (CPSSs) have been developed using linear control theory to damp the oscillation of synchronous machine rotor under transient conditions [10]. Power systems are highly non-linear and stochastic in nature because of non-linear loads like induction motor, FACTS and HVDC controllers. Also day-by-day increase in demand and competition in power market, the power system is becoming very large and complex in nature. The control parameters which are optimal for one set of operating conditions may not be optimum for another set of operating conditions. This is also demonstrated in previous chapter. In some cases, the fixed parameter of PSS may have detrimental effect on system dynamic performance. For example when a severe disturbance occurs in the system, the AVR forces the field voltage to increase up to the ceiling voltage which is known as field forcing [19]. But the CPSS will try to take it out of the ceiling as soon as possible, which may lead to system instability.

Limitations of fixed parameter of conventional PSS has lead to advanced control schemes such as self tuning control [22], rule based PSS [14], and fuzzy logic control [14]. Adaptive control and self tuning techniques require intensive computations and difficult to implement. Unlike the classical approach which requires a deep understanding of the system, fuzzy logic incorporates an alternative way of thinking, allowing complex system to be modeled from accumulated knowledge and experience. A detailed knowledge or mathematical model of power system is not required to design Fuzzy Logic PSS (FLPSS). The basic feature of fuzzy logic controllers is that the control strategy can be simply expressed by a set of rules which describe the behaviour of the controller using linguistic terms [22]. Proper control action is then inferred from these rules. In addition, FLC are relatively easy to develop and robust as compared to CPSSs.

4.2 Fuzzy Logic Controller (FLC)

In conventional control, the amount of control is determined in relation to a number of data inputs using a set of equations to express the entire control process. Expressing human experience in the form of a mathematical formula is a very difficult task. Fuzzy logic provides a simple tool to interpret this experience into reality. In recent years, fuzzy logic has emerged as a powerful tool and is starting to be used in various power system applications. The application of fuzzy logic control technique appears to be most suitable one whenever a well-defined control objective can not be specified and the system to be controlled is a complex one or its exact mathematical model is not available. Fuzzy Logic Controllers (FLCs) are robust and have relatively low computational requirements. They could be constructed easily using a simple microcomputer.

Fuzzy logic controllers are rule-based controllers. The structure of the FLC resembles a knowledge-based controller except that the FLC utilizes the principle of fuzzy set theory [26] in its data representation and its logic. The basic configuration of the FLC can be simply represented in four parts as shown in Fig.4.1

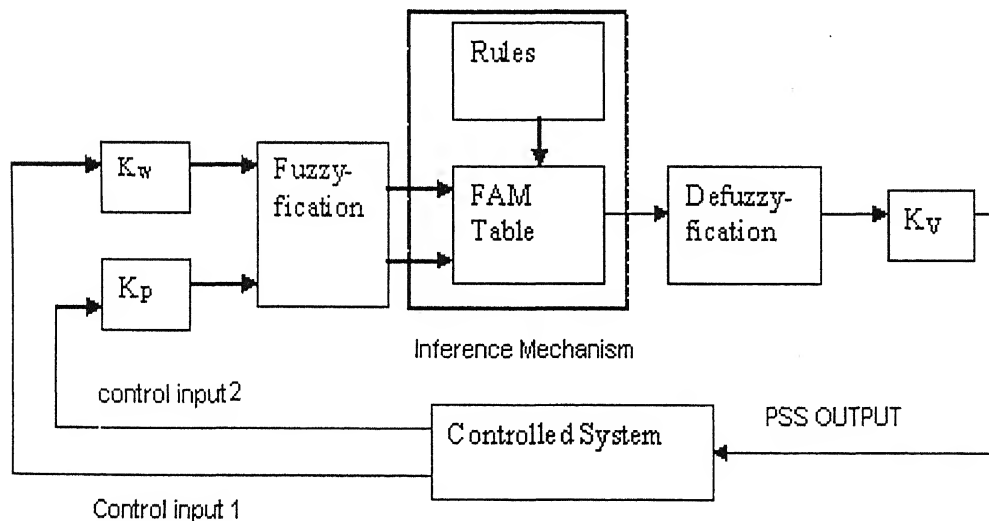


Fig. 4.1: Schematic diagram of the FLC building blocks

1. Fuzzification module

Fuzzification is a process whereby the crisp inputs are mapped onto corresponding linguistic (fuzzy) variables. These linguistic variables are used for making decisions. Each

linguistic variable or Fuzzy set has a certain membership function. The membership function assigns a certain degree of membership or weight to each of the linguistic variables. The membership value is nothing but the truth of belongingness of a certain input to that fuzzy set or linguistic variable.

2. Inference mechanism

Control decisions can now be made based on the linguistic variables. It performs two functions. Firstly assigns degree of membership or weight to the variables and secondly determines the output decisions or output linguistic variables based on input linguistic variables. The definitions of the fuzzy membership functions corresponding to each fuzzy set and the necessary rules defining the output goal are included in a knowledge base

3. Defuzzification mechanism

This converts the fuzzy set of output variables to crisp numerical outputs. These crisp values are the final control inputs to the controlled system.

4.3 FLC Design

The design process of an FLC may be divided into the five steps described below.

(I) Selection of Control Variables

The selection of control variables (controller inputs and outputs) depends on the nature of the controlled system and the desired output. It is more common to use the output error (e) and the rate or derivative of the output (e') as controller inputs.

(II) Membership Function Definition

Each of the FLC input signals and output signals, fuzzy variables, have the real line R as the universe of discourse. In practice, the universe of discourse is restricted to a comparatively small interval $[X_{\min}, X_{\max}]$. The number of fuzzy sets for each fuzzy variable varies according to the application. A common and reasonable number of variables are odd number. Increasing the number of fuzzy sets results in a corresponding increase in the number of rules. A membership function is assigned to each fuzzy set. The membership

function maps the crisp values into fuzzy values. A set of membership functions defined for seven linguistic variables NB, NM, NS, Z, PS, PM, PB, which stand for Negative Big, Negative Medium, Negative Small, Zero, Positive Small, Positive Medium, Positive Big, respectively as shown in Fig. 4.2.

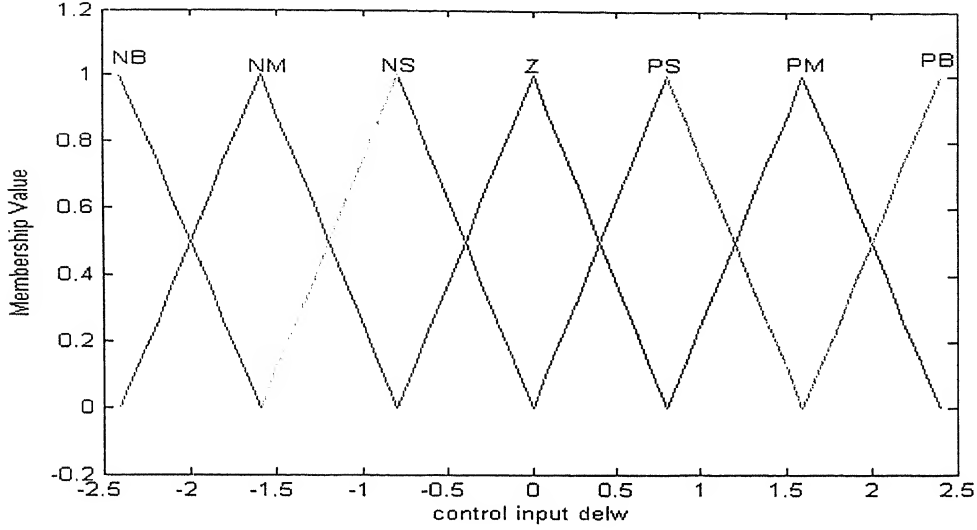


Fig. 4.2: Seven triangular membership functions

Membership function can be of a variety of shapes, the most usual being triangular, trapezoidal, or a bell shaped. The Fig. 4.2 shows a triangular membership function for speed deviation as fuzzy variable and is used for design of FLPSS. For simplicity, it is assumed that the membership functions are symmetrical and each one overlaps with the adjacent functions by 50%. In practice, the membership functions are normalized in the interval $[-L, L]$, which is symmetrical around zero. Thus control signal amplitudes (fuzzy variables) are expressed in terms of controller parameters (gain). These parameters can be defined as:

$$K_j = \frac{2L}{X_{rangej}} \quad (4.1)$$

where X_{rangej} defines full range of the control variable X_j , that is,

$$X_{rangej} = X_{maxj} - X_{minj} \quad (4.2)$$

X_{minj} and X_{maxj} are the maximum and the minimum values, respectively of the control variable X_j . The input and output gains K_j are referred to as FLC parameters. The selection of these parameters is usually based on the previous knowledge of the controlled system.

(III) Rule Creation and Inference

In general, fuzzy systems, as function estimators, map an input fuzzy set to an output fuzzy set $S: I^n \rightarrow I^p$. Fuzzy rules are the relations between the fuzzy sets. They usually are in the form, "if A , then B ," where A is the rule antecedent and B is the rule consequence. Each rule defines a fuzzy patch in the Cartesian product $A \times B$ (system state space). The antecedents of each fuzzy rule describe a fuzzy input region in the state space. This enables one to effectively quantize continuous state space so that it covers a finite number of such regions [22]. In terms of associative memory definition (FAM), each rule represents an association $(A_i; B_i)$. A fuzzy system using two antecedents and one consequence $(A, B; C)$ is shown in Fig.3.3. The association $(A_i, B_i; C_i)$ or the rule of " A_i and B_i then C_i " maps inputs A, B to C^i , a partially activated version of C . The corresponding output fuzzy set C combines the partially activated sets C^1, C^2, \dots, C^m , that is,

$$C = \sum_{i=1}^m C^i \quad (4.3)$$

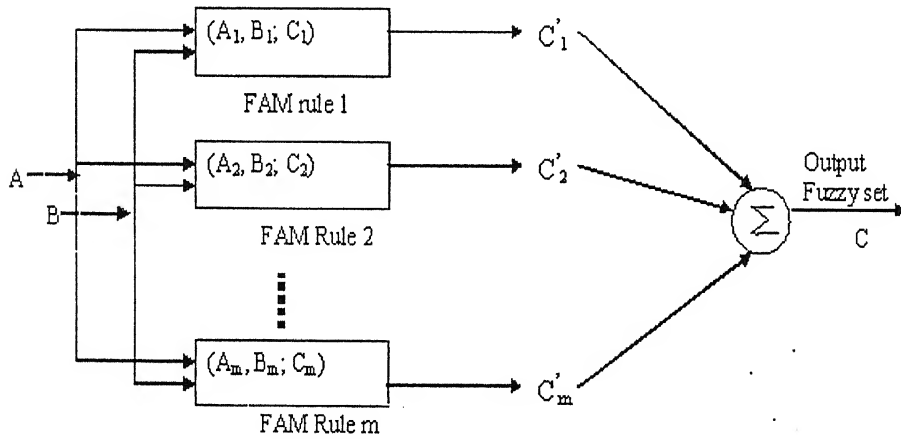


Fig. 4.3: FAM system architecture for two fuzzy antecedents and one consequence

Consider a controller of two fuzzy variables, error (e) and derivative of output (e'), and one output fuzzy variable, control strategy (μ), each quantized to seven fuzzy sets. This leads to a 7 X 7 FAM rule matrix, as shown in Fig. 3.4. Every entry in the matrix represents a rule, for example,

If e is NB and e' is NM, then U is NB.

Error Derivative

	NB	NM	NS	Z	PS	PM	PB
Error	NB	NB	NB	NB	NM	NS	Z
	NM	NB	NB	NM	NS	Z	PS
	NS	NB	NM	NS	Z	PS	PM
	Z	NM	NM	NS	Z	PS	PM
	PS	NM	NS	Z	PS	PM	PB
	PM	NS	Z	PS	PM	PB	PB
	PB	Z	PS	PM	PB	PB	PB

Fig. 4.4: Fuzzy control rule matrix

The activation of the i th rule consequent is a scalar value w_i , which equals the minimum of the two antecedent conjuncts' values. For example, if e belongs to NB with a membership of 0.3 and e' belongs to NM with a membership of 0.7, then the rule consequence w_i will be 0.3. The knowledge required to generate the fuzzy rules can be derived from an off-line simulation, an expert operator, and/or a design engineer. Some of the knowledge can be based on understanding of the dynamic system being controlled.

(IV) Fuzzy Inference

The well-known inference mechanisms in fuzzy logic are the correlation –minimum-encoding and the co-relation-product encoding. The correlation minimum encoding is based on the fuzzy outer product notation. The max-min composition operator is denoted by the composition operator ' \circ '. Thus the fuzzy outer product of the fit row vectors A and B , which forms the FAM matrix M :

$$M = A \circ B, \text{ where } m_{ij} = \min(a_i, b_j) \quad (4.4)$$

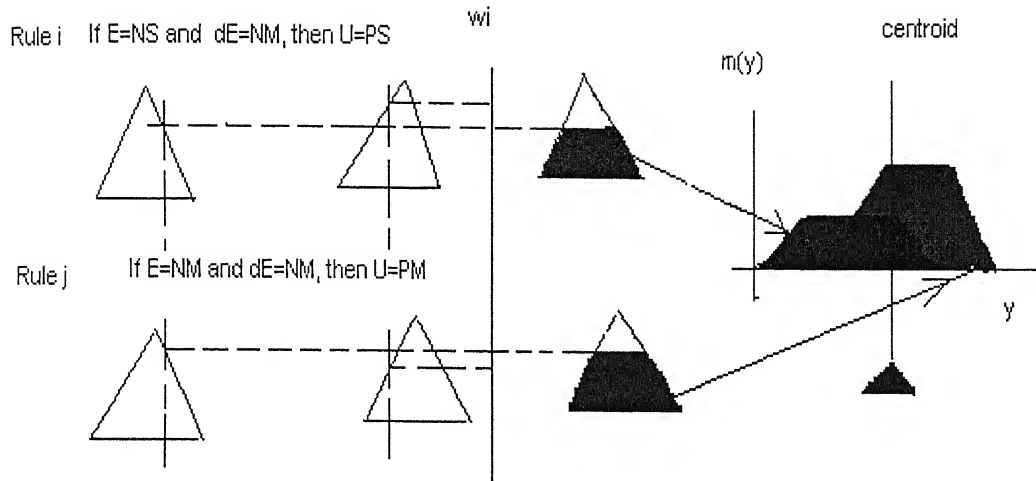


Fig. 4.5: Generation of the output fuzzy set using correlation minimum encoding

The correlation product encoding uses the standard mathematical outer product of the fit vectors A and B to form the FAM matrix M:

$$\mathbf{M} = \mathbf{A}^T \mathbf{B}, \text{ where } m_{ij} = a_i b_j \quad (4.5)$$

(V) Defuzzification Strategy

Defuzzification is a process of converting the FLC inferred control actions from fuzzy values to crisp values. This process depends on the output fuzzy set, which is generated from the fired rules [Eq. (4.3)]. The output fuzzy set is formed by either a correlation-minimum encoding or the correlation product encoding as discussed in (IV).

Commonly used defuzzification methods are discussed here:

(1) Centroid Method

This procedure also known as center of area or center of gravity method is the most prevalent and physically appealing of all the defuzzification methods. It is given by the algebraic expression

$$Z^* = \frac{\int \mu(z) \cdot z \, dz}{\int \mu(z) \, dz} \quad (4.6)$$

where, $\mu(z)$ is the control strategy for the input variable 'z'. Here \int denotes an algebraic integration.

(2) Weighted Average Method

This method is valid only for symmetrical membership functions. It is given by the algebraic expression

$$z^* = \frac{\sum \mu(z).z}{\sum \mu(z)} \quad (4.7)$$

where, $\mu(z)$ is the control strategy for the input variable 'z'. The weighted average method is formed by weighting each membership function in the output by its respective maximum membership value.

(3) Max-membership Principle

Also known as height method, this scheme is limited to peaked output functions. This method is given by the algebraic expression

$$\mu(z^*) \geq \mu(z) \quad (4.8)$$

4.4 FLPSS Design

A power system stabilizer based on the FLC algorithm can be designed for damping the power system oscillations. Since the goal of this application is to stabilize and improve the damping of the synchronous machine, speed deviation and active power deviation have been selected as controller input [10]. Other options like speed deviation and rate of speed deviation, speed deviation and field voltage deviation are also considered. Field voltage deviation as one of the inputs is very appealing from the practical point of view, because it is very easy to measure as compared to other machine states. As shown in Fig. 4.6 the FLC has two input parameters, K_v and K_p , and one output parameter, K_U . The selection of these parameters is usually subjective and requires previous knowledge of the fuzzy control variables (input and output signals). Also previous experience of the controlled system dynamics is commonly used in the creation of the fuzzy control rules.

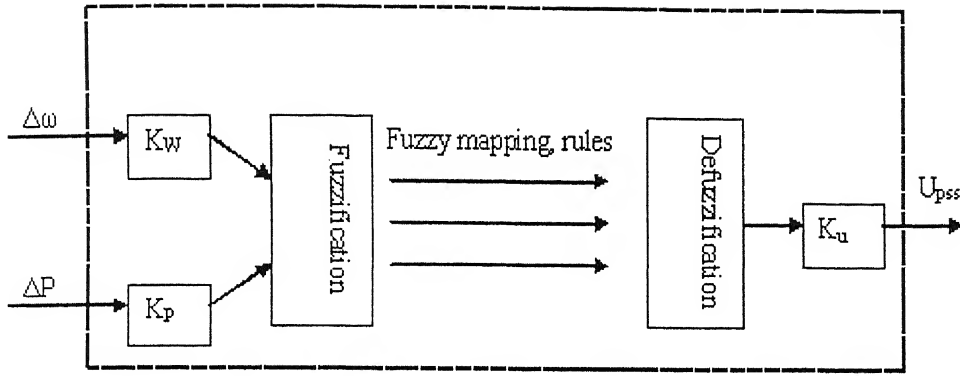


Fig. 4.6: Schematic diagram of the FLPSS

4.4.1 FAM table formation

The previous knowledge of the system parameter variations with conventional PSS is used here for the rule base formation. For that, a three phase fault is simulated at the generator terminals (the worst case of a fault), and the variation of the required parameters is observed. The PSS output is also observed. Same as the FLC design procedures the input and output signals of the FLPSS are divided into seven linguistic variables or fuzzy sets, such as NB, NM, NS, Z, PS, PM, PB. They have their usual meaning as described above. Depending on the variation in conventional case the FAM table was formed, where each entry in the table represents a rule.

1. Rule Base for $\Delta\omega$ and ΔP_e as Input Signals (Fig. 4.7)

		Active Power Deviation						
		NB	NM	NS	Z	PS	PM	PB
Speed Deviation	NB	NB	NB	NB	NB	NM	NS	Z
	NM	NB	NB	NM	NM	NS	Z	PS
	NS	NB	NM	NS	NS	Z	PS	PM
	Z	NM	NM	NS	Z	PS	PM	PM
	PS	NM	NS	Z	PS	PS	PM	PB
	PM	NS	Z	PS	PM	PM	PB	PB
	PB	Z	PS	PM	PB	PB	PB	PB

Fig. 4.7: Fuzzy control rule matrix for $\Delta\omega$ and ΔP_e as PSS inputs

2. Rule base for $\Delta\omega$ and ΔE_{Fd} as Input Signals (Fig. 4.8)

		Change in Field Voltage						
Speed Deviation		NB	NM	NS	Z	PS	PM	PB
	NB	PB	PM	PS	Z	NS	NM	NB
	NM	PM	Z	NM	NS	NS	NM	NM
	NS	PM	PM	PS	Z	Z	NS	NM
	Z	PB	PS	PS	Z	NS	NS	NM
	PS	PM	PS	PS	Z	NS	NM	NB
	PM	PB	PM	PS	Z	NS	NS	NS
	PB	PB	PB	PM	Z	NS	NS	NB

Fig. 4.8: Fuzzy control rule matrix for $\Delta\omega$ and ΔE_{Fd} as PSS inputs

3. Rule base for $\Delta\omega$ and $\Delta \dot{\omega}$ as Input Signals

When rate change of speed $\Delta \dot{\omega}$ is used as input signal, it can be analyzed as the active power signal [2]. So instead of going for observation of the variation in case of the fault, the same rule base as rule base 1 is sufficient. Only during implementation, the rate change of speed signal has to be multiplied by twice of the inertia constant of the machine and inverted before feeding it to the FLPSS.

4.4.2 FLPSS Parameter Tuning

Once the proper rules are obtained, the proper parameter (K_w , K_p , and K_I) tuning should be done in order to achieve good performance. Tuning of FLPSS parameters can be a tedious trial-and-error process if not enough information is available about the range of the control variables and how they change with different disturbances.

4.5 Simulink Model for FLPSS

Fig. 4.9 shows the simulink model used for FLPSS realization. Fuzzy Inference System, (FIS) editor of Fuzzy logic toolbox is used for simulation. The inference mechanism used is correlation-minimum encoding type (Mamdani type, [22]). So it is

called as a Mamdani type FIS system. Centroid method or centre of gravity method is used for defuzzification. FLPSS output is given at the AVR summing point in place of CPSS as shown in the Fig. 3.10. The inputs to the controller are sampled at a rate of 20ms by a Zero Order Hold (ZOH) block. The MUX converts the dual inputs to a vector input to the controller. The input and output gains are the PSS parameters.

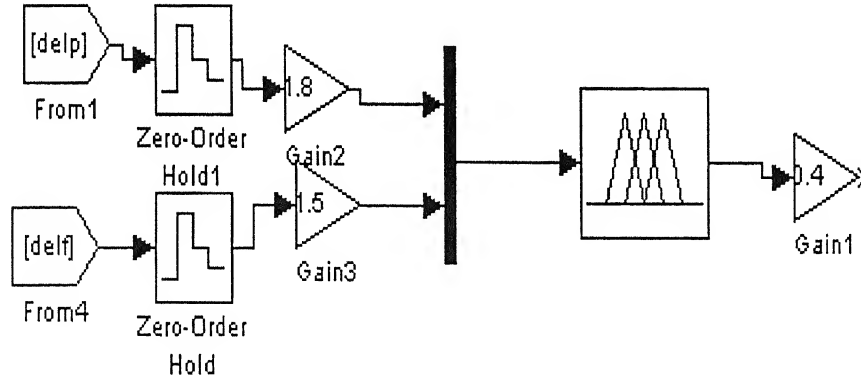


Fig. 4.9: FLPSS simulink block.

4.6 Simulation and Results

The method of defining the fuzzy membership functions used is same as that of FLC design, section 4.3. The fuzzy rules in the FAM tables of Fig.4.7 and 4.8 are defined in the FIS editor. The input and output ranges are calculated with a three phase fault at generator terminal. The different cases as discussed in section 3.5 are simulated with the CPSS replaced by FLPSS.

(a) Reduced NPC system with FLPSS

The parameters of FLPSS are set as $K_P=1.8$, $K_w=1.5$, $K_U=0.4$ obtained by generalized GA approach [22]. Load angle of Kaiga-1 and swing generator are shown in Fig. 4.10 and Fig. 4.11, respectively. Speed deviation between Kaiga-1 and swing generator, and Kaiga-1 and 2 are shown in Fig. 4.12 and Fig. 4.13 respectively. Power output, terminal voltage and PSS output for Kaiga-1 are given in Fig. 4.14-Fig.4.16. From Fig. 4.10 to Fig. 4.16 it is observed that, with FLPSS the oscillations are getting damped within less than 5 seconds. However, with CPSS, oscillations are damped out in almost 15 second for $T_1/T_2=0.25$.

(b) Detailed NPC System

The FLPSS parameters are maintained at the same value, and the simulation was performed for the detailed model. Load angles of Kaiga, swing generator and Kadra generator are shown in Fig. 4.17, Fig. 4.18 and Fig. 4.20, respectively. Speed difference between Kaiga-1 and swing generator and PSS output at Kaiga-1 are shown in Fig. 4.19 and Fig. 4.21 respectively. FLPSS also improves the system performance in this case as compared to CPSS.

c) Kaiga System with Other 16 Generators

Other generators remain the same; FLPSS is installed only at Kaiga-1. The load angles of Kaiga-1, swing generator and Kadra hydro are shown in Fig. 4.22, Fig. 4.23 and Fig. 4.24, respectively. Speed deviation between Kaiga-1 and Kadra, Kaiga-1 and 2 generators are shown in Fig. 4.25 and Fig. 4.26 respectively. Kaiga-1 terminal voltage is given in Fig. 4.27. The Fig. 4.22- Fig. 4.27 shows that system FLPSS is able to damp the system oscillations very quickly following a three phase fault and subsequent opening of the line

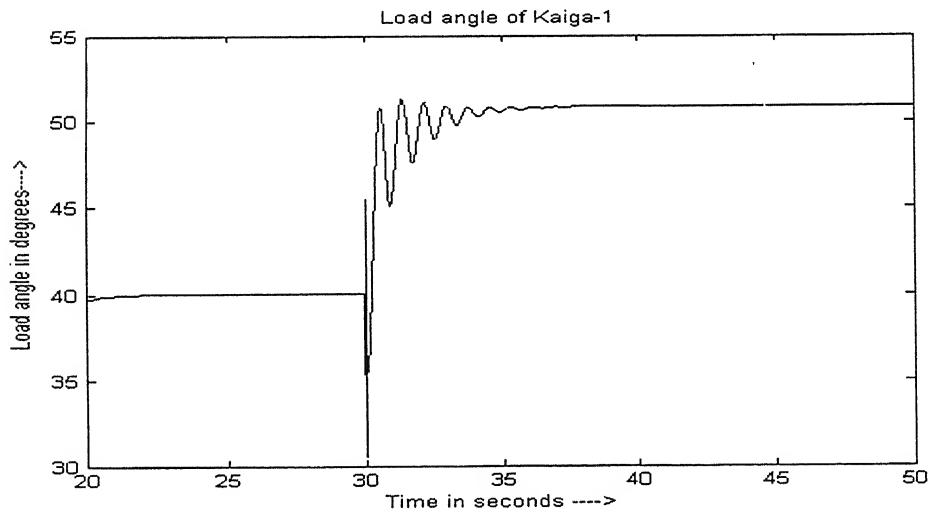


Fig. 4.10: Load angle of Kaiga-1 for reduced NPC system

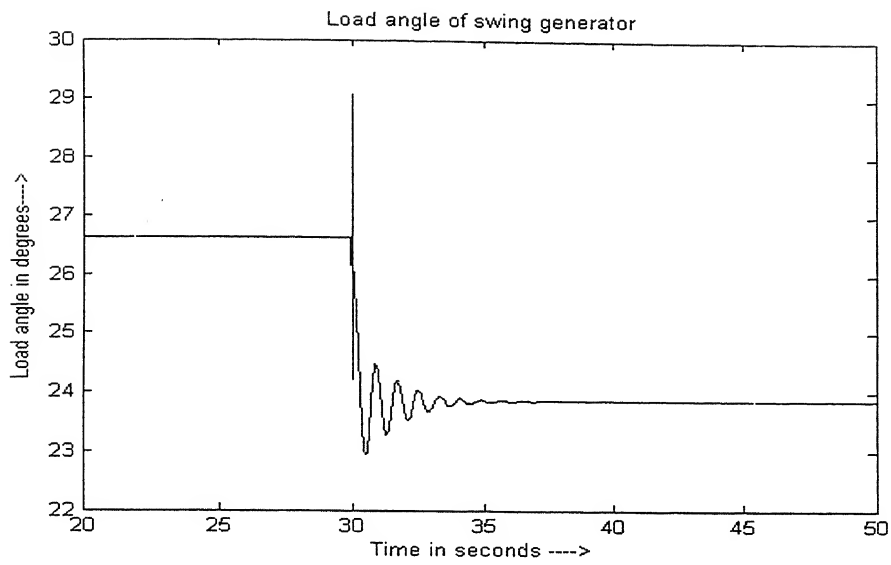


Fig. 4.11: Load angle of swing generator

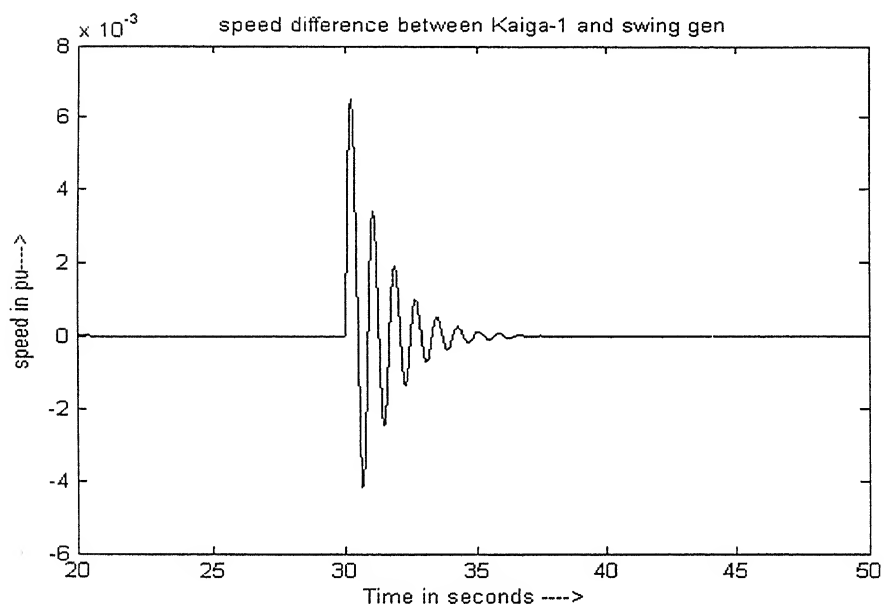


Fig. 4.12: Speed difference between Kaiga-1 and swing generator

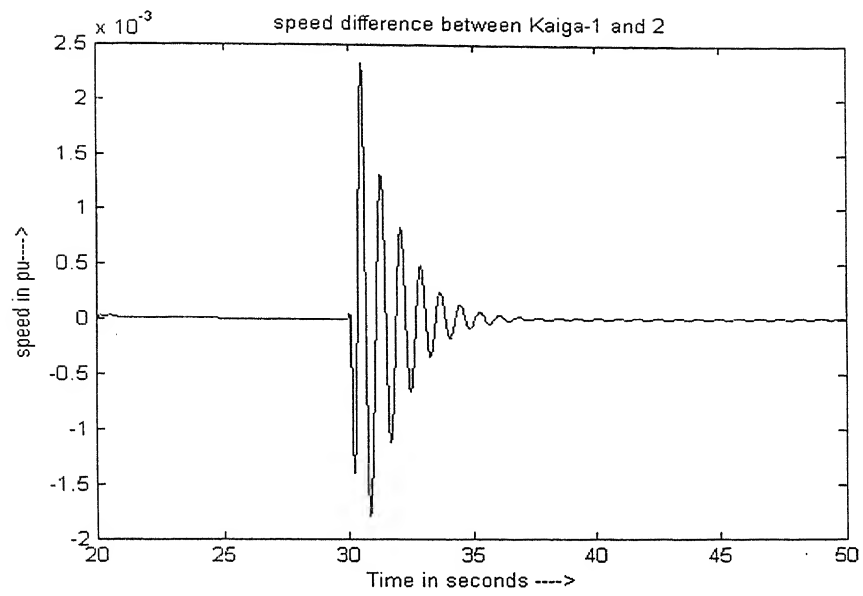


Fig. 4.13: Speed difference between Kaiga-1 and 2

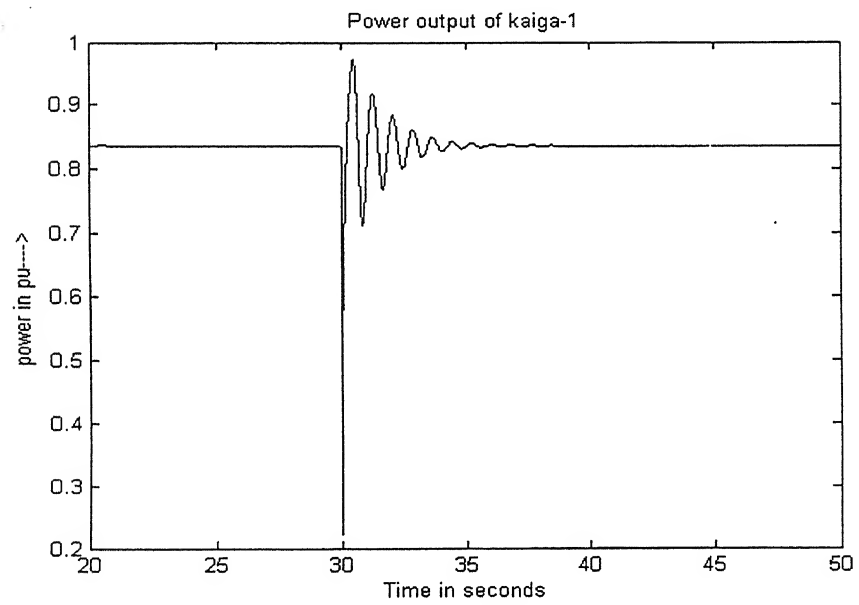


Fig. 4.14: Power output of Kaiga-1

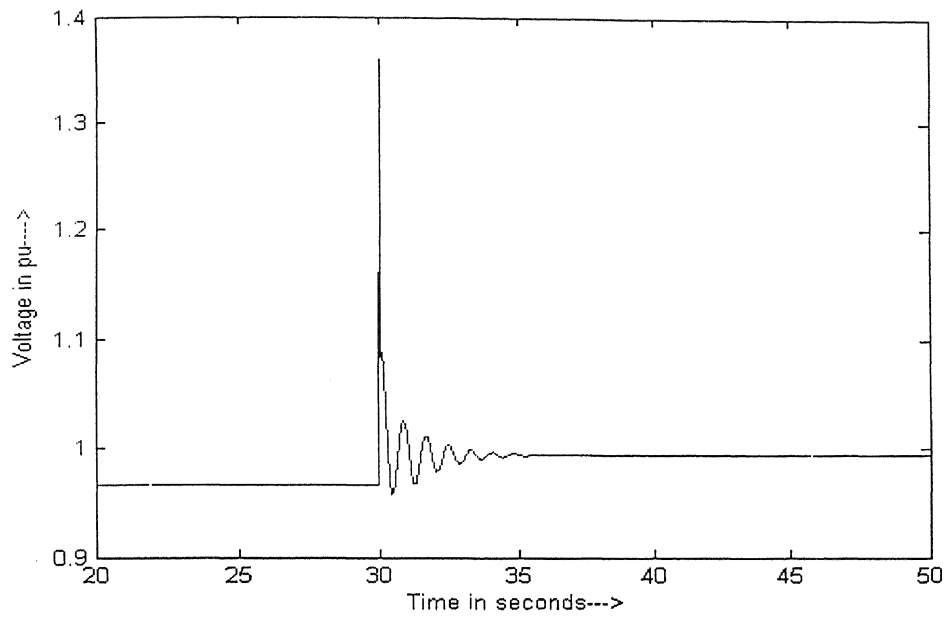


Fig. 4.15: Terminal voltage at Kaiga-1

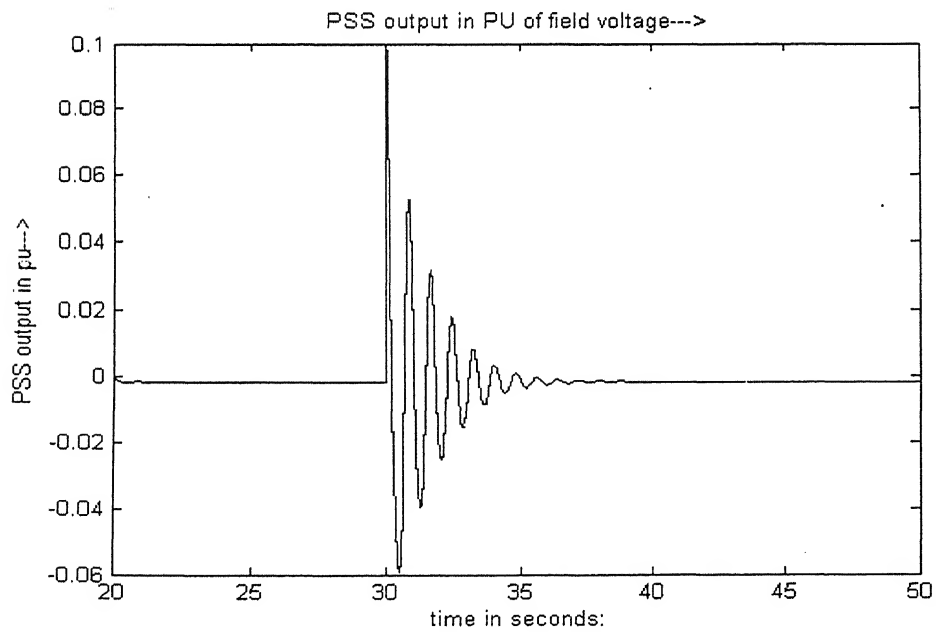


Fig. 4.16: FLPSS output in PU of field voltage

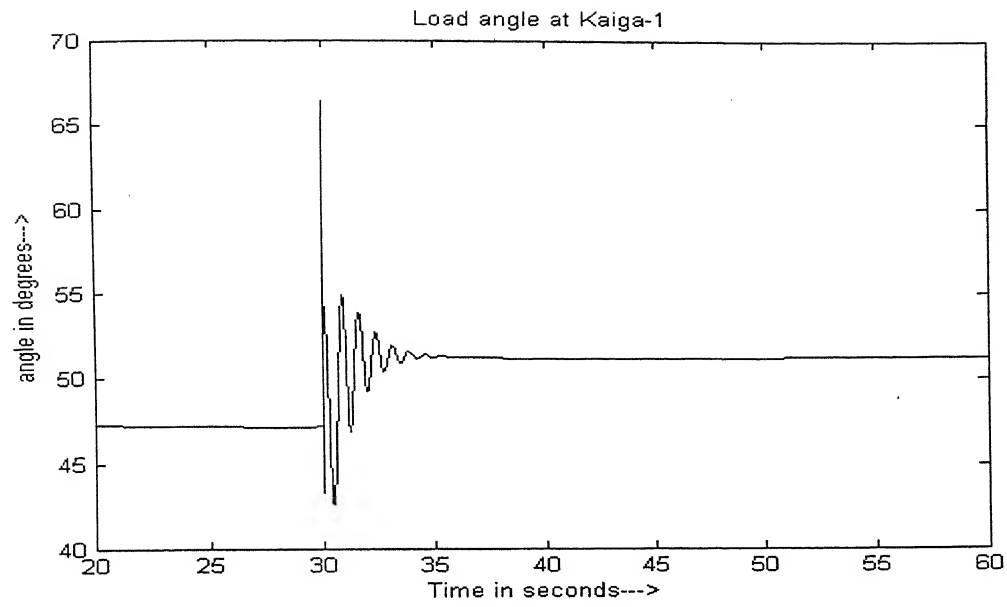


Fig. 4.17: Load angle at Kaiga-1 with Fuzzy PSS, for detailed NPC system

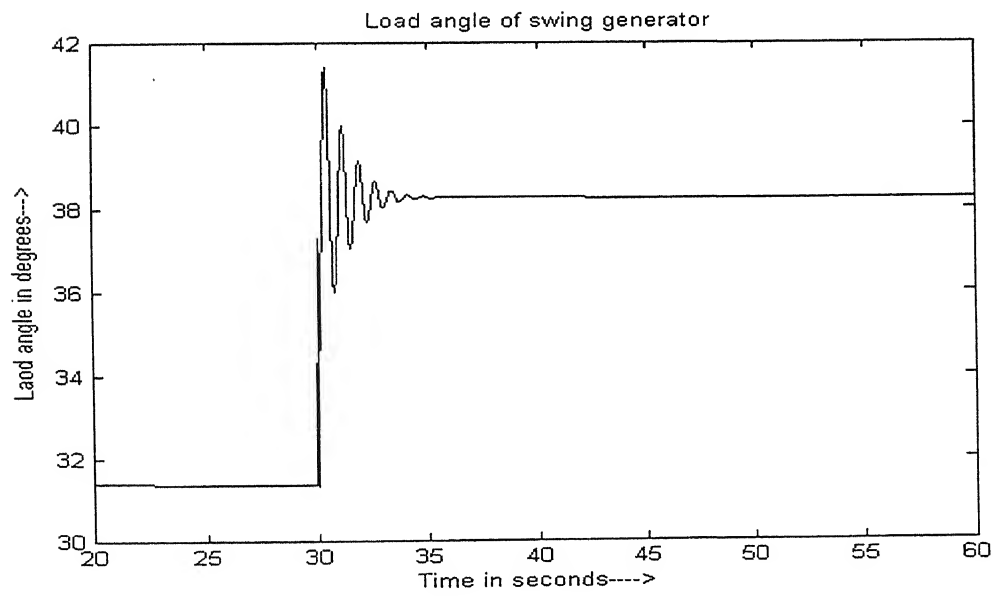


Fig. 4.18: Load angle of swing generator

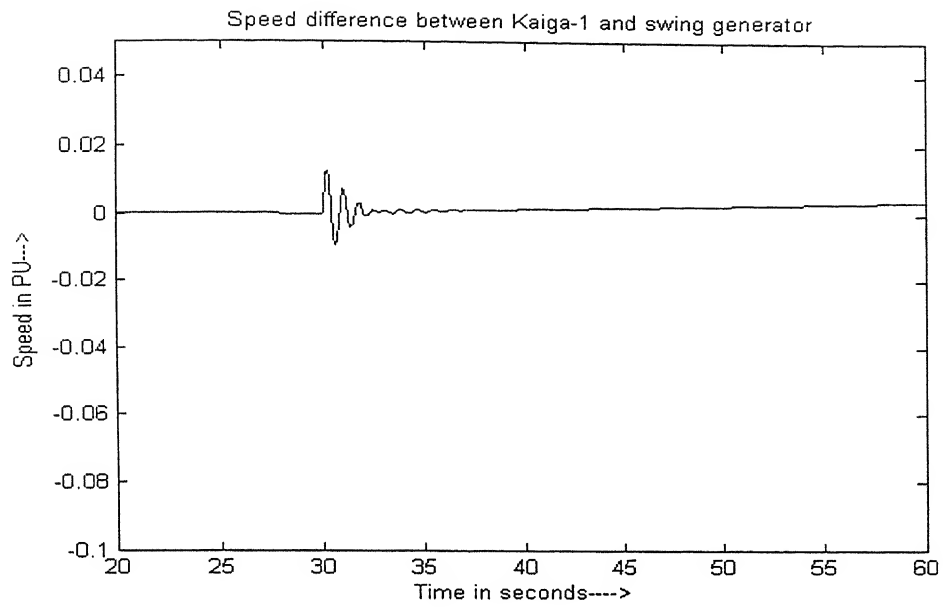


Fig. 4.19: Speed difference between Kaiga-1 and swing generator

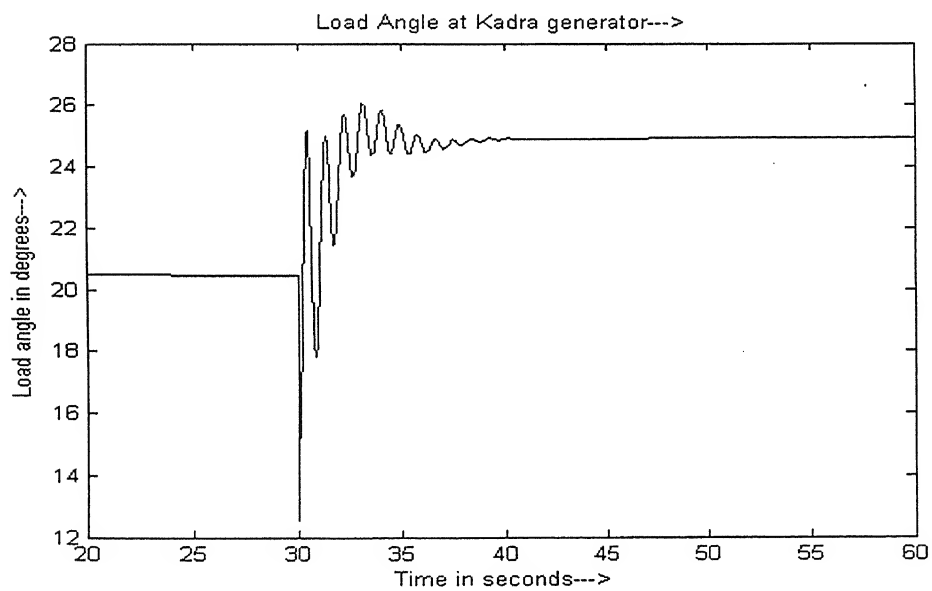


Fig. 4.20: Load angle at Kadra generator

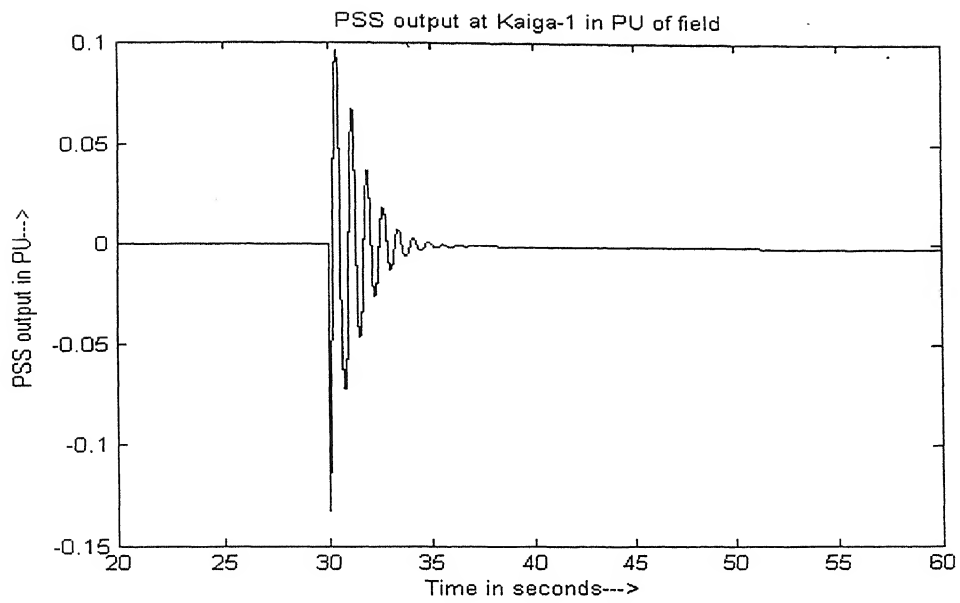


Fig.4.21: PSS output at Kaiga-1 in PU of field voltage

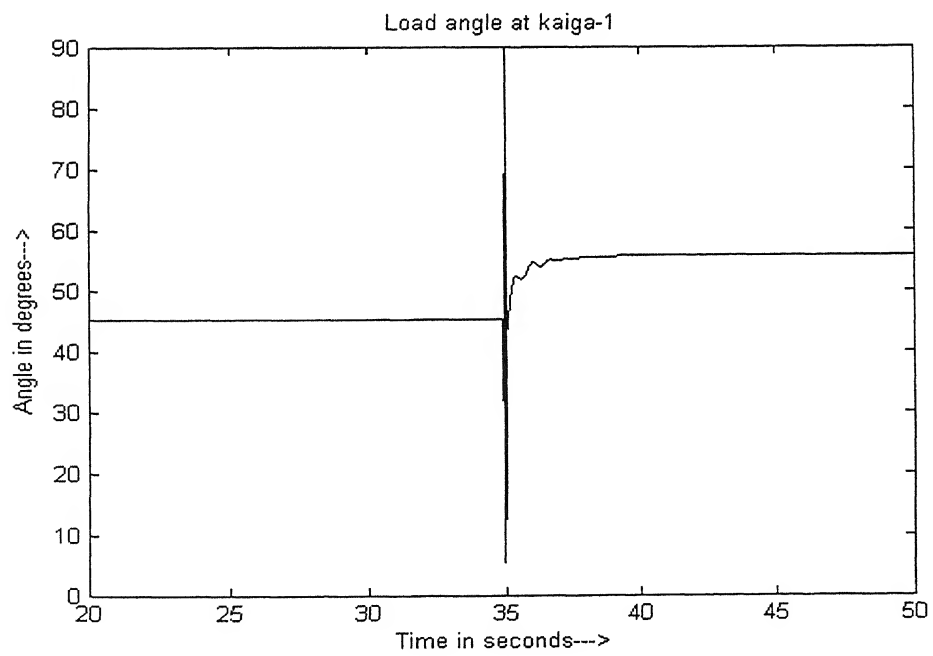


Fig. 4.22: Load angle at Kaiga-1 with fuzzy PSS for other 16 gen connected

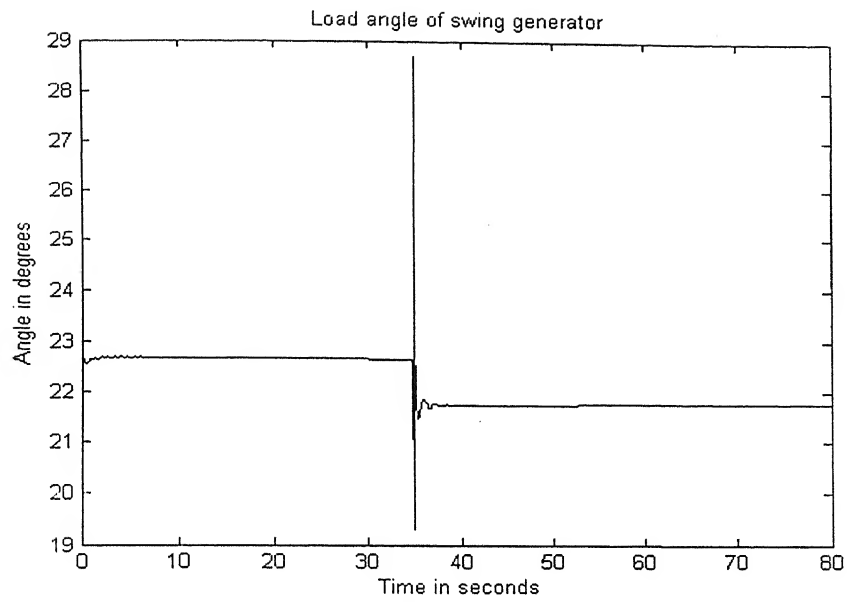


Fig. 4.23 Load angle of swing generator

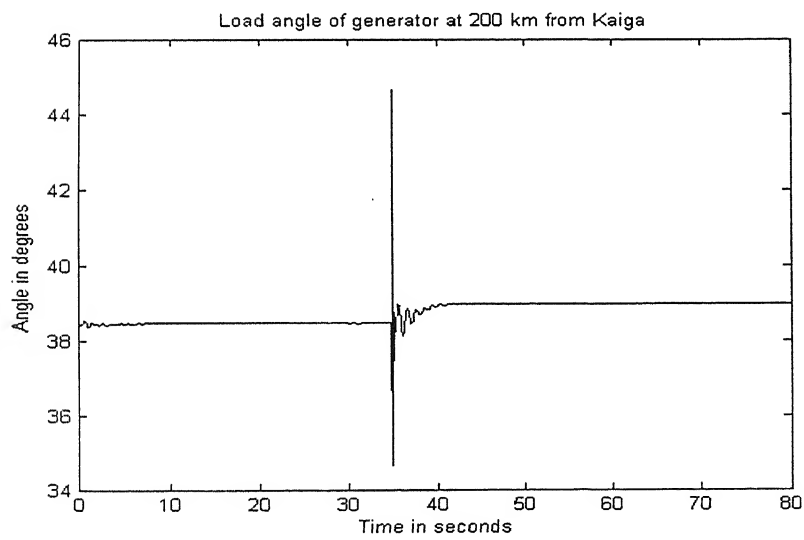


Fig. 4.24: Load angle of generator 200km from Kaiga

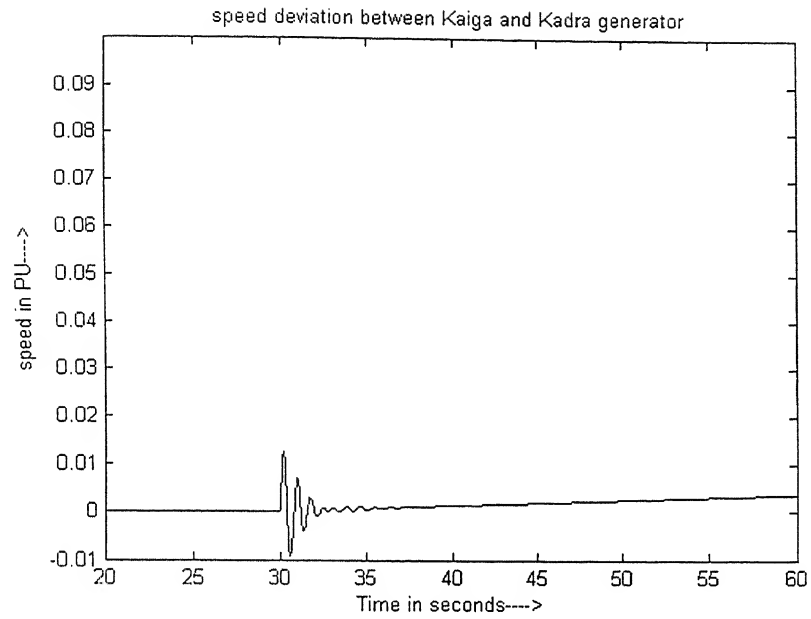


Fig. 4.25: Speed deviation between Kaiga-1 and Kadra generator

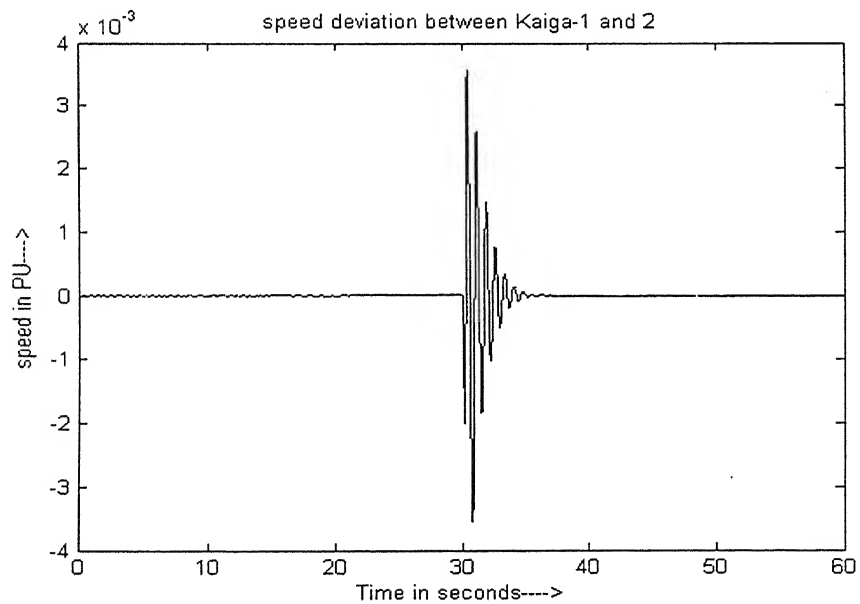


Fig. 4.26: Speed deviation between kaiga-1 and 2

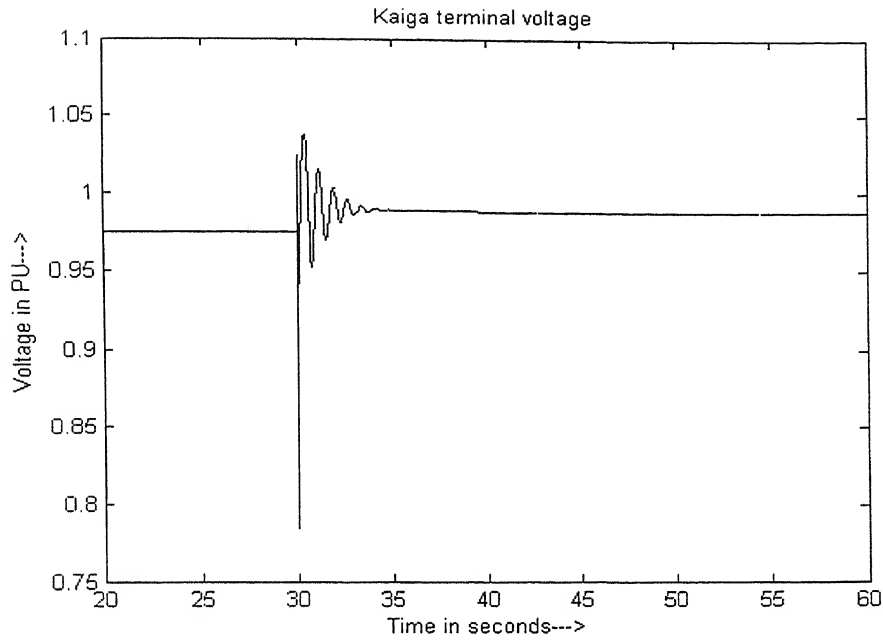


Fig. 4.27 terminal voltage of Kaiga-1

4.7 Conclusion

FLPSS can be used as a better alternative for CPSS to damp the rotor oscillations. The FLPSS input and output parameters do not vary for a change in system configuration. The range of the control inputs change with change in system configuration, but to certain extent the same PSS parameters are able to damp the rotor oscillations. Only for extreme contingency cases, the PSS may not be able to damp the oscillations within reasonable time if the input parameters range exceeds the specified range. For this reason adaptive FLPSS is preferred, where the input and output parameters are determined depending on the severity of contingency. The input and output parameters are optimized for a three phase fault at generator terminal of reduced NPC system.

Conclusions

5.1 General

Because of long transmission lines, operation of the generators near to their full load capacity and poor tuning of AVR parameters, present day practical power systems are facing the problem due to poor damping of small signal oscillations. Load centers and generating stations are placed far from each other because of various reasons. So long transmission line (weak system) is inevitable. Because of heavy demand mostly in developing countries, the generator has to operated near the full load capacity. Higher settings of AVR increases the field forcing capability, thereby increases the steady state stability limit. But simultaneously magnifies the oscillations by reducing the damping torque [15]-[16]. The problem of long transmission line can be solved by application of FACTS devices; which is beyond the scope of the present thesis. This thesis identifies poor tuning of AVR parameters as the main cause of undamped oscillations in a practical system and prescribes tuning of PSS for damping these oscillations.

In this thesis, the causes of small signal oscillations in Kaiga generators were found out. The remedial measure to damp these oscillations was provided by tuning the PSS and a Fuzzy Logic PSS is proposed to replace the conventional PSS.

The main findings of the studies carried out in chapter-2 are as follows:

- In the 9 bus system, all the eigen values had negative real parts but the damping was poor with one critical mode in the system. Application of strip eigen value placement method and pseudo decentralization method improved the system damping.
- In the 39-bus system there were three under damped modes with damping ratio < 0.05 . Application of pseudo decentralization method improved the system damping ratio. But strip eigen vale method could not be applied to this system.

In chapter 3, the SMIB approach was used for tuning of Kaiga PSS, as there is no lead-lag block as there in practice. The main findings of this chapter are

- The PSS signal had to overcome considerable phase lag in the GEP(s) block to produce the final torque on the rotor in phase with speed deviation signal.
- Eigen value analysis showed that there are two critical modes and both the generators had maximum participation in $\Delta\delta$ and $\Delta\omega$ states corresponding to these modes. After introduction of PSS the damping ratio had improved to safe values
- With T_i/T_2 setting of 0.5, the simulation of the reduced NPC system exhibited similar oscillations at 1.2 Hz. But with $T_i/T_2=0.5$, the oscillations damped out. This proved the improper tuning of AVR at Kaiga. After inclusion of PSS with the settings found through eigen value analysis, the oscillations were damped out.
- The detailed model considering the dynamics of near by hydro generators had similar oscillating response without PSS. After inclusion of PSS the oscillations were damped out.
- The NPC system was tested for a three phase fault case, with and without PSS. The PSS was able to damp the oscillations. Which proved that, this setting of PSS can also improve the system performance during severe fault conditions?

Chapter-4, CPSS was replaced by FLPSS. The main findings of this chapter are

- The rule base was prepared for the FLPSS through the simulation of the NPC system with a 3 phase fault at the generator terminal. So a detailed knowledge of the system dynamics is not required for finding the rule base, as it can also be designed from operating experience of the system
- The FLPSS was able to damp the oscillations within few seconds, so it can be used as an alternative to CPSS.

5.2 Future Scope of Research

During the course of research, following areas were found out for further research and development

- The decentralization method can be improved further, so that an effective method to find out the \mathbf{Q} matrix can be obtained. This will reduce the burden of arbitrary selection and variation of PSS parameters. So that practical application of this method will be feasible.
- The actual settings of nearby generators to Kaiga were not available for analysis. The analysis can be made more realistic if those settings are obtained from the site.
- FLPSS needs some adaptive technique, so that it can take care of different operating conditions. This remains as a future area of research.

References

1. Francisco P.Demello and Charles Concordia, "Concepts of Synchronous Machine Stability as Affected by Excitation System", *IEEE Transactions on Power System apparatus and Systems*, Vol.PAS-88, No. 4, April 1969, PP 316-328
2. E.V.Larsen and D.A. Swann, "Applying Power System Stabilizer, I, II, III", *IEEE Transaction on Power Apparatus and System*, Vol. PAS-100, No.6, June 1981,PP 3017-1045
3. F.P. Demello, L.N. Hennett and J.M. Undrill, "Practical Approach to Supplementary Stabilizing from Accelerating Power", *IEEE Transactions on Power Apparatus and Systems*, PAS-97, 1978, PP 1515-1522.
4. P. Kundur, M Klein, G.J. Rogers and M.S. Zywno, "Application of Power System Stabilizer for Enhancement of Overall System Stability", *IEEE Transactions on Power System*, Vol 4, 1989, PP.614 -629
5. A.J.A Simoes Costa, F.D. Freitas and H.E. Pena, "Power System Stabilizer Design via Structurally Constrained Optimal Control", *Electric Power System Research*, 1995, PP.33-40
6. A.J.A. Simoes Costa, F.D. Feritas and A.S.e Silva, "Design of Decentralized Controllers for Large Power Systems Considering Sparsity", *IEEE Transactions on Power Systems*, Vol.12, No.1, Feb. 1997,pp. 144-152
7. A.Jafari Koshkouei and A.S.I. Zinober, "Comments on "Linear Quadratic Regulators with Eigen Value Placement in a Vertical Strip", *IEEE Transaction on Automatic Control*, Vol.44. No.7. July 1999,pp.1417-1419

8. Y.C. Lee, C.J. Wu, "Damping of Power System Oscillations with Output Feedback and Strip Eigenvalue Assignment", *IEEE Transactions on Power Systems*, Vol. 10, No. 3, August 1995, pp. 1620-1626.
9. Kei Ohiska and Yauso Morioka, "A Decentralized Control System for Stabilizing a Longitudinal power System Using Tie Line Power Flow Measurement", *IEEE Transaction on Power System*, Vol.12, No.3, August 1997, pp.1202-1209.
10. "IEEE Recommended Practice for Excitation System Models for Power System Stability Studies", *IEEE std.*, 421.5, 1992
11. Chern-Lin Chen, Yuan-Yih Hsu, "An Efficient Algorithm for the Design of Decentralized Output Feedback", *IEEE transactions on Power Systems*, Vol. 3, No. 3, August 1988, pp. 999-1004.
12. D.C.Lee, R.E. Beaulieu, J.R.R. Service, "A Power System Stabilizer Using Speed and Electrical Power Inputs- Design and Field Experience", *IEEE Transaction on Power Apparatus and Systems*, Vol. PAS-100, No.9, September 1981, pp.4151-4157
13. N. Hossseinzadeh, A.kalam, "A Rule-Based Fuzzy Power System Stabilizer Tuned by a Neural Network", *IEEE Transaction on Energy Conversion*, Vol.14, No.3, September 1999, pp.773-779.
14. K.A. El-Metwally, O.P.malik, "Application of Fuzzy Logic Stabilizers in a Multimachine Power System Environment", *IEE Proceedings on Gen. Transm. Distrib*, Vol.143, No.3, May 1996, PP. 263-268
15. J.Wen, S. Cheng, O.P. Malik, "A Synchronous Generator Fuzzy Excitation Controller Optimally Designed with a Genetic Algorithm", *IEEE Transactions on Power Systems*, Vol.13, No. 3, 1998, pp.339-347.

16. P.Laxmi, M. Abdullah Khan, "Stability Enhancement of a Multi Machine Power System Using Fuzzy Logic Based Power System Stabilizer Tuned Through Genetic Algorithm", *International Journal of Electric Power and Systems*, No.22, 2000, pp. 137-145.
17. Indraneel Sen and Ritwik Majumder, "Design and Implementation of a Novel Fuzzy Logic Based Power System Stabilizer", International Conference on Power Systems, ICPS2004, Nov3-5, Kathmandu, Nepal
18. B. Kalyan Kumar," Coordination of Power System Stabilizer and Supplementary Control Parameters in a Multi Machine System", MTech Thesis, February 2003, IIT Kanpur
19. P.Kundur, *Power System Stability and Control*, McGraw-Hill, New York, U.S.A, 1994
20. K.R.Padiyar, *Power System Dynamic Stability and Control*, John Wiley & sons (Asia) Pte Ltd.
21. Peter W. Sauer, M.A.Pai, *Power System Dynamics and Stability*, Prentice Hall, New Jersey, U.S.A.
22. *Electric Power Applications of Fuzzy Systems*, IEEE Press Power Systems Engineering Series, New York
23. P.M. Anderson and A.A. Fouad, *Power System Stability and Control*, the Iowa State University Press, 1977

24. P.S. Kundur, "Power System Security in the New Industry Environment: Challenges and Solutions", International Conference on Power Systems, ICPS2004, Nov 3-5, Kathmandu, Nepal
25. Stanislaw H.Zak, *Systems and Control*, Oxford University Press, New York, 2003
26. Timothy J. Ross, *Fuzzy Logic with Engineering Applications*, McGraw-Hill International Edition, Singapore, 1997
27. System Models and Data Sheets, BHEL

WSSC 3-Machine, 9-Bus System

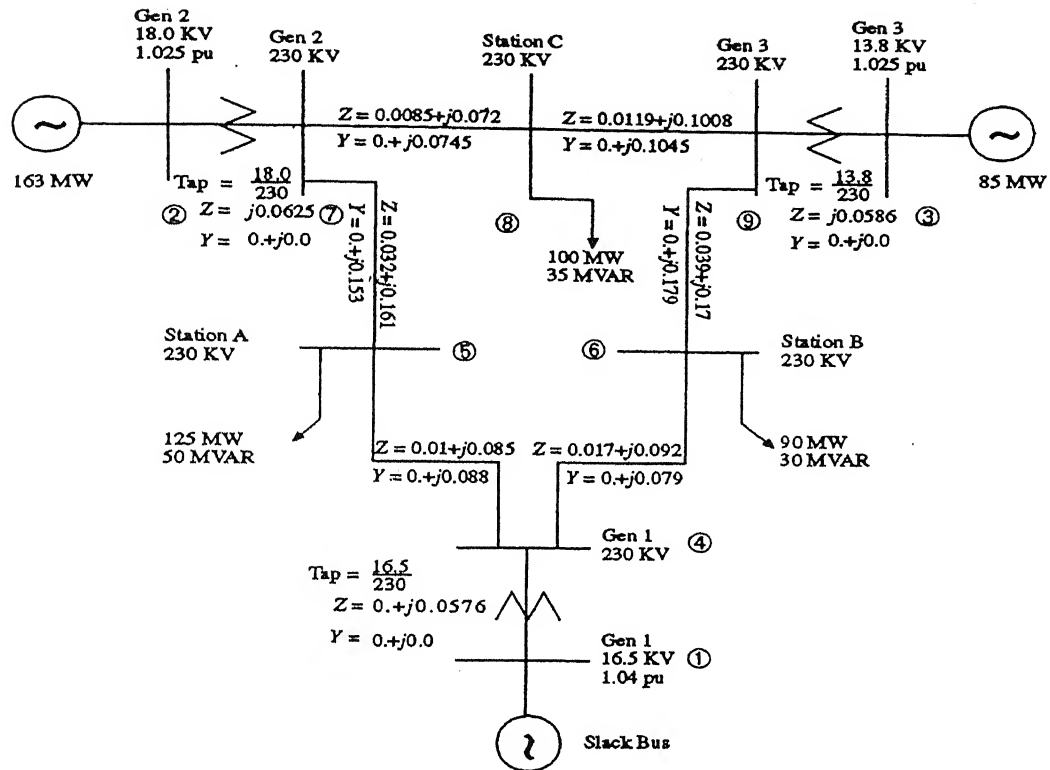


Fig A-1 one line diagram of WSSC 9-bus system.

Table A-1 Base case load flow Results

Bus	Voltage	Phase (deg)	Pgen	Qgen	Pload	Qload
1	1.040	0.00	0.7164	0.2705	0.0000	0.0000
2	1.025	9.28	1.6300	0.0665	0.0000	0.0000
3	1.025	4.66	0.8500	-0.1086	0.0000	0.0000
4	1.026	-2.22	0.0000	0.0000	0.0000	0.0000
5	0.996	-3.99	0.0000	0.0000	1.2500	0.5000
6	1.026	3.72	0.0000	0.0000	0.9000	0.3000
7	1.026	3.72	0.0000	0.0000	0.0000	0.0000
8	1.016	0.73	0.0000	0.0000	1.0000	0.3500
9	1.032	1.97	0.0000	0.0000	0.0000	0.0000

Table A-2 Line Data

From	To	R_line	X_line	Y_charging	Tapping
4	1	0.0000	0.0576	0.0000	1
7	2	0.0000	0.0625	0.0000	1
9	3	0.0000	0.0586	0.0000	1
4	6	0.0170	0.0920	0.1580	0
4	5	0.0100	0.0850	0.1760	0
5	7	0.0320	0.1610	0.3060	0
6	9	0.0390	0.1700	0.3580	0
7	8	0.0085	0.0720	0.1490	0
8	9	0.0119	0.1008	0.2090	0

Table A-3 Machine Data

Gen	H	X _d	X _d '	X _q	X _q '	T _{do} '	T _{qo} '
1	23.6	0.1460	0.0608	0.0969	0.0969	8.96	0.31
2	6.4	0.8958	0.1198	0.8645	0.1969	6.00	0.54
3	3.0	1.3125	0.1813	1.2578	0.2500	5.89	0.60

Table A-4 Exciter Data

The IEEE type-1 exciter having identical parameters has been used in all the three generators. The exciter data is given below:

$$K_A = 20.00$$

$$T_A = 0.2 \text{ sec}$$

$$K_E = 1.0$$

$$T_E = 0.314 \text{ sec}$$

$$K_F = 0.063$$

$$T_F = 0.35 \text{ sec}$$

$$S_E(E_{fd}) = 0.0039e^{1.555E_{fd}}$$

New England 39-Bus, 10-Machine System

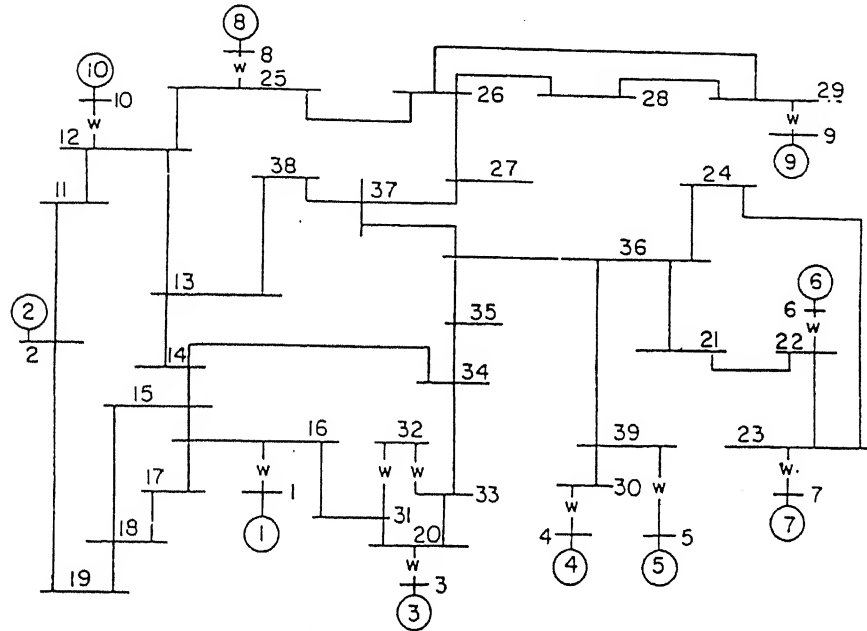


Fig B-1: One line diagram of New England 39-bus system.

Table B-1 Base case Load-flow Results

Bus	Voltage	Phase (deg)	Pgen	Qgen	Pload	Qload
1	0.980	0.00	5.527	1.687	0.092	0.046
2	1.03	-11.06	10.000	2.425	11.040	2.500
3	0.980	2.36	6.500	1.705	0.000	0.000
4	1.010	3.22	5.080	1.673	0.000	0.000
5	0.990	4.30	6.32	0.760	0.000	0.000
6	1.040	5.35	6.500	2.669	0.000	0.000
7	1.060	8.13	5.600	2.415	0.000	0.000
8	1.020	1.95	5.400	0.239	0.000	0.000
9	1.020	7.71	8.300	0.631	0.000	0.000
10	1.040	-4.01	2.500	1.767	0.000	0.000
11	1.033	-9.40	0.000	0.000	0.000	0.000
12	1.010	-6.48	0.000	0.000	0.000	0.000
13	0.979	-9.51	0.000	0.000	3.220	0.024
14	0.945	-10.45	0.000	0.000	5.000	1.840

15	0.947	-9.19	0.000	0.000	0.000	0.000
16	0.948	-8.41	0.000	0.000	0.000	0.000
17	0.940	-10.88	0.000	0.000	2.338	0.840
18	0.941	-11.45	0.000	0.000	5.220	1.760
19	1.006	-11.27	0.000	0.000	0.000	0.000
20	0954	-563	0.000	0.000	0.000	0.000
21	0.978	-4.34	0.000	0.000	2740	1.150
22	1.007	0.26	0.000	0.000	0.000	0.000
23	1.006	-0.02	0.000	0.000	2.745	0.840
24	0.967	-6.83	0.000	0.000	3.086	0.922
25	1.019	-4.97	0.000	0.000	2.240	0.472
26	1.005	-6.23	0.000	0.000	1.390	0.170
27	0.985	-8.38	0.000	0.000	2.810	0.755
28	1.009	-243	0.000	0.000	2.060	0.276
29	1.012	0.53	0.000	0.000	2835	0.269
30	0980	-1.99	0.000	0.000	6.28	1.030
31	0.951	-6.57	0.000	0.000	0.000	0.000
32	0.931	-6.56	0.000	0.000	0.075	0.880
33	0.952	-6.42	0.000	0.000	0.000	0.000
34	0.950	-827	0.000	0.000	0.000	0.000
35	0.951	-859	0.000	0.000	3.200	1.530
36	0.967	-6.93	0.000	0.000	3.294	0.323
37	0.975	-8.15	0.000	0.000	0.000	0.000
38	0.975	-9.15	0.000	0.000	1.580	0.300
39	0.979	-0.98	0.000	0.000	0.000	0.000

Table B-2 Line Data

From	To	R_line	X_line	Y_charging	Tapping
39	30	0.0007	0.0138	0.0000	1
39	5	0.0007	0.0142	0.0000	1
32	33	0.0016	0.0435	0.0000	1
32	31	0.0016	0.0435	0.0000	1
30	4	0.0009	0.0180	0.0000	1
29	9	0.0008	0.0156	0.0000	1
25	8	0.0006	0.0232	0.0000	1
23	7	0.0005	0.0272	0.0000	1
22	6	0.0000	0.0143	0.0000	1
20	3	0.0000	0.0200	0.0000	1
16	1	0.0000	0.0250	0.0000	1
37	27	0.0013	0.0173	0.3216	0
37	38	0.0007	0.0082	0.1319	0
36	24	0.0003	0.0059	0.0680	0
36	21	0.0008	0.0135	0.2548	0

36	39	0.0016	0.0195	0.3040	0
36	37	0.0007	0.0089	0.1342	0
35	36	0.0009	0.0094	0.1710	0
34	35	0.0018	0.0217	0.3660	0
33	34	0.0009	0.0101	0.1723	0
28	29	0.0057	0.0625	1.0290	0
26	29	0.0057	0.0625	1.0290	0
26	28	0.0043	0.0474	0.7802	0
26	27	0.0014	0.0147	0.2396	0
25	26	0.0032	0.0323	0.5130	0
23	24	0.0022	0.0350	0.3610	0
22	23	0.0006	0.0096	0.1846	0
21	22	0.0008	0.0135	0.2548	0
20	33	0.0004	0.0043	0.0729	0
20	31	0.0004	0.0043	0.0729	0
19	2	0.0010	0.0250	1.2000	0
18	19	0.0023	0.0363	0.3804	0
17	18	0.0004	0.0046	0.0780	0
16	31	0.0007	0.0082	0.1389	0
16	17	0.0006	0.0092	0.1130	0
15	18	0.0008	0.0112	0.1476	0
15	16	0.0002	0.0026	0.0434	0
14	34	0.0008	0.0129	0.1342	0
14	15	0.0008	0.0129	0.1382	0
13	38	0.0011	0.0133	0.2138	0
13	14	0.0013	0.0213	0.2214	0
12	25	0.0070	0.0086	0.1460	0
12	13	0.0013	0.0151	0.2572	0
11	12	0.0035	0.0411	0.6987	0
11	2	0.0010	0.0250	0.7500	0

Table B-3 Machine data

Gen	H	X_d	X_d'	X_q	X_q'	T_{do}'	T_{qo}'
1	30.3	0.2950	0.0647	0.2820	0.0647	6.56	1.50
2	500.0	0.0200	0.0060	0.0190	0.0060	6.00	0.70
3	35.8	0.2495	0.0531	0.2370	0.0531	5.77	1.5
4	26.0	0.3300	0.0660	0.3100	0.0660	5.40	0.44
5	28.6	0.2620	0.0436	0.2580	0.0436	5.69	1.50
6	34.8	0.2540	0.0500	0.2410	0.0500	7.30	0.40
7	26.4	0.2950	0.0490	0.2920	0.0490	5.66	1.50
8	24.3	0.2900	0.0570	0.2800	0.0570	6.70	0.41
9	34.5	0.2106	0.0570	0.2050	0.0570	4.79	1.96
10	420	0.2000	0.0040	0.1960	0.0040	5.70	0.05

For all machines $R_a = 0$

Table B-4 AVR data

Machine no.	K_a	T_a	K_e	T_e	K_f	T_F
1	5.0	0.06	-0.05	0.25	0.04	1.000
2	6.2	0.05	0.63	0.41	0.06	0.500
3	5.0	0.06	-0.02	0.5	0.08	1.000
4	5.0	0.06	-0.05	0.5	0.08	1.000
5	40.0	0.02	-0.04	0.785	0.03	1.000
6	5.0	0.02	1.00	0.471	0.08	1.250
7	40.0	0.02	1.00	0.730	0.03	1.000
8	5.0	0.02	-0.05	0.528	0.09	1.260
9	40.0	0.02	1.0	1.4	0.03	1.000
10	5.0	0.02	1.0	1.4	0.03	1.000

System and Machine Parameters for Kaiga NPP

- | | |
|-----------------------------|-------------|
| 1. M/C inertia constant (H) | 1.91 MJ/MVA |
| 2. M/C Voltage | 16.5 kV |

Table C-1 Machine reactances in PU on machine voltage and power base

	Unsaturated	Saturated
Direct axis synchronous reactance (X_d)	1.94	1.72
Quadrature axis synch. Reactance (X_q)	1.84	1.63
Direct axis transient reactance (X'_d)	0.28	0.238
Quadrature axis transient reactance (X'_q)	0.82	0.74
Direct axis subtransient reactance(X''_d)	0.209	0.167
Quadrature axis subtransient reactance(X''_q)	0.23	0.184
Potier reactance (X_p)	0.209	0.167

Table C-2 Machine time constants in second

Open circuit Direct axis transient time constant (T'_{do})	6.3
Open circuit Quadrature axis transient time constant (T'_{qo})	2.0
Open circuit direct axis subtransient time constant (T''_{do})	0.04
Open circuit Quadrature axis subtransient time constant (T''_{qo})	0.17

Table C-3 Exciter and AVR parameters

	Range	Typical values
V_0 =steady state gain	10-126	40
V_p =Proportional gain	0.8-25.6	10
V_{inf}	8-257	200
T_R =transducer time constant	-	0.025sec
T_a =AVR time constant	-	1 sec
T_b =AVR time constant	-	10msec

T_S =Thyristor time constant - 3.3 μ sec

Table C-4 Line and Transformer data

Line data in ohms/km/circuit, in 100MVA and 220kV base

	R_1	X_1	R_0	X_0
For single circuit lines	0.08	0.399	0	0
For all double circuit lines	0.029792	0.322	0.16192	1.24

Transformer data on Machine base

	X_1	X_0	X_1/R_1	X_0/R_0
All two winding transformers	0.14	0.14	20	20
Three winding transformer on machine base	X_1	X_2		X_0
Primary-secondary reactance	45%	45%		95%
Secondary to tertiary reactance	12.5%	12.5%		95%
Primary to tertiary reactance	30%	30%		95%